SANDIA REPORT
SAND97-0991 • UC-704
Unlimited Release
Printed May 1997

A Microstructural Analysis of Solder Joints from the Electronic Assemblies of Dismantled Nuclear Weapons

P. T. Vianco, J. A. Rejent

Prepared by
Sandia National Laboratories
Albuquerque, New Mexico 87185 and Livermore, California 94550

Sandia is a multiprogram laboratory operated by Sandia Corporation, a Lockheed Martin Company, for the United States Department of Energy under Contract DE-AC04-94AL85000.

Approved for public release; distribution is unlimited.

Sandia National Laboratories

SF2900Q(8-81)

Issued by Sandia National Laboratories, operated for the United States Department of Energy by Sandia Corporation.
NOTICE: This report was prepared as an account of work sponsored by an agency of the United States Government. Neither the United States Government nor any agency thereof, nor any of their employees, nor any of their contractors, subcontractors, or their employees, makes any warranty, express or implied, or assumes any legal liability or responsibility for the accuracy, completeness, or usefulness of any information, apparatus, product, or process disclosed, or represents that its use would not infringe privately owned rights. Reference herein to any specific commercial product, process, or service by trade name, trademark, manufacturer, or otherwise, does not necessarily constitute or imply its endorsement, recommendation, or favoring by the United States Government, any agency thereof, or any of their contractors or subcontractors. The views and opinions expressed herein do not necessarily state or reflect those of the United States Government, any agency thereof, or any of their contractors.

Printed in the United States of America. This report has been reproduced directly from the best available copy.

Available to DOE and DOE contractors from
Office of Scientific and Technical Information
P.O. Box 62
Oak Ridge, TN 37831

Prices available from (615) 576-8401, FTS 626-8401

Available to the public from
National Technical Information Service
U.S. Department of Commerce
5285 Port Royal Rd
Springfield, VA 22161

NTIS price codes
Printed copy: A05
Microfiche copy: A01

SAND97-0991
Unlimited Release
Printed May 1997

Distribution
Category UC-704

A Microstructural Analysis of Solder Joints from the Electronic Assemblies of Dismantled Nuclear Weapons

P.T. Vianco and J.A. Rejent
Materials Joining Department

Sandia National Laboratories
P.O. Box 5800
Albuquerque, NM 87185-1411

Abstract

MC1814 Interconnection Boxes from dismantled B57 bombs, and MC2839 Firing Sets from retired W70-1 warheads were obtained from the Pantex facility. Printed circuit boards were selected from these components for microstructural analysis of their solder joints. The analysis included a qualitative examination of the solder joints and quantitative assessments of (1) the thickness of the intermetallic compound layer that formed between the solder and circuit board Cu features, and (2) the Pb-rich phase particle distribution within the solder joint microstructure. The MC2839 solder joints had very good workmanship qualities. The intermetallic compound layer stoichiometry was determined to be that of Cu6Sn5. The mean intermetallic compound layer thickness for all solder joints was 0.885 mm. The magnitude of these values did not indicate significant growth over the weapon lifetime. The size distribution of the Pb-rich phase particles for each of the joints were represented by the mean of 9.85 × 10-6 mm2. Assuming a spherical geometry, the mean particle diameter would be 3.54 mm. The joint-to-joint difference of intermetallic compound layer thickness and Pb-rich particle size distribution was not caused by varying thermal environments, but rather, was a result of "natural" variations in the joint microstructure that probably existed at the time of manufacture.

The MC1814 solder joints were "through-hole" in nature; however, in place of the electrodeposited Cu conducting layer used on the barrel walls, the copper sleeve ("eyelet") technology was used to transmit signals between the two sides of the circuit board. The joints exhibited very good workmanship with no appreciable voiding and demonstrated excellent surface wetting. However, the solder connection between the sleeve and surface traces on the circuit boards exhibited cracking. The mean intermetallic compound layer thickness that was determined by the combined evaluation of all of the solder joints Cu lands was 1.102 μm. The layer thickness magnitude did not indicate significant growth over the weapon lifetime. The intermetallic compound layer was entirely Cu_6Sn_5. The mean particle size of the combined data was 15.3×10^{-6} mm^2. Assuming a spherical geometry, the mean particle diameter would be 4.41 μm. Trends in the joint-to-joint intermetallic compound layer thickness and mean particle size did not indicate variations in mean particle sizes were due to elevated temperature exposures. Rather, they were a result of random fluctuations from manufacture of the joint.

Abstract (Continued)

The microstructural evaluation of the through-hole solder joints from the MC2839 and MC1814 components indicated that the environmental conditions to which these electronic units were exposed in the stockpile, were benign regarding solder joint aging. There was an absence of thermal fatigue damage in MC2839 circuit board, through-hole solder joints. The damage to the eyelet solder joints of the MC1814 more likely represented infant mortality failures at or very near the time of manufacture, resulting from a marginal design status of this type of solder joint design. The few defects that were observed in MC2839 solder joints were those brought about at the time of assembly (manufacture) of the circuit board.

Acknowledgments

The authors wish to thank the following laboratory personnel: A. Carter, R. Chavez, F. Greulich, and A. Kilgo for preparation of the solder joint samples. The authors also wish to thank W. Dickenmann for still photographic efforts, B. Ritchey for the SEM analyses, and M. Dvorack for his careful review of the manuscript.

Contents

1.0 Introduction 1
1.1 Stockpile Reliability 1
1.2 Tri-labs Dismantlement Program 1
1.3 Dismantled Hardware Acquisition 2
1.4 The Sn-Pb Solder Joint 4
1.5 Objectives 8

2.0 Experimental Procedures and Data Analysis 10
2.1 MC2839 Power Supply 10
2.1.1 Procedures for the Extrication of Targeted Parts 10
2.1.2 Results and Discussion 19
2.2 MC1814 Junction Box 42
2.2.1 Procedures for the Extrication of Targeted Parts 42
2.2.2 Results and Discussion 49

3.0 Conclusions 71

4.0 References 73

Appendix A - Chemical Dissolution for Depotting MC2839 Assemblies 74

Appendix B - Procedures for Analyzing Intermetallic Compound Layer Thicknesses 75

Appendix C - Procedures for Analyzing Lead-Rich Phase Distribution 76

Figures

1a Equilibrium phase diagram of the Sn-Pb binary alloy. 5
1b Microstructure of a ^{63}Sn-^{37}Pb solder joint. 5
2a Plated through-hole solder joint used in present-day printed circuit board technology. 7
2b Schematic diagram of the sleeve-fitted through-hole solder joint used in printed circuit boards of weapons evaluated in this study (c. late 1950s to middle 1960s). 8
3 MC2839 Power Supply from the W70-1 weapon: (a) side view and (b) top view made clear by removal the potting foam. 11
4 Two views (a) and (b) of the position of the 234010-00 circuit board within the MC2839 housing after depotting. 12
5 (a) Top view (with components) and (b) bottom view (without components) of the 234010 printed wiring board sub-assembly. 13
6 Schematic diagram of the abrasive water jet apparatus. 14
7 Set up of MC2839 unit in the abrasive water jet apparatus....15
8 Abrasive water jet cutting process in action. 16
9 A photograph of the bisected unit, showing the cut faces. 16
10 Photograph of 234010 circuit board showing the solder joints selected for cross sectioning and subsequent microstructural analysis. 17
11 Schematic diagram of a through-hole solder joint showing the locations of the quantitative analyses performed on the MC2839, 234010-00 circuit board solder joints. 19
12 Optical micrograph of the solid lead joint "B" from unit 316030 showing an absence of voids in the solder. 20
13 Optical micrograph of the stranded lead joint "I" from unit 316030 showing the presence of voids. 21
14a Low magnification optical micrograph of the "L" joint from unit 526676 showing the gap between the lead and the hole wall, and the coarsening phenomenon in the solder at the lead interface. 22
14b Higher magnification of the coarsening effect. 22
15 Optical micrograph of location III (land) of joint F from unit 469565 showing the intermetallic compound layer between the solder and the copper substrate. 23
16 Effect of cross sectional cut on the measured intermetallic compound layer thickness at the barrel wall (I). 27
17 Optical micrographs of the fillet region II in joint C from unit 526676 at (a) 500x and (b)1000x. 33
18 Pb-rich phase particle size distributions from the micrograph in Fig. 17a from an MC2839 solder joint. 34
19 (a) Standard deviation and (b) percent error as a function of mean Pb-rich phase particle size for the data compiled from the MC2839 units. 40
20 Area percent of Pb-rich phase versus the mean Pb-rich phase particle size for all of the solder joints. 42
21 Photographs of the MC1814 junction box: (a) general view, (b) top view, and (c) bottom view. 43
22a Positive print of an x-ray of the MC1814 junction box. 45
22b The circuit boards targeted for analysis have been identified by a schematic diagram of the junction box showing their location. 45
23 An MC1814 unit in place in the abrasive water jet cutting machine. 46

Figures (continued)

24 Segment of the MC1814 unit after water jet cutting which contains the targeted circuit boards: (a) First cut from the unit to separate the segment of interest. Segment of interest in (b) the front view and (c) rear view. 47

25 Photograph of the circuit board segments labeled "S", "M", and an unlabelled part, taken from circuit boards #5, #4, and #3 of the MC1814 unit, respectively. 48

26 Schematic diagram of the hole construction for the circuit boards in the MC1814 junction box....................50

27 (a) Scanning electron micrograph of the top side of a solder joint from the unit serial number 65517 of the MC1814 assembly. Locations for higher magnification images have been noted; those regions are shown in (b) as "G" and (c) as "D". 51

28 (a) Scanning electron micrograph of the bottom side of a solder joint from the unit serial number 65517 of the MC1814 assembly. Locations for higher magnification images have been noted; those regions are shown in (b) as "J" and (c) as "N". 53

29a Optical micrograph from one quadrant of a unit #65517 solder joint at the point where the sleeve ends on the surface at the conductor....................55

29b A second quadrant showing partial cracking of the sleeve-to-conductor surface solder joint 55

29c A third quadrant in which complete cracking of the connection has occurred. 56

30 Optical micrograph of the intermetallic compound layer in the M1B solder joint (unit #65517) at the solder/copper land interface (location III)....................58

31 Optical micrograph of the solder microstructure in the M1B solder joint (unit #65517) in the fillet region (II)....................63

32 Pb-rich phase particle frequency distribution for the (II) regions of the S1 solder joint in the MC1814, #65517 unit. The ranges are: (a) $0 - 5 \times 10^{-4}$ mm^2; (b) $0 - 2 \times 10^{-4}$ mm^2; (c) $0 - 2 \times 10^{-5}$ mm^2; and (d) $0 - 2 \times 10^{-6}$ mm^2. 64

33 Pb-rich phase particle sizes (mean and ± one standard deviation) for each of the joints in the MC1814 units. 66

34 (a) Standard deviation and (b) percent error as a function of mean Pb-rich phase particle size for the data compiled from the MC1814 units....................68

35 Area percent of Pb-rich phase versus the mean Pb-rich phase particle size for the top-side (A), solder fillet (G) location from all of the solder joints compiled for the MC1814 units. 69

36 Mean Pb-rich phase particle size as a function of the solder/copper intermetallic compound layer thicknesses at (a) region (I) and (b) region (III). 70

Tables

1 Proposed Weapon Components for Dismantlement Evaluation 2
2 Hardware Acquired from Dismantlement Program 3
3 Intermetallic Compound Layer Thickness MC2839 Power Supply Circuit Board 24
4 Intermetallic Compound (IMC) Layer Thickness MC2839 Power Supply Circuit Board Test for Equivalence of Positions I and III 26
5 Frequency of Equal Mean Thickness for Solder Joint Pairings within Each of Three Units. 27
6 Intermetallic Compound Layer Thicknesses MC2839 Power Supply Circuit Board Units 28
7 Intermetallic Compound Layer Thickness Combination Levels 5, 4, 3, 2, and 1 Units 30
8 Pb-rich Particle Size Statistics from the MC2839 Units 37
9 Equality of MC2839 Solder Joint Mean Pb-Rich Particle Sizes versus Total Number of Pairwise Comparisons per Unit 38
10 Intermetallic Compound Layer Thickness MC1814 Junction Box Circuit Board 59
11 Intermetallic Compound Layer Thickness for MC1814 Junction Box Circuit Boards -Unit Summaries for III Locations (A or B) 60
12 Intermetallic Compound Layer Thickness MC1814 Junction Box Circuit Boards Frequency of Equivalence, All Joints per Unit, Location IIIA 61
13 Pb-Rich Particle Phase Distribution MC1814 Junction Box Circuit Boards Frequency of Equivalence of the Mean Size of Paired Locations (A or B, versus H) of Unit Joints 66

1.0 Introduction

1.1 Stockpile Reliability

The safeguarding, arming, fusing, and firing of a nuclear weapon each use a complex arrangement of electronic systems in order to prevent, or realize, a detonation event. The coincidental need for reduced weapon size and increased functionality in the warhead, have placed a greater demand on the electronic packages. The critical reliance on electronics performance for nuclear safety and weapon functionality necessitates that assemblies have a long term reliability in various storage environments that is commiserate with deployment of the particular system. A significant part of electrical system reliability rests upon the integrity of the *solder interconnects.*

While gross manufacturing defects in solder joints can be identified at the time of assembly through proper inspection techniques and subsequently can be corrected through repair or rework procedures, the occurrence of longer term failures due to aging of the electronics is much more difficult to fully anticipate at the design phase, even following extensive, near term testing of prototype units. Although currently available computational techniques have made in-roads into the lifetime predictions of engineering systems, their applicability for materials' response to aging environments is far from mature. Such limitations have included not only the development of accurate codes, but also the availability of empirical data to provide input parameters as well as to validate the numerical results.

Lifetime predictions of solder joints can be significantly streamlined if the failure modes could be compiled and ranked in order of importance to system functionality (through criticality, frequency probability for failure, etc.). Of particular importance is identification of unknown, yet significant, failure mechanisms. The large scale implementation of electronics in both commercial and military products has occurred over roughly the same time frame as they have been used in nuclear weapons (approximately 35 to 40 years). No prior data base of electronic materials performance for such time scales has been available; rather, it is being generated in real time for those applications. Therefore, it becomes necessary to access the integrity of solder joints from field hardware with such lifetimes in order to establish a reliability database that documents failure modes from the past 35 to 40 year lifetimes, as well as provide an "initial condition" from which to apply reliability models that will predict performance for the next 35 to 40 year cycle as part of weapon lifetime extension activities.

1.2 Tri-labs Dismantlement Program

Several international treaties have been negotiated between the U.S. and the former Soviet Union which have reduced the size of both nuclear arsenals. As a result of implementing the provisions of those agreements, nuclear weapons hardware, some with lifetimes of 35 to 40 years, was decommissioned from the U.S. stockpile and targeted for dismantlement. The act of "dismantlement" included retrieval of the physics package for storage followed by the destruction of non-nuclear components, including the electronic systems. Realizing the tremendous value of these older electronic systems towards establishing a reliability database, procedures were put into place for the acquisition of

several electronic systems from decommissioned weapons. The objective of that program began by obtaining one or two electronic systems from weapons targeted for dismantlement. Those units were further broken down into their circuits board elements with the follow-up task of examining the condition of the solder joint interconnects. Low magnification examination and cross sectional analyses were performed to document the integrity of the joints. These analyses included both qualitative evaluations of the joint as well as a study of the solder microstructure in search for quantitative metrics that would describe the aging condition of the electronics.

1.3 Dismantled Hardware Acquisition

Limited to the list of available hardware and extent of dismantlement to which the technicians would proceed on a particular warhead, an effort was mounted to identify those systems available from the Pantex (Mason and Hanger) facility. An important criterion for the selection of hardware was that it be *non-explosive*. Although non-radioactive components were also desired, Environmental Safety and Health provisions were put into place in order to accept such hardware. Shown in Table 1 is a list of the weapon systems projected for dismantlement, the fiscal year targeted for dismantlement, the approximate production period, and the particular components proposed for retrieval from the respective systems.

Table 1. Proposed Weapon Components for Dismantlement Evaluation

Weapon	FY of Dismantle	Period of Production	Component(s)
B57	FY93	early 60's	MC1804/311751 Firing Set
			MC1814/311761 Interconn. Box
W70	FY93	late 60's to early 70's	MC2840/211515 Firing Set
			MC2841A/211552 Power Supply
W79	FY94	early 80's	MC3048/211575 Firing Set
W56	FY95	early to mid 60's	MC1793/211236 Firing Set
B61-0	FY95	mid to late 60's	MC1850/311801 Firing Set
			MC1838/311787 Programmer

During the course of the program, the request for MC3048 firing sets from W79 units was withdrawn because of the presence of an explosive device that could not be removed by dismantlement in place at the Pantex facility. Because storage capabilities and dismantlement procedures were not in place at Sandia at the time, the units could not be received and stored at Sandia and hence, were declined.

A request was made for ten units of each of the components. The request stipulated that the ten weapons were to be selected at random rather than be selected from a particular build or serial number group. It was also designated that the weapon serial numbers be provided with the parts so that a full history of each unit could be obtained for later reference.

Shown in Table 2 is a list of those components which have, in fact, been received from dismantlement activities at Pantex. Quantities, classification, hazards, and serial numbers/description are also provided in the listing. Discussions with B57 and W70 weapon technologists that were interim to the initial proposal of components (represented by Table 1 data) and the date of hardware shipment, resulted in some changes to the list of requested hardware; those changes are reflected in Table 2.

Table 2. Hardware Acquired from Dismantlement Program

Weapon	Qty. of Units	Classification/ Radioactivity	Serial Number	Component(s)
B57	6	CRD/Radio.	BBN1911	MC1380/311188-00
			BBN2109	
			BBN1463	
			BBN1330	
			BBN2303	
			BBN2315	
	4	CRD/Radio.	BBN1399	MC1938/311910-00
			BBN1503	
			BBN1583	
			BBN1975	
	10	UNC/None	26705	MC1814/311761-01
			50462	
			83079	
			81735	
			65517	
			83035	
			51470	
			79909	
			30912	
			22020	
W70-1	10	UNC/None	526676	MC2839/211514-02
			487553	
			863997	
			661860	
			316030	
			469565	
			971521	
			706268	
			199602	
			219214	
	8	CRD/None	1395	MC2841A/211552-00
			1444	
			1451	
			BBN1453	
			1404	
			1450	
			BBN1470	
			1465	
	2	CRD/None	2431	MC2841A/211552-01
			2000	

In the case of the B57 components, a quantity of ten MC1814 Interconnection Box units were acquired as planned upon at the project outset. On the other hand, the MC1804 Firing Set, which came off of the Mod.-2 version, had had its dismantlement schedule slipped to FY94 (as projected at that time). Therefore, that component was substituted with a quantity of six, MC1380 (Mod.-0 and Mod.-1) Firing Sets and a quantity of four MC1938 (Mod.-1) Firing Sets. The MC1380 and MC1938 units were classified CRD. The explosive elements were removed; however, the units were *radioactive.* The source of the radioactivity was Ni^{63} (β-emitter). Radiological analysis was performed by qualified personnel and determined that the level of radioactivity was not a hazard under conventional handling and storage practices.

The requested components from the W70 warhead were also changed from the initial request. These included a quantity of ten MC2839 Power Supplies (new addition) and a quantity of ten MC2841A Power Supplies. The MC2839 units were unclassified; the MC2841A units were classified CRD; neither was radioactive. In the latter case, two mods. of the units were delivered; a quantity of eight MC2841A/211552-00 and a quantity of two MC2841A/211552-01 assemblies. In all cases, the units were made non-explosive prior to receipt. The MC2840 firing sets were not available from the Pantex facility at the time of the study and hence, were dropped from consideration.

Components from the W56 were to have been replaced with W48 components (production: 10/63) or W33 units (production: 1/57) due to changes in the dismantlement schedule and weapon availability. The Dismantlement Program was ended prior to FY95. Therefore, units from the W79, W56 (W48 or W33) , and B61-0 systems were not provided to Sandia for analysis at the time of hardware procurement.

1.4 The Sn-Pb Solder Joint

The solder interconnect analysis begins by recognizing the important features of solder joints fabricated with Sn-Pb solder. The equilibrium phase diagram of the Sn-Pb binary system is shown in Figure 1a[1]. At a eutectic composition of 61.8Sn-38.2Pb, the liquidus and solidus temperatures are identical, having a value of 183°C. Some resources consider the 63Sn-37Pb composition as the eutectic value, and it is often quoted as such. Between the two compositions that are said to represent the eutectic point, the differences in microstructure, physical, and mechanical properties are insignificant. Therefore, the typically-quoted eutectic composition of 63Sn-37Pb will be utilized in this text, where necessary.

The microstructure of the solder is shown in Figure 1b[2]. The phase diagram shows the two equilibrium terminus phases that are present in Figure 1b (at 25°C). The lighter matrix is the Sn-rich phase which is effectively pure Sn due to the insolubility of Pb in Sn at room temperature. The dark particles are the Pb-rich phase. Tin particles are observed as the lighter phase within the dark, Pb-rich phase particles. Tin has an equilibrium solubility of approximately 1 wt.% in Pb at room temperature. However, that solubility increases significantly at higher temperatures. Fast cooling rates from the solidification temperature for Sn-Pb solder joints can cause a non-equilibrium condition to exist in which the Pb-rich phase becomes supersaturated with Sn upon the joint reaching room temperature. However, because of the relatively low melting point of

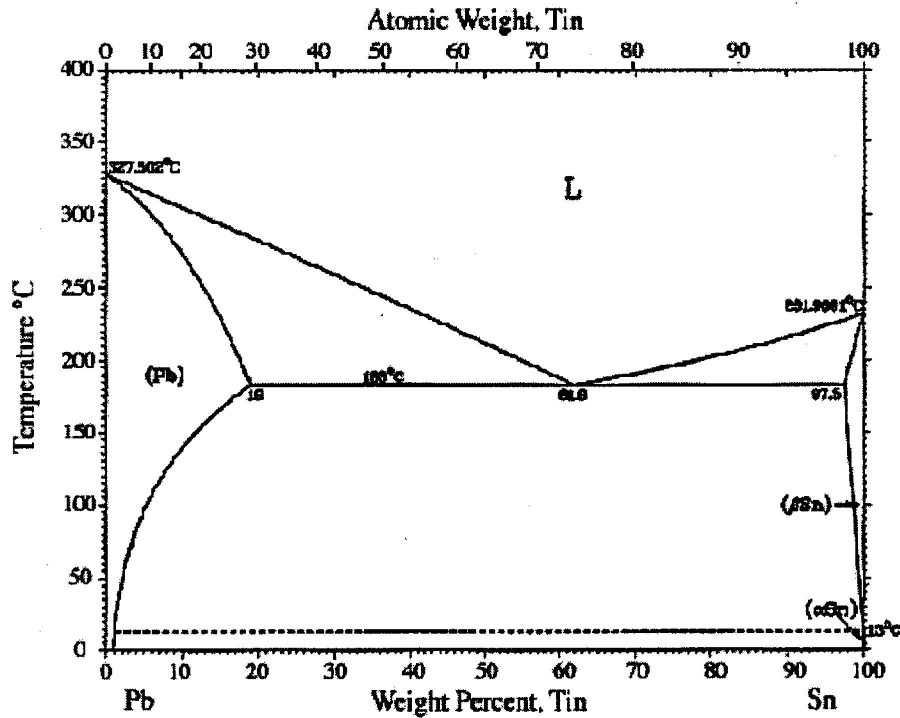

From [Metals].

Figure 1a. Equilibrium phase diagram of the Sn-Pb binary alloy.

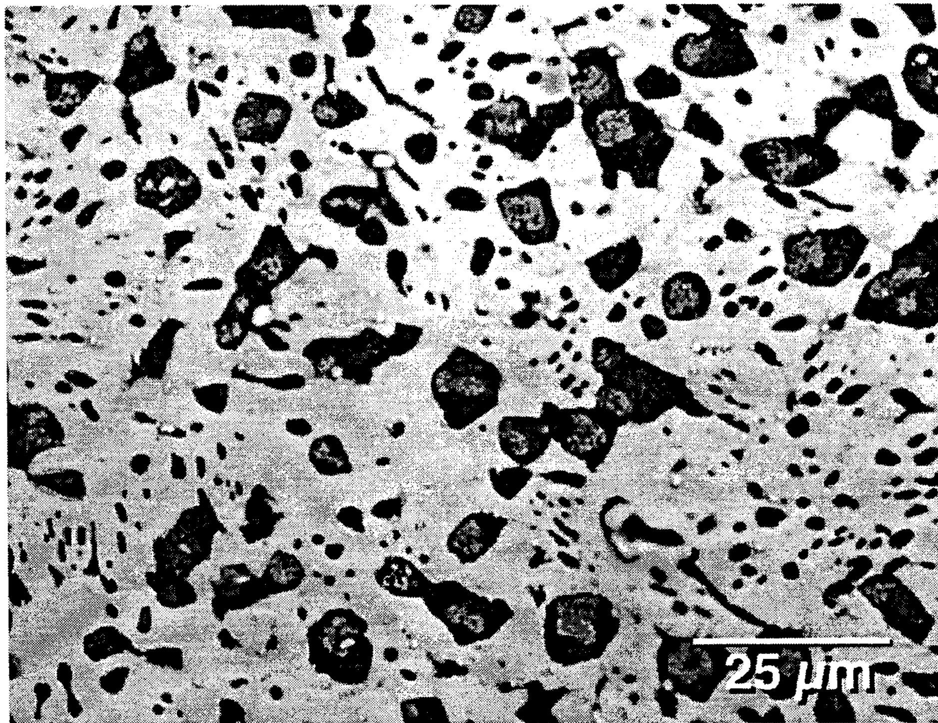

Figure 1b. Microstructure of a ^{63}Sn-^{37}Pb solder joint. The light areas are the Sn-rich phase and the dark areas are Pb-rich phase. The light areas within the Pb-rich phase are regions of dissolved Sn which had since the time of manufacture, precipitated out as per the equilibrium state dictated in the phase diagram.

solder with respect to ambient temperature conditions (and as represented by the *homologous temperature*, T_h, given by $T_{environ.}/T_{liquidus}$), room temperature provides adequate thermal activation for diffusion processes to reduce the non-equilibrium microstructure to the equilibrium configuration over time.

The solder joints on electronic printed circuit board assemblies at the time of manufacture for the systems noted above, used the through-hole configuration. An optical micrograph of a present day *plated* through-hole is shown in Figure 2a. A distinctive difference between the solder joint shown in Figure 2a (today) and the through-hole assembly technology used in a number of early weapons was the absence of the electroplated Cu conductor on the hole walls. That Cu layer allowed signal transmission between the two surfaces of the circuit board. In its place, Cu sleeves or *eyelets* were inserted into the hole as a means of providing that electrical continuity. This latter configuration is shown schematically in Figure 2b.

Whether present-day plated through-hole geometry (Figure 2a) or the earlier eyelet configuration (Figure 2b), the joint is completed by solder having wetted to the wire lead as well as to the surfaces of circuit board Cu features. Those latter features are the hole wall (or "barrel") and the pads or, "lands" around the top and bottom of each hole. The metallurgical bond between the solder and the Cu results from the development of a third material between them. That material, which forms as a layer at the solder/Cu interface, is an intermetallic (or covalent) compound comprised of Cu and Sn. The intermetallic compound layer may be comprised of one or more sub-layer stoichiometries. In the case of the Cu/Sn binary system, those sub-layer compositions are Cu_6Sn_5 and Cu_3Sn[3]. The former composition is always formed; the presence and, like the Cu_6Sn_5 sub-layer, the thickness of the Cu_3Sn stoichiometry are dependent upon the thermal environment (time and temperature history) to which the joints have been exposed[3].

As remarked upon earlier, the physical metallurgy of 63Sn-37Pb solder joints evolve with time. The mean size of the Pb-rich phase increases due to thermally activated coarsening of the particle colonies by solid state diffusion processes. In addition, the size distribution of the Pb-rich colonies would be expected to become much tighter as material from smaller particles migrate to the larger ones as part of the coarsening process. Coincidental with evolution of the solder microstructure are the changes to the alloy mechanical properties. Typically, a decrease in the strength values of the solder is observed[4]. However, the magnitude of this strength loss is generally not of sufficient severity to jeopardize the functionality of most electronic solder joints. The solder microstructure provides an important metric with which to document solder joint aging.

The intermetallic compound layer which forms at the Cu/solder interface will also undergo changes arising from thermally activated, solid state diffusion processes. Growth of the layer thickness as well as evolution of the layer stoichiometry have been documented for a number of solder alloys[5,6,7]. The extent of growth of the intermetallic compound layer at the Cu/solder interface has several repercussions with respect to the integrity, and ultimately, the functionality of the joint. First of all, growth of the intermetallic compound layer requires the consumption of both Cu from the

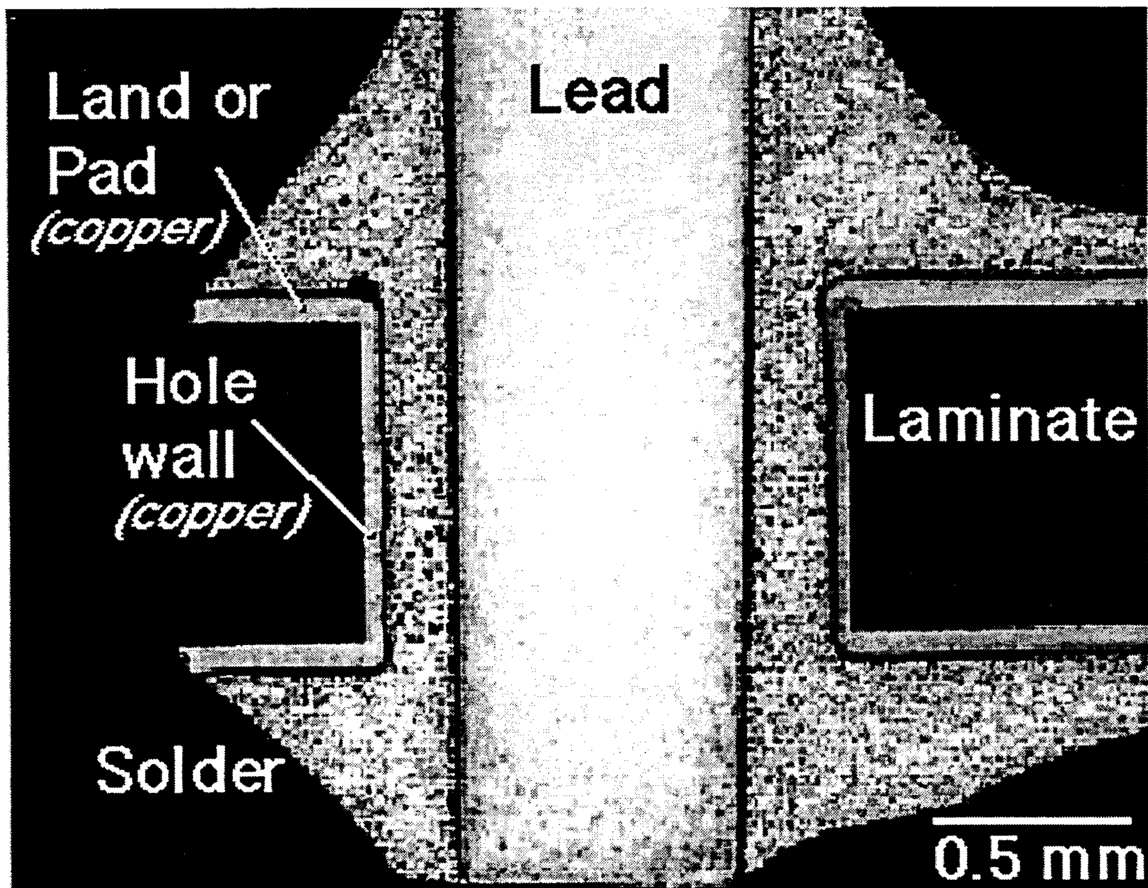

Figure 2a. Plated through-hole solder joint used in present-day printed circuit board technology.

conductor feature and Sn from the 63Sn-37Pb alloy in order to form the interface stoichiometry. In the case of very thin Cu layers or Cu thin films, intermetallic compound layer growth can fully consume the Cu substrate, thus jeopardizing the connectivity of the joint structure. Turning attention to the Sn-Pb solder coating, the loss of solder to intermetallic compound layer formation can result in the poor solderability of such features in follow-up repair and rework procedures.

The second concern of excessive intermetallic compound layer growth is the mechanical integrity of the solder joint. The intermetallic compound layer, being a covalently bonded solid, has very limited ductility. As a brittle material located at the interface between two other dissimilar materials, the mechanical strength of the solder joint can be sensitive to intermetallic compound layer development. The potential for compromise of the solder joint integrity due to I intermetallic compound layer growth is greatest when loads are applied at high rates (impact loads) as opposed to the more benign strain rates that are observed in thermal fatigue environments. Therefore, it is necessary to determine the extent of intermetallic compound layer growth in solder joints over long stockpile storage lifetimes, particularly for weapon systems that are designed for use in high-g service environments.

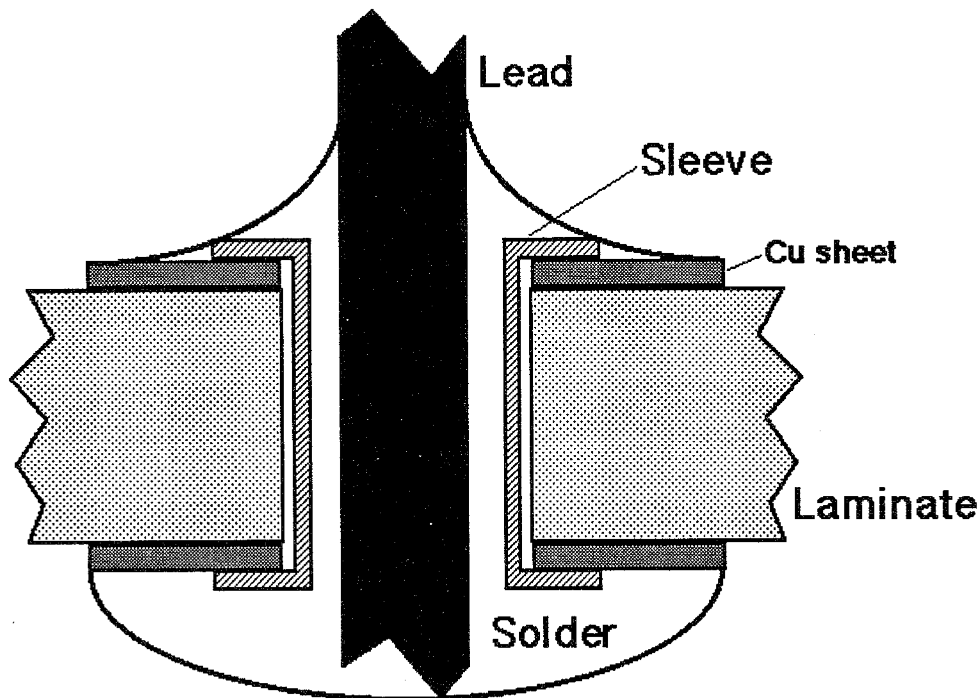

Figure 2b. Schematic diagram of the sleeve-fitted through-hole solder joint used in printed circuit boards of weapons evaluated in this study (c. late 1950s to middle 1960s).

Finally, it would be advantageous to be able to perform a relative comparison of solder joint microstructure (i.e., intermetallic compound layer thickness and Pb-rich phase size) from aged joints and those from the time of manufacture. However, the latter information had not been suitably documented and hence, is not presently available. The reader must be cognizant of the fact that circuit board materials and soldering techniques have changed since the time that a number of the production units in Table 1 were assembled. Therefore, the use of present day solder joints as a representation of as-assembled (baseline) specimens for units with nearly 40 years of age, must be accepted with some trepidation.

1.5 Objectives

Two primary objectives drove this study. The first goal was to make a general survey of solder joints from fielded weapon electronics in order to identify gross failures or defects that would jeopardize the performance of similar joints in those and other systems. This qualitative assessment would also allow for a comparison between present day technology or best-practices and assembly procedures used at the time of hardware fabrication. The assessment would look to such issues as overall solder joint design, solder wetting, solder quantity at the fillets, and residue formation as could be determined by visual inspection of the circuit board sample as well as through metallographic cross sections.

The second goal of the study considered the development of protocols with which to quantitatively assess the microstructural characteristics of the solder joints. These techniques would be used to document the variability of the solder joint microstructures, not only within a particular joint, but also, the microstructures between joints on the same circuit board, joints on different circuit boards of the same component, and so on to include the comparison of solder microstructures between entirely different weapon systems (and associated build dates). Those microstructures would include information on both the manufacturing process used to make the joint and the storage conditions to which it was exposed while in the stockpile.

The quantitative properties that were assessed were *(1) the intermetallic compound layer thickness* that developed between the solder and the Cu features of the joint and *(2) the Pb-rich phase size distribution* in the solder comprising the joint. Intermetallic compound layer thickness and Pb-rich phase particle size provide quantitative metrics describing the aging of solder joints under thermally activated environments. The intermetallic compound layer thickens with time; the rate of growth increases with environmental temperature. Likewise, the Pb-rich phase particles will coarsen with time, with the rate of coarsening also being greater at higher temperatures. In addition, the statistical distribution of particle sizes is expected to narrow as the mean size increases with aging. Although Pb-rich phase particle coarsening does not pose an immediate concern for the integrity of the solder joint, it can serve as a precursor to a loss in solder joint fatigue resistance, particularly under thermal cycling environments.

Once a suitable baseline is in place, then the temperature/time history of the solder joint, or an equivalent description, can be established.

In the following section, the experimental procedures, data results, and discussion will be presented for each of two components: (1) the MC2839 Power Supply from the W70, Mod.-1 weapon and (2) the MC1814 Junction Box from the B57 weapon. Both components served weapon function tasks.

2.0 Experimental Procedures and Data Analysis

2.1 MC2839 Power Supply

2.1.1 Procedures for the Extrication of Targeted Parts

Prior to commencing analysis of the MC2839, the drawing package belonging to this component was reviewed for sub-assemblies that were, or contained, printed circuit boards. Two such sub-assemblies were identified: (1) 234010-00 (agency design number), "Printed Wiring Board" with "Printed Wiring Assembly" drawing AY234011-000 and (2) 231248-00, "Terminal Board" with "Terminal Board Assembly" drawing AY231249-001. The 234010-00 circuit board was the preferred part because of the ease of its retrieval from the dismantled power supply as well as having a large number of solder joints available for examination.

Shown in Figure 3 is an MC2839 Power Supply unit. Figure 3a shows a side view while Figure 3b shows the top view looking into the housing following removal of the potting material by chemical dissolution (Appendix A). The location of the 234010 sub-assembly inside the depotted housing is shown by the two views in Figure 4. Wire leads were clipped in order to extricate the circuit board from the assembly. The top and bottom views of the 234010-00 printed circuit board sub-assembly are shown in Figure 5. The circuit board was double sided with plated-through holes, made of glass fabric impregnated with epoxy resin (drawing 2141004, "Plastic Sheet, Laminated, Epoxy Glass Cloth Base"). The laminate was 0.813 mm (0.032 in.) thick. The Cu features (including conductor lines, lands, and barrel plating on the hole walls) were built up from a "1 oz." clad base on both surfaces, to a *final* metal thickness between 0.51 mm and 0.76 mm (0.002 in. and 0.003 in.). There were ten clipped leads on the top side that served as connection wires between the circuit board and several components within the power supply. The assembly had seven resistors with either solid Cu or Cu-plated alloy leads. Connector wires were stranded Cu or solid Cu. It is evident that the housing material on three of the resistors was attacked during the depotting process. However, the circuit board laminate was not noticeably damaged by the chemicals. Only a thin film of the potting material remained on the circuit board surfaces after the depotting procedure.

Seven MC2839 power supplies had the 234010-00 electronic circuit board sub-assembly extracted by the procedure described in Appendix A, which involved the removal of potting material from the entire inside of the MC2839 housing by means of chemical dissolution. The serial numbers of those units were: 526676, 487553, 863997, 661860, 316030, 469565, and 971521. The remaining MC2839 units (706268, 199602, and 219214) were used in trials that would replace the chemical dissolution techniques for acquiring the circuit board sub-assembly with a relatively new procedure: *(abrasive) water jet machining.*

Use of water jet machining or cutting was identified as an alternative method to the large-scale chemical depotting of the component interior. Not only was the water jet process quicker than the time required for chemical dissolution of the potting, but the specimen did not have to be exposed either to the elevated temperatures required to expedite the depotting process or to the chemicals themselves, which were damaging to

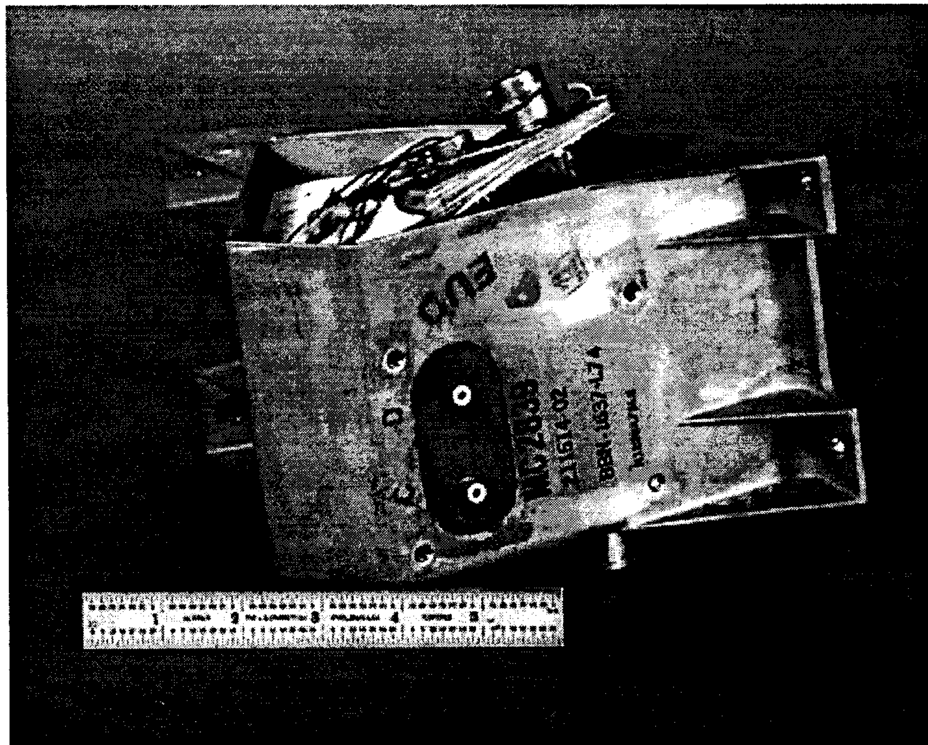

(a)

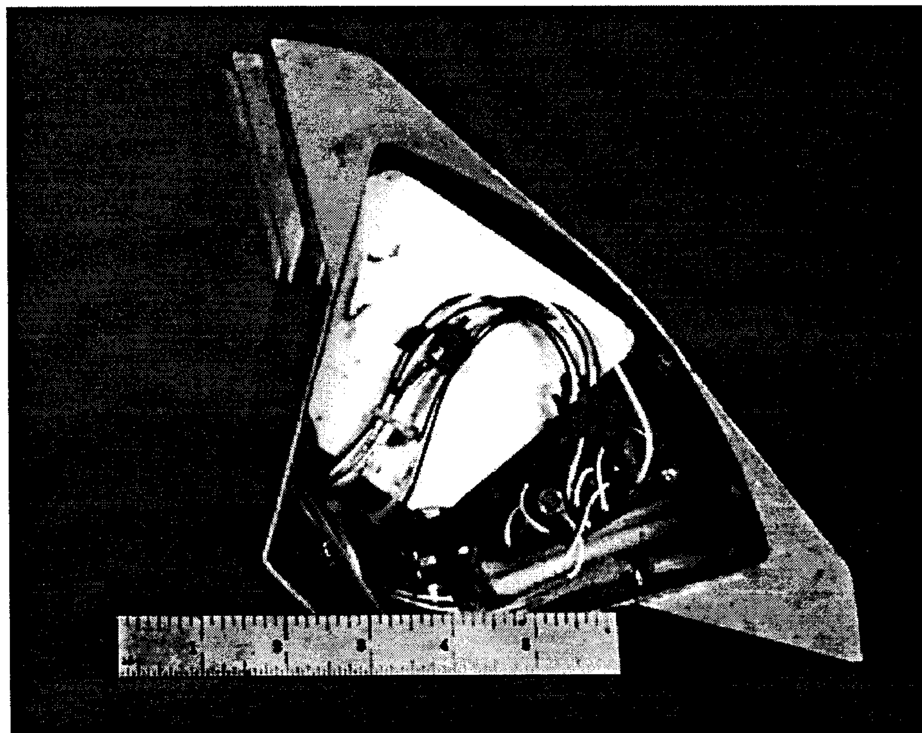

(b)

Figure 3. MC2839 Power Supply from the W70-1 weapon: (a) side view and (b) top view made clear by removal the potting foam.

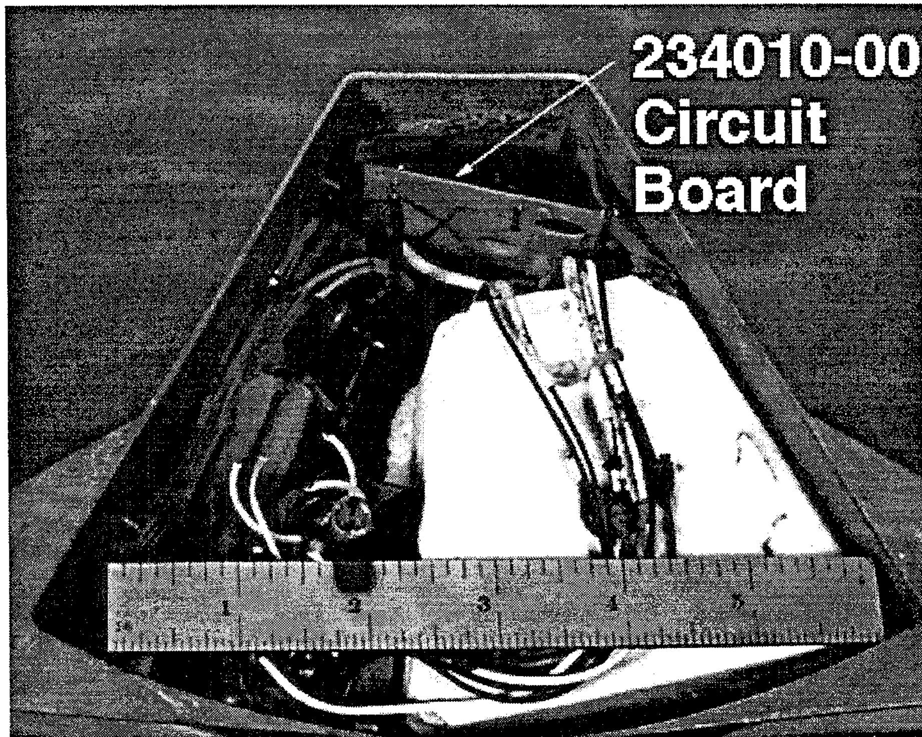

(a)

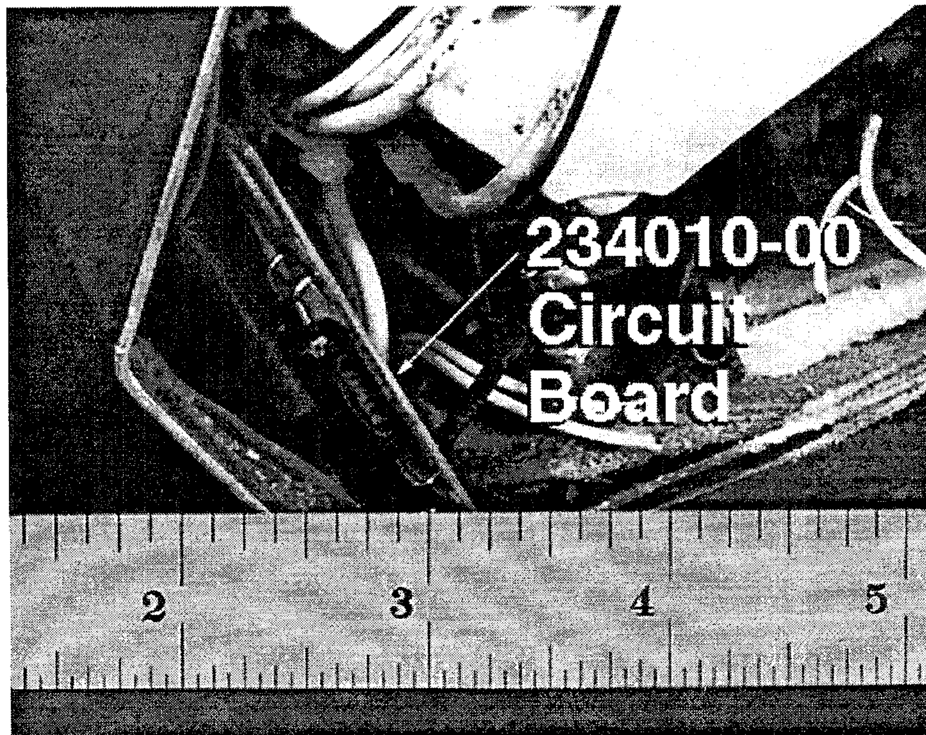

(b)

Figure 4. Two views (a) and (b) of the position of the 234010-00 circuit board within the MC2839 housing after depotting.

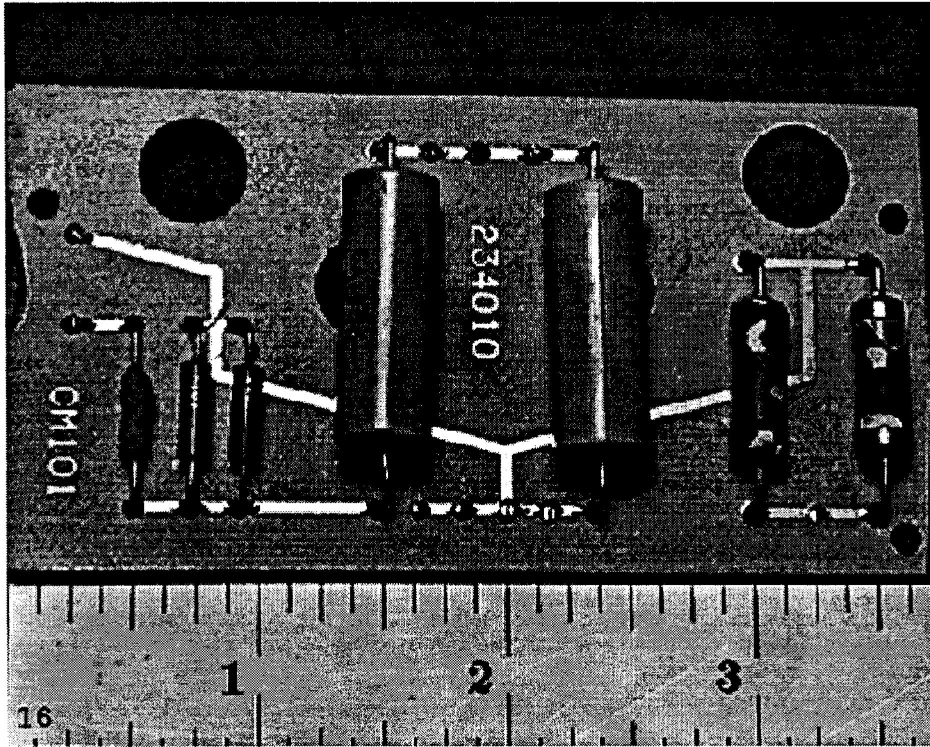

(a)

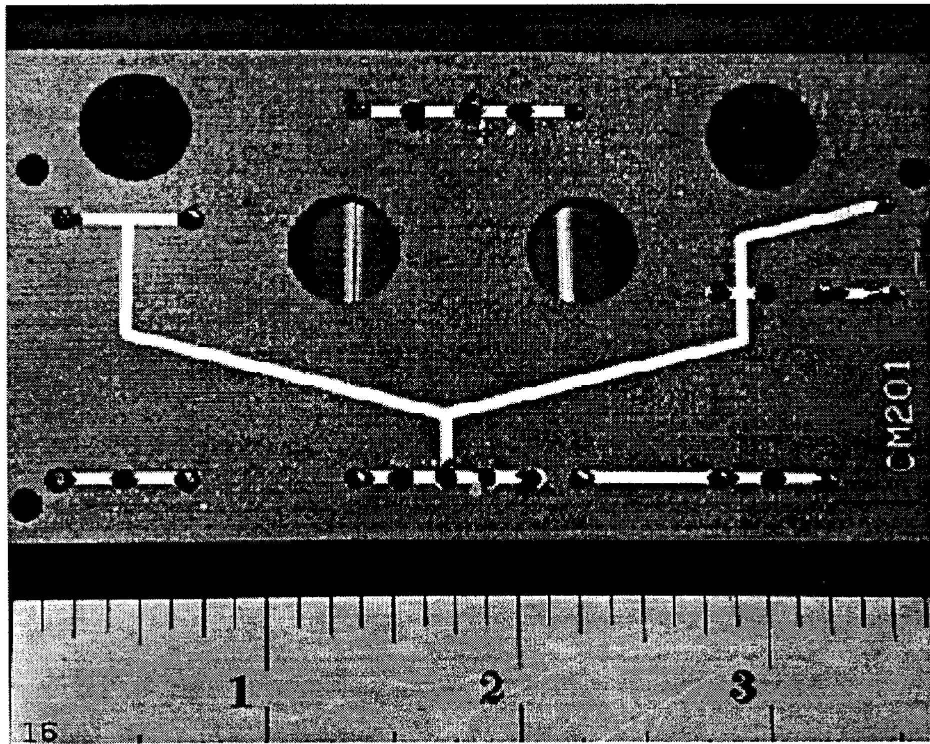

(b)

Figure 5. (a) Top view (with components) and (b) bottom view (without components) of the 234010 printed wiring board sub-assembly.

some of the plastic materials and other components. Numerous sources of information are available that detail the technique and the equipment used in water jet cutting[8,9,10]. A summary of the process is given here. Shown in Figure 6 is a schematic diagram of the water jet apparatus. In this process, a high velocity water stream is generated by a multistage pressure booster system. The water jet is combined with abrasive particles to form a "saw" which cuts through the material. Water velocity (which is controlled by the pressure) as well as the particle size and quantity (or "loading") determine the cutting efficiency of the jet. In addition, the type of material(s) being cut, as well as their dimensions also affect the cutting process. For example, as the water jet progresses through the material, the stream begins to widen or *disperse*, thereby increasing the amount of material that is removed by the water jet cut, its so-called *kerf*. It was important to consider the kerf of the cutting path initially, so that the cuts were made without inadvertently damaging the targeted part. The kerf was also dependent upon the travel speed of the nozzle. The slower the travel speed, the wider was the kerf generated in the part.

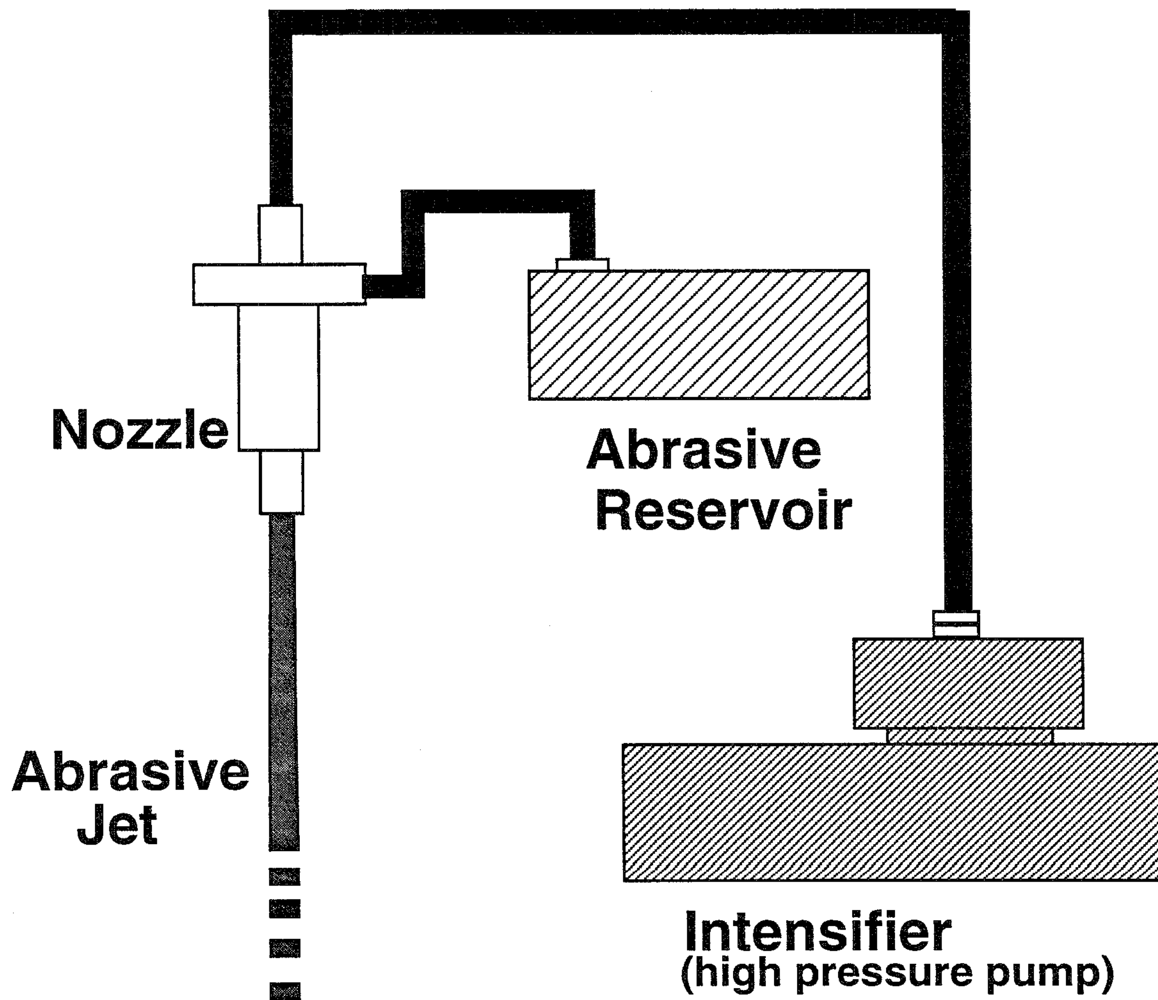

Figure 6. Schematic diagram of the abrasive water jet apparatus.

The water jet process required that the 234010-00 circuit board position be located within the MC2839 assembly. Therefore, first, X-ray photographs were first taken of the unit. The circuit board position and orientation were documented. Then, the unit was set up in the water jet equipment. Shown in Figure 7 is an MC2839 unit that has been placed into the apparatus. The water jet nozzle can be seen at the top of the photograph. The operating parameters were: (1) 50 ksi water pressure, (2) 0.012 in. diameter sapphire orifice, (3) 0.045 in. diameter silicon carbide nozzle, (4) 80 mesh garnet abrasive, (5) 1.5 lb/min abrasive flow rate, and (6) a nozzle-to-part standoff distance of approximately 0.25 in. A single pass at a rate of 10-20 in./min was determined adequate to cut through the part. Figure 8 is a photograph of the cutting process in action. A photograph of the two sections formed from the bisected unit is shown in Figure 9, which also shows that the cut is somewhat uneven. This variability is caused by the composite nature of the assembly; that is, the water jet must pass through several different types of materials (aluminum housing, foam, copper wires, etc.), each material having a different cutting rate. Also, the kerf of the stream increased with depth into the unit (that is, in the direction of the water flow that is downwards in the Figure 9 photograph).

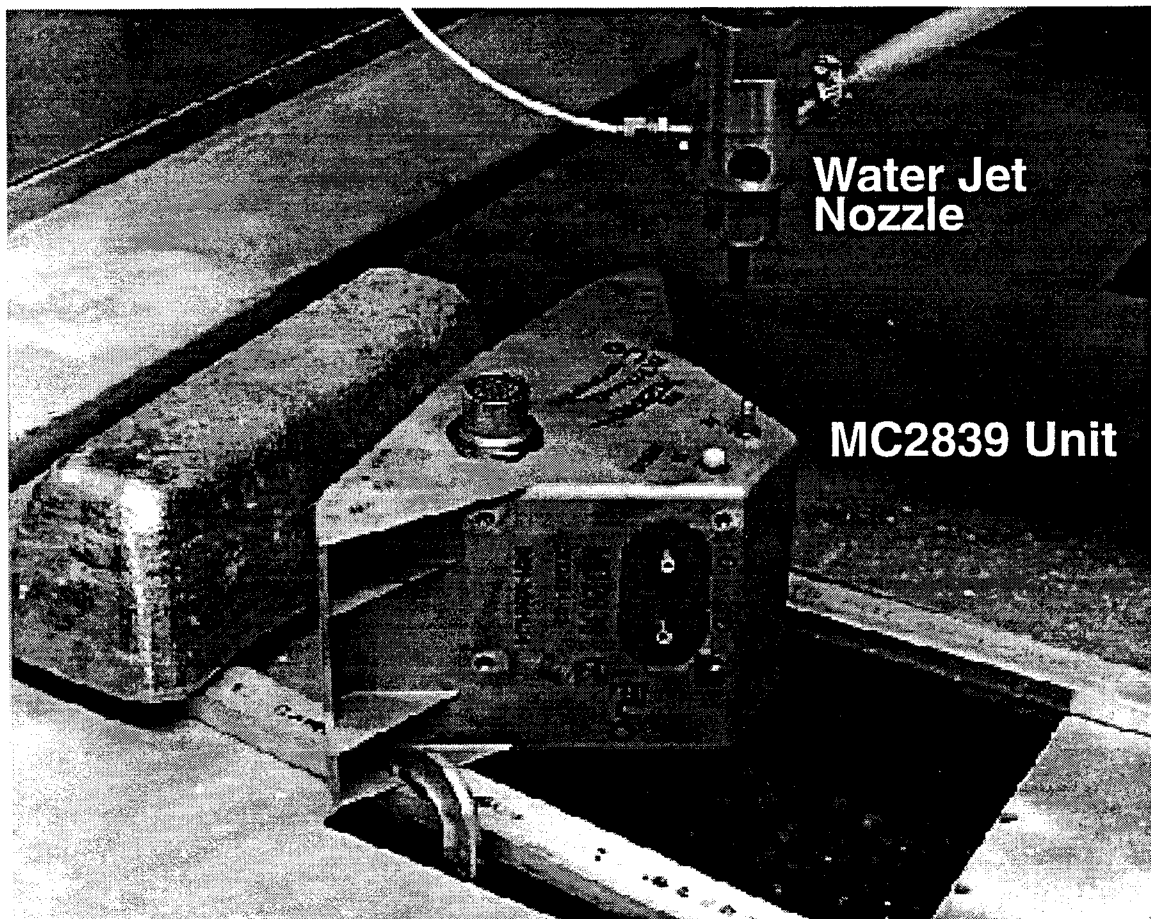

Figure 7. Set up of MC2839 unit in the abrasive water jet apparatus. The water jet nozzle can be seen at the top of the photograph.

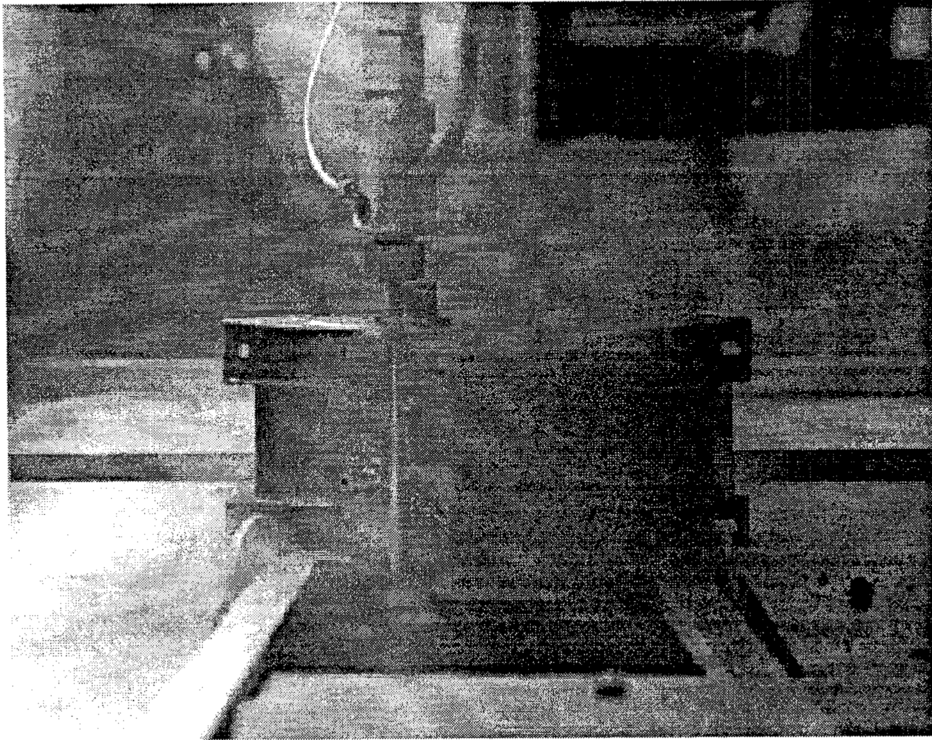

Figure 8. Abrasive water jet cutting process in action.

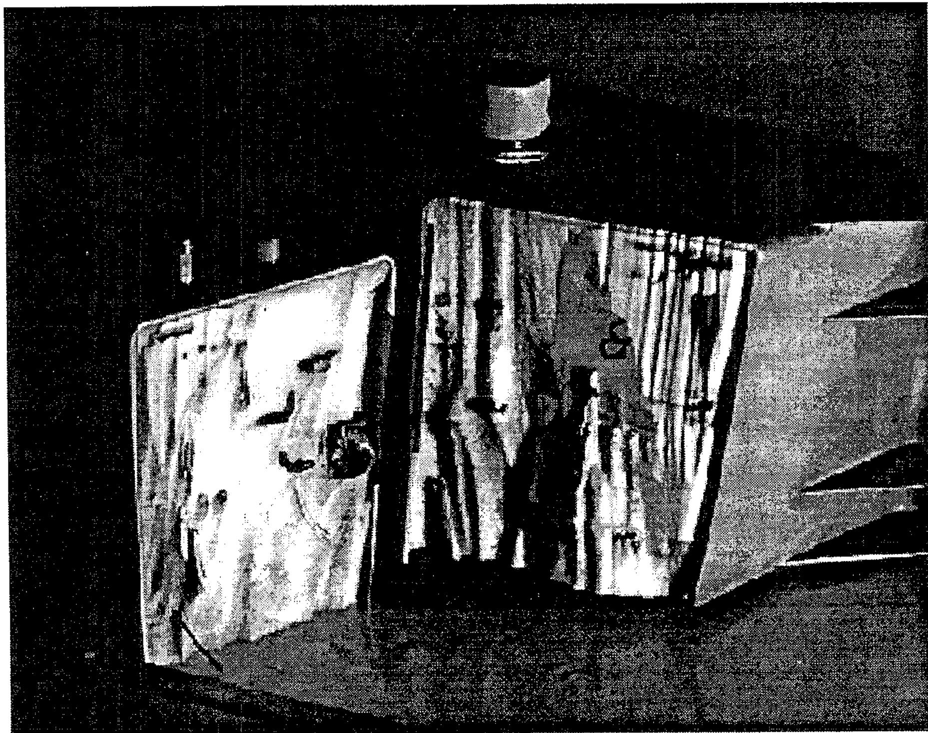

Figure 9. A photograph of the bisected unit, showing the cut faces.

The cut-out segments of the MC2839 unit containing the circuit board were of a size that could be further sectioned in the metallography laboratory, down to the solder joints of interest. However, because the 234010-00 circuit board was resistant to attack by the depotting chemicals, coupled with the fact that the soak time in the solvent would be significantly reduced by the smaller size of the segment, the chemical dissolution process described in Appendix A was used once again, this time to supplement subsequent cutting of the circuit board in order to the solder joint level. After chemical depotting, but prior to any further cutting of the circuit boards, the solder joints from each unit were visually inspected. The objective of this inspection was the detection and documentation of flaws and workmanship defects. Catastrophic damage to the laminate and/or passive devices was also documented; however, cosmetic disparities were largely ignored due to their prevalence arising from the depotting chemicals.

The solder joints selected for cross sectioning are shown in Figure 10. The joints were labeled A, B, ..., L and required four cuts through the circuit board. The sections were selected to sample the joints from each of the different passive components as well as to include views of the solder-coated conductor lines. The assessment performed on the solder joints cross sections performed in two parts: a qualitative evaluation and a quantitative analysis. The qualitative evaluation examined (1) void formation, (2) bulk circuit board laminate damage, and (3) the integrity of the interface between the copper conductor feature and the laminate, as well as any other noteworthy features. All joint cross sections were examined for qualitative evaluation.

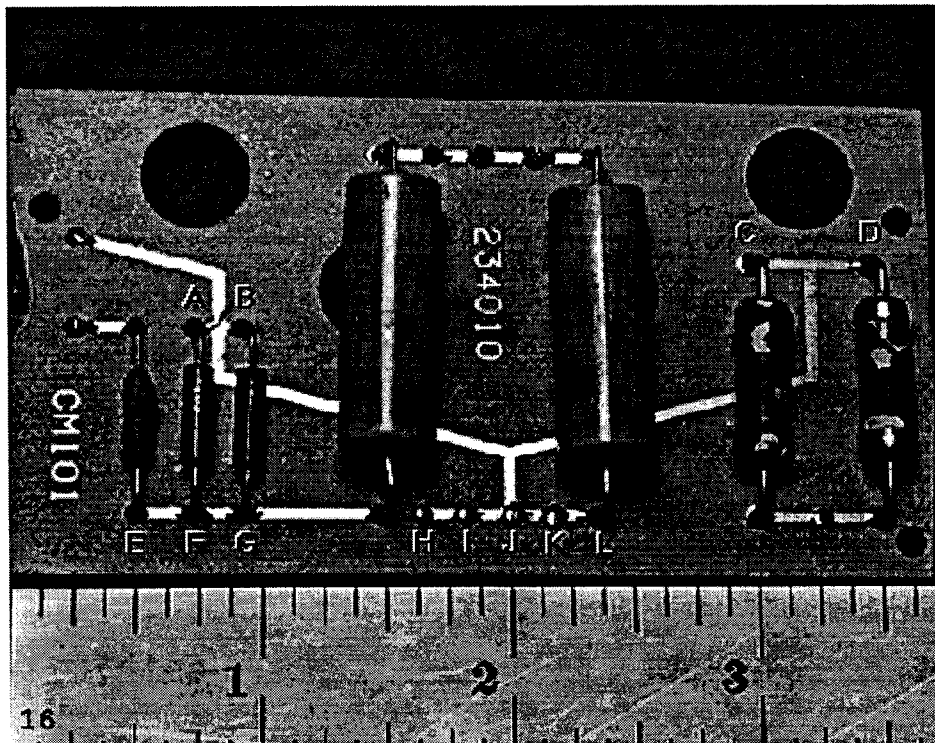

Figure 10. Photograph of 234010 circuit board showing the solder joints selected for cross sectioning and subsequent microstructural analysis.

The quantitative evaluation targeted: (1) intermetallic compound layer thickness at the interface between the Cu features (device leads or circuit board conductor) and (2) the Pb-rich phase particle size distribution. All quantitative analyses were performed on high magnification photomicrographs of selected regions of the solder joints. Shown in Figure 11 is a reference diagram of the through-hole joint and the three areas, I, II, and III selected for examination. Intermetallic compound layer thickness measurements were performed at the Cu barrel wall/solder interface (I) and at the Cu land/solder interface (III). These two locations were selected in order to determine whether a variability of layer thickness existed between them, and the extent of that variability. A single photomicrograph of nominal 1000x magnification was taken at each location. A National Institute of Standards and Technology calibration standard was used to establish the precise magnification of the photomicrographs. The intermetallic compound layer thickness was determined at ten equally spaced locations along the interface; the layer thickness was represented as the mean and ± one standard deviation of the ten data points. The measurement process, data storage, and manipulation were all performed with computer software packages (Appendix B).

The Pb-rich phase size distributions were determined by the following procedure. For each solder joint, a 500x micrograph was taken at position II in one of the four fillet quadrants provided by the cross section. The solder fillets offered the largest area from which to sample the microstructure. The image was then processed via several computer software packages (Appendix C). The particle size output was comprised of a series of histograms showing the frequency distribution of particle sizes between a range of nominal values.

The examination logistics for solder joints A through L on the 234010-00 sub-assembly are described below:

- **Joints A and B:** Low magnification photomicrographs of each joint only; no quantitative analysis. Leads A and B were solid Cu wires.
- **Joints C and D:** Low magnification photomicrographs of each joint for qualitative analysis; high magnification (500x and 1000x) photomicrographs at locations I, II, and III in each of the joints for quantitative analysis. Leads C and D were Cu-plated alloy.

- **Joints E, F, and G:** Low magnification photomicrographs of each joint for qualitative analysis; 500x and 1000x at locations I, II, and III in each of the joints for quantitative analysis. Lead E was Cu-plated alloy and leads F and G were solid Cu wire.

- **Joints H, I, J, K, and L:** Low magnification photomicrographs of each joint for qualitative analysis; 500x and 1000x at locations I, II, and III of the **L** joint for quantitative analysis. Leads H, I, J, and K were stranded Cu wires; lead L was a solid Cu pin. Intermetallic compound layer measurements were also made at the solder/pin interface of the L joint.

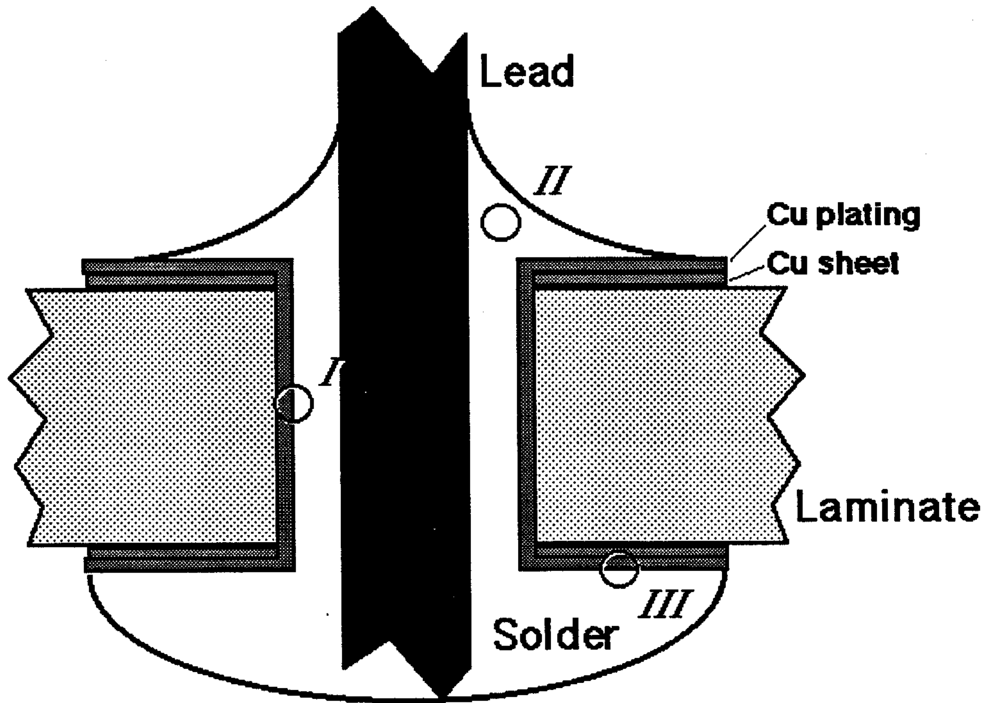

Figure 11. Schematic diagram of a through-hole solder joint showing the locations of the quantitative analyses performed on the MC2839, 234010-00 circuit board solder joints.

2.1.2 Results and Discussion

2.1.2.1 Qualitative Assessment

Visual observations were made of the 234010-00 circuit boards from MC2839 units prior to metallographic cross sectioning. There was no gross damage in the form of cracks, gouges or delamination that was observed on the devices, the device leads, solder fillets, conductor features, or the laminate. Corrosion products were absent from the surfaces of the solder fillets and circuit board. This latter observation must, of course, be taken with some reservation because of the possible removal of such residues by the chemical depotting process. Generally, the solder joints exhibited good workmanship; they were slightly heavy on the solder volume (perhaps reflecting the "more-is-better" approach, given the limited engineering knowledge of electronic soldering at the time). The lead extension from the bottom of the circuit board was clipped after the soldering operation; however, no damage was observed at the solder fillets.

Next, an assessment of the solder joint microstructure was performed on the cross section samples. Bonding of the Cu conductor traces to the top side and bottom side of the laminate was excellent. Isolated discontinuities were noted between the hole wall and the Cu plating; however, there was no evidence that the Cu barrel integrity was compromised. Voids were absent from within the solder joints in the case of the solid wire leads or pins. This point is exemplified in Figure 12, which shows the "B" joint

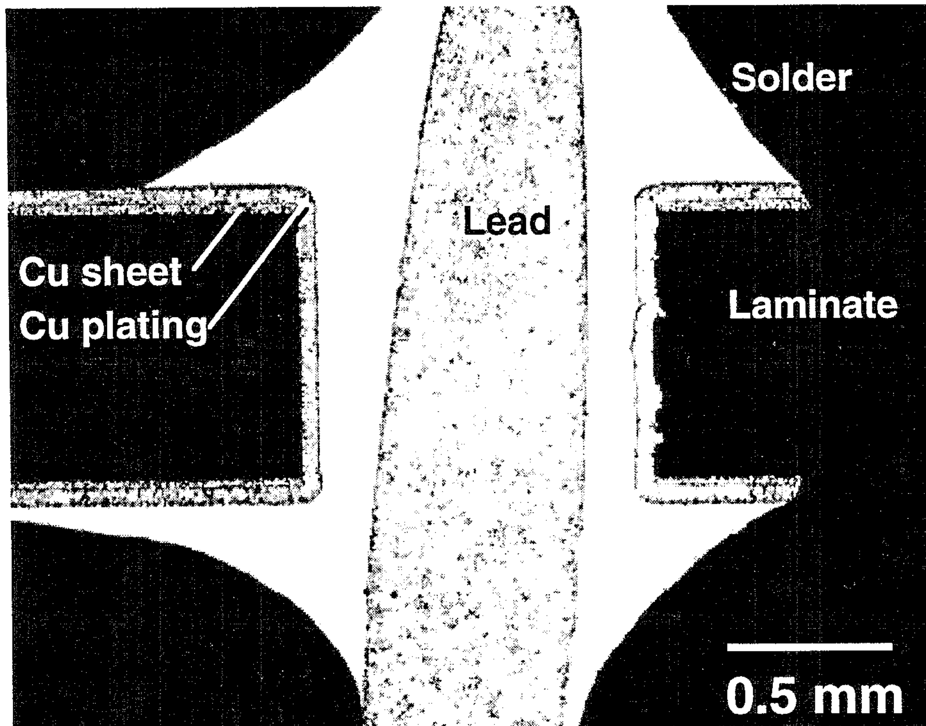

Figure 12. Optical micrograph of the solid lead joint "B" from unit 316030 showing an absence of voids in the solder.

from the board in the unit having serial number 316030. On the other hand, voids were more significant in the stranded wire joints. The micrograph in Figure 13 of the joint "I" from unit 316030 illustrates the presence of voids in both the solder volume between the wire and the hole wall, as well as in the solder that filled between the strands. An increased degree of volatile formation during soldering was expected from the stranded wire due to the greater amount of flux trapped by capillary action between the individual strands. It was also observed that the leads were generally not oriented precisely parallel with the hole axis; rather, the wires were tilted with respect to the axis. This configuration did not appear to cause a consistent defect to the solder joint such as void formation, poor solder fill, or damage to the wall plating.

Finally, it was observed on the 526676 unit that the interface between the "L" lead and the solder exhibited an apparent coarsening of the solder microstructure at the immediate interface. This effect is illustrated by a low magnification optical micrograph in Figure 14a, showing the gap between the lead and the hole wall; a higher magnification micrograph appears in Figure 14b. The region next to the lead shows a coarsened Pb-rich phase. In addition the coarsening of the Pb-rich phase particles, the grain boundaries of the Sn-rich phase are clearly delineated; *grain boundary sliding* is a likely source of the accented boundaries. Closer examination of this region also showed that recrystallization had also taken place in some areas. The coarsening phenomenon was also observed on the H, I, J, and L joints of the 199602 unit as well as several joints on 661860 and 219214 units. The phenomenon was not observed in the other units. Coarsening did not appear to favor any particular joint type.

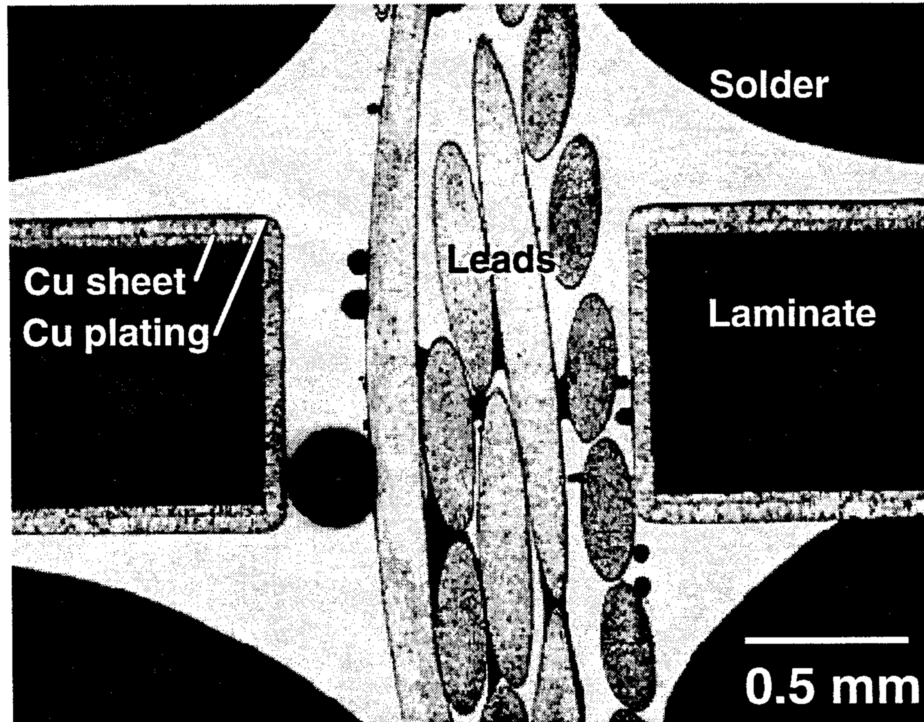

Figure 13. Optical micrograph of the stranded lead joint "I" from unit 316030 showing the presence of voids.

The location of the coarsening zone being adjacent to the lead suggests that a source of the phenomenon is local thermal expansion mismatch between the solder (with a thermal expansion coefficient of 23 ppm/°C[11]) and the Cu (17 ppm/°C). Thermal strains induced into 63Sn-37Pb solder by thermal expansion mismatches have been shown to induce a coarsening of the solder microstructure[12]. However, chemical effects arising from the dissolution of lead material adjacent to the interface may also have had a role in the coarsening process. The coarsening of the solder caused by thermal mismatch strains has been shown to be a prelude to thermal fatigue cracking; it is not certain whether the localized phenomenon shown in Figure 14 would have significantly impacted the mechanical and electrical reliability of the solder joint under further service. There was clearly no indication of voids as a precursor to general cracking, or the presence of cracks, themselves, in the coarsened regions.

2.1.2.2 Quantitative Assessment - Intermetallic Compound Layer Thickness

As noted above, measurements of the intermetallic compound layer thickness were made at locations I and III in Figure 11, the "I" location being the hole (or barrel) wall and the "III" thickness values having been taken from the land/solder interface. A micrograph of the intermetallic compound layer at location III of joint F in unit 469565 is shown in Figure 15. The stoichiometry of the layer was Cu_6Sn_5. There were no unusual features in the physical appearance of the layer. The thickness values, which ranged from 0.54 to 1.28 μm, were comparable to those observed in freshly-made hand solder and machine-made solder joints (infrared reflow or vapor phase reflow techniques). This

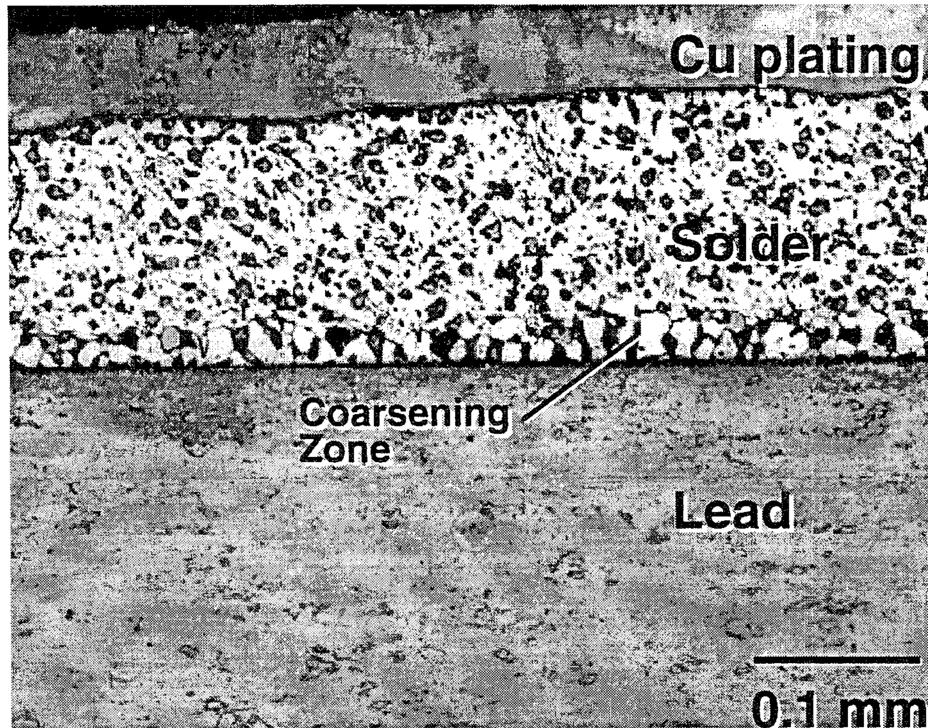

Figure 14a. Low magnification optical micrograph of the "L" joint from unit 526676 showing the gap between the lead and the hole wall, and the coarsening phenomenon in the solder at the lead interface.

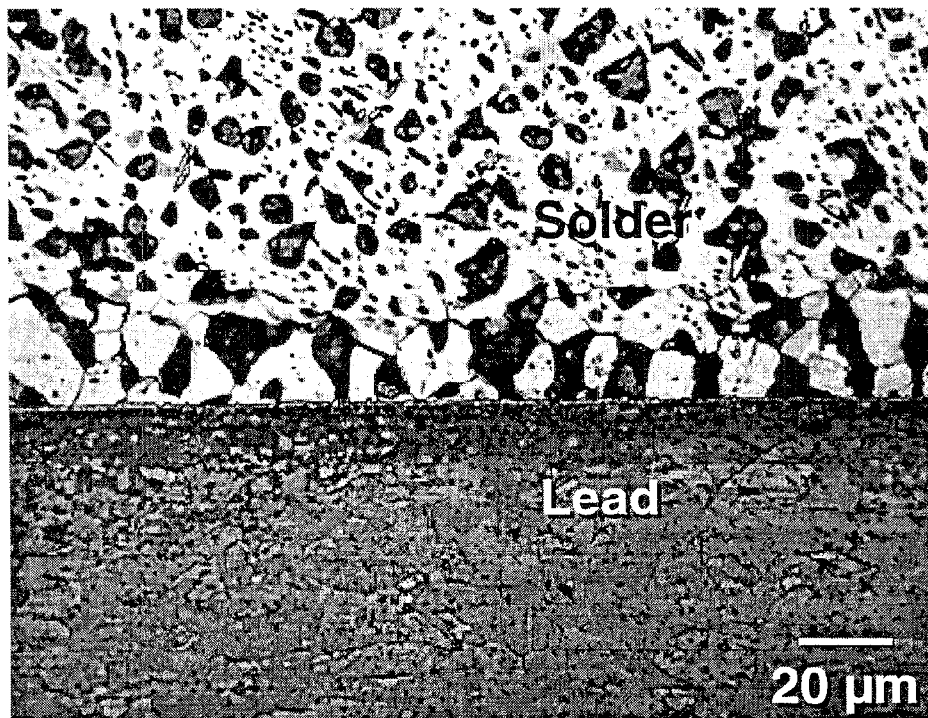

Figure 14b. Higher magnification of the coarsening effect.

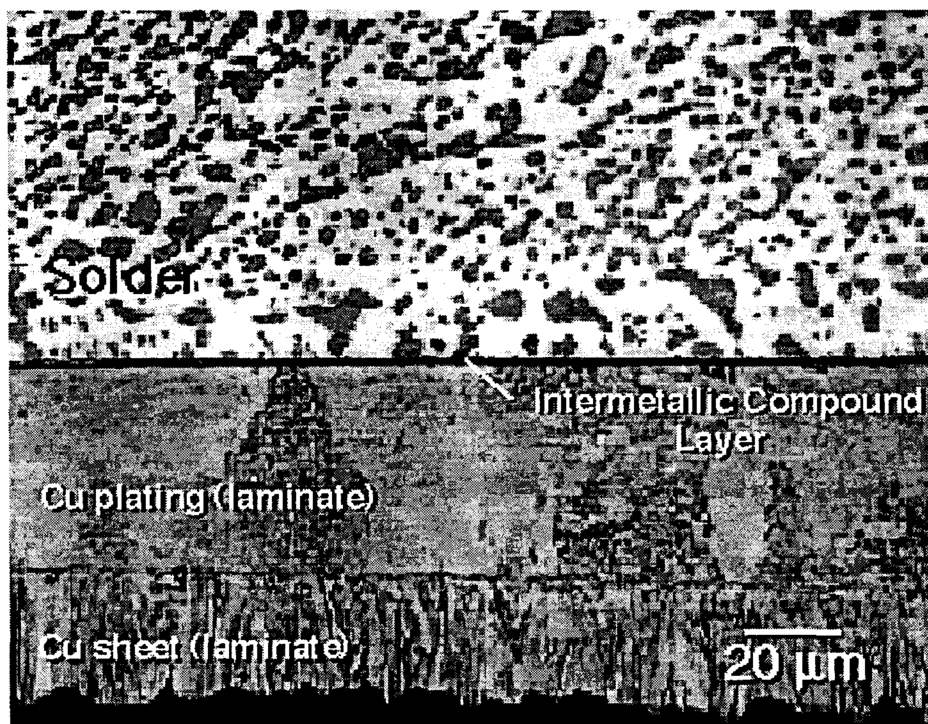

Figure 15. Optical micrograph of location III (land) of joint F from unit 469565 showing the intermetallic compound layer between the solder and the copper substrate.

preliminary analysis indicated that the solder joints did not undergo any unusual assembly anomalies, nor were they exposed to significantly elevated temperature environments. A conclusive statement as to the change in intermetallic compound layer thickness would need to await the baseline data.

Shown in Table 3 is a summary of the intermetallic compound thickness data for the two locations in each of the solder joints from all five of the MC2839 units. These data include: (1) the mean layer thicknesses; (2) the standard deviations; and (3) the 95% confidence interval for the mean for each data set.

A statistical analysis procedure was developed that tested the hypothesis of whether the population means of intermetallic compound layer measurements (as represented by the sample means) taken from the two locations (I and III on the same joint) were equal or unequal. The Student's t-test was used to provide this evaluation. Prior to testing the mean hypothesis between two data sets by the t-test, it was necessary to determine whether the population variances (represented by the sample variances) were equivalent. The F-test of equality of variances was used to make this assessment. Therefore, the equivalence of the intermetallic compound layer thickness between two data sets began with an assessment of the variances between the data sets, using the F-test. The equivalence (or non-equivalence) of the variances determined which of the t-tests would be used to actually test the hypothesis of equivalence of (sample) means between the two data sets.

Table 3. Intermetallic Compound Layer Thickness MC2839 Power Supply Circuit Board

Unit #	Solder Joint/Location	Mean Thickness (μm)	Standard Deviation (μm)	Confidence Interval (95%) (μm)
526676	C/I	0.891	0.364	0.226
	C/III	0.645	0.166	0.103
	D/I	0.911	0.186	0.115
	D/III	0.664	0.138	0.085
	E/I	0.979	0.351	0.218
	E/III	0.961	0.438	0.272
	F/I	1.033	0.253	0.157
	F/III	0.802	0.251	0.155
	G/I	1.279	0.596	0.369
	G/III	0.803	0.171	0.106
219214	C/I	1.502	0.476	0.295
	C/III	1.293	0.370	0.229
	D/I	1.608	0.442	0.274
	D/III	1.188	0.272	0.169
	E/I	1.293	0.288	0.179
	E/III	1.048	0.404	0.250
	F/I	1.013	0.260	0.161
	F/III	0.995	0.288	0.178
	G/I	1.117	0.331	0.205
	G/III	1.066	0.316	0.196
316030	C/I	0.909	0.161	0.100
	C/III	0.645	0.166	0.103
	D/I	0.872	0.233	0.144
	D/III	1.346	0.237	0.147
	E/I	0.732	0.138	0.086
	E/III	0.857	0.293	0.182
	F/I	0.837	0.110	0.068
	F/III	1.118	0.323	0.200
	G/I	1.117	0.331	0.205
	G/III	1.066	0.316	0.196
469565	C/I	0.577	0.381	0.236
	C/III	0.679	0.153	0.095
	D/I	0.596	0.184	0.114
	D/III	0.663	0.199	0.124
	E/I	0.716	0.433	0.268
	E/III	0.558	0.139	0.086
	F/I	0.716	0.154	0.095
	F/III	0.575	0.202	0.125
	G/I	0.644	0.299	0.185
	G/III	0.524	0.165	0.102

Table 3. Intermetallic Compound Layer Thickness MC2839 Power Supply Circuit Board (Continued)

Unit #	Solder Joint/Location	Mean Thickness (μm)	Standard Deviation (μm)	Confidence Interval (95%) (μm)
661860	C/I	1.046	0.320	0.198
	C/III	0.822	0.350	0.217
	D/I	0.750	0.204	0.126
	D/III	0.960	0.222	0.138
	E/I	0.697	0.458	0.284
	E/III	0.977	0.311	0.193
	F/I	0.752	0.312	0.193
	F/III	0.487	0.110	0.068
	G/I	0.751	0.219	0.136
	G/III	0.756	0.246	0.153

As noted, the comparison of intermetallic compound layer thicknesses began by assessing the equivalence of each mean thickness at location I versus the corresponding value at location III on the joint. Shown in Table 4 is a listing of all the I/III solder joint pairs identified by joint letter and by the unit from which they came. It was observed from the pair-wise comparison of joints that the case of equal, mean intermetallic compound thicknesses between locations I and III was observed nearly as many times (11 or 55%) as was the case of unequal intermetallic compound layer thicknesses (9 or 45%). These results suggested that the chances are largely random that the mean intermetallic compound layer thickness within the barrel wall will be the same, or will differ, from that on the bonding pad or land; therefore, no trend was observed for the intermetallic compound layer thickness between the two locations.

The cases of unequal mean thicknesses at the two joint locations in Table 4 were further examined. It was observed that the thickness at the barrel wall (I) always exceeded that at the pad (III). Two likely causes were identified for this trend. The first source was that the intermetallic compound layer that developed on the barrel wall was, in fact, thicker. Such a trend could have developed from the temperature profile of the solder within the hole. If the solder in the hole is the last location to solidify, then the exposure time between the molten solder and the Cu finish would be the longest, resulting in a thickening of the intermetallic compound layer there as opposed to that which developed on the land (III) surface. The second hypothesis suggests that the thicker intermetallic compound layer on the hole wall was an artifact of the metallographic sectioning technique. If the sectional cut was made off of the longitudinal axis of the hole, then the profile at the interface would not be normal to that interface, but rather, would present an angle to it (Fig 16). As a consequence, the measured intermetallic compound layer thickness would appear *larger* than was truly the case, because the section through the layer is tapered to the normal. A further analysis of the two hypotheses, in order to determine conclusively which was responsible for the observed trend, was beyond the resources of this study. *Because artifacts caused by metallographic preparation would least impact the intermetallic compound layer thickness measurements of the pad location (III), data from those measurements were deemed as "representative" of the particular joint.*

Table 4. Intermetallic Compound (IMC) Layer Thickness MC2839 Power Supply Circuit Board Test for Equivalence of Positions I and III

Unit #	Solder Joint	Equality of IMC Thickness Positions I vs. III
526676	C	UNEQUAL
	D	UNEQUAL
	E	equal
	F	UNEQUAL
	G	UNEQUAL
219214	C	qual
	D	UNEQUAL
	E	equal
	F	equal
	G	equal
316030	C	UNEQUAL
	D	UNEQUAL
	E	equal
	F	UNEQUAL
	G	equal
469565	C	equal
	D	equal
	E	equal
	F	UNEQUAL
	G	equal
661860	C	equal
	D	UNEQUAL
	E	equal
	F	UNEQUAL
	G	equal

Next, the intermetallic compound layer thickness data were compared between the five solder joints that were analyzed per circuit board; again, each circuit board represented one of the five units (i.e., #526676, #219214, #316030, #469565, and #661860). This analysis documented the equivalence of the intermetallic compound layer thickness amongst solder joints from the *same* board. Only the layer thickness at the hole pad (location III) was included from each joint. The intermetallic compound layer data, including the mean thickness, ± one standard deviation, and the 95% confidence interval were listed in Table 3. To determine the variability of layer thicknesses amongst solder joints in a given unit, a pair-wise comparison was performed between the solder joints in three of the five units. In performing this comparison, the mean layer thicknesses of each of ten possible solder joint pairs from amongst the five joints per unit, were subjected to Student's t-test to assess the hypothesis that the means were equal or not equal. As in the comparison of I versus III locations, the F-test was initially performed to determine the equivalence of variances between the two data sets in order to select the proper t-test format to be used.

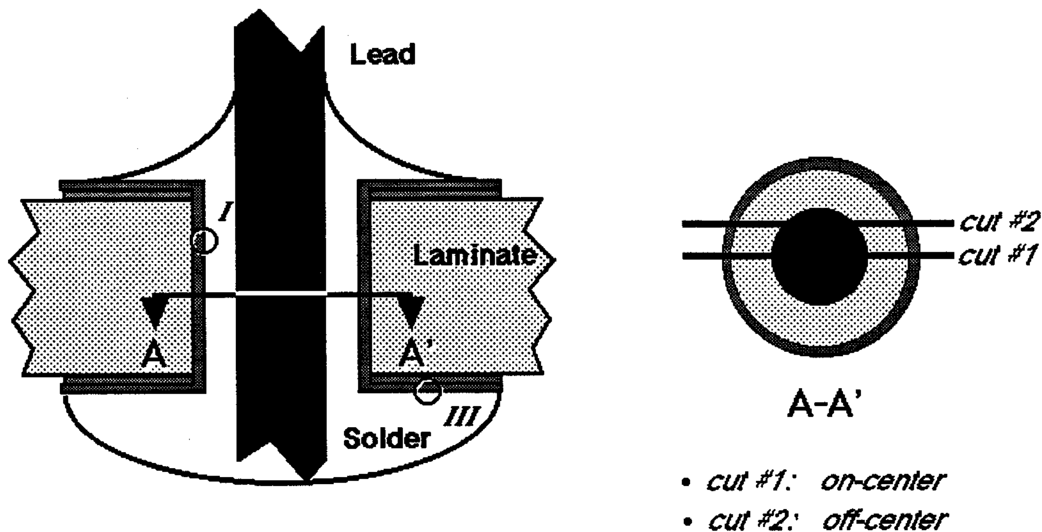

Figure 16. Effect of cross sectional cut on the measured intermetallic compound layer thickness at the barrel wall (I).

The results of the pairwise tests for joints within each of the three units #526676, #219214, and #316030 were summarized in Table 5 (joints with equal means in each of the three units). It was observed that in unit #526676, five of ten solder joint pairs (50%) had equal mean intermetallic compound layer thicknesses. In the case of unit #219214, nine of ten solder joint pairs (90%) were equal. Lastly, unit #316030 had only two of ten possible pairs (20%) that had equivalent mean thicknesses.

Table 5. Frequency of Equal Mean Thickness for Solder Joint Pairings within Each of Three Units.

Unit #	Frequency of Equal Means Thickness Between Solder Joint Pairs
526676	5/10
219214	9/10
316030	2/10

The results in Table 5 document the variability of intermetallic compound layer thickness to be expected from solder joints on the same board. Those data demonstrated the following: (1) that there could be considerable variation in the solder joint intermetallic compound layer thickness at the pad/solder interface (e.g., #316030); (2) the mean thickness values could be similar (#219214); or (3) the thickness variations could be largely random (#526676). That is, the state of variability observed in a particular unit was not necessarily reproduced by the other units.

In the next analysis, the variability between different units was assessed by combining together, as one sample, all of the location III, intermetallic compound layer

thickness measurements from solder joints on a given unit (circuit board). The data were described by a mean, standard deviation value, and a 95% confidence interval value and these results are summarized in Table 6.

Table 6. Intermetallic Compound Layer Thicknesses
MC2839 Power Supply Circuit Board Units

Unit #	Mean Thickness (μm)	Standard Deviation (μm)	Confidence Interval (95%) (μm)
526676	0.775	0.272	0.075
219214	1.118	0.338	0.094
316030	1.006	0.356	0.099
469565	0.600	0.177	0.049
661860	0.800	0.308	0.085

Again, in order to assess the similarity of the representative intermetallic compound layer thickness from amongst the different units, a pairwise comparison of mean layer thickness values was performed by testing the hypothesis of equivalent means using the Student's t-test. A total of 10 such pairings was created from amongst the five mean values in Table 6. The analysis revealed that eight of the ten pairs had significantly different mean thickness values (80%). The fact that eight of the ten pairs had dissimilar mean thicknesses serves as a benchmark for the variability of the layer thickness between the various units.

At a more detailed level, a relative ranking of layer thicknesses amongst the various units was determined based upon the statistical hypothesis of equivalent mean values. That evaluation was performed in the following manner: Examining the ten pairings, it was observed that in those eight cases in which non-equivalent means were observed, the units #219214 and #316030 each had mean values that were greater than their respective counterparts in the pair-wise tests. On the other hand, unit #469565 had a mean thickness value that was always less than its counterpart in all three hypothesis tests. The units #526676 and #661860 had mixed results. Between units #219214 and #316030, the pair had equal mean thicknesses. Likewise, the units #526676 and #661860 had statistically similar mean thickness values. Therefore, based upon the frequency of pair-wise inequality or equality of means (via the t-test), the units can be grouped as follows:

<table>
<tr><td>#469565 (0.600 μm)</td><td>#526676 (0.775 μm)
#661860 (0.800 μm)</td><td>#219214 (1.118 μm)
#316030 (0.893 μm)</td></tr>
</table>

→Increasing thickness

Units within the same group (groups 2 and 3 from the left) had statistically equal mean layer thicknesses.

The mean thickness data in Table 6, together with the pairwise analyses, served as a benchmark describing the magnitude of those thicknesses and the degree to which those

thicknesses differed on the circuit boards from the five different units. The differences in layer thicknesses observed between the several units may have been caused by variations in the technique of the solder operator. Also, the source of variations could have been small differences in thermal environments experienced by the selected units. Finally, it should be noted that the dissimilarity in thickness values would not impact the predictability of solder joint function while in service.

The intermetallic compound layer thickness statistics from *all* of the evaluated units that were combined to represent the MC2839, were as follows: *mean thickness, 0.86; standard deviation, 0.35; and the 95% confidence interval, 0.04.*

Finally, an important aspect of this study was the development of a protocol with which to determine the number of units required from the stockpile and that would provide a desired confidence interval on the intermetallic compound thickness data. As a review, the experimental logistics that were followed in the above analysis have been listed below:

- per joint: 10 thickness measurements
- per unit (PWB): 5 joints (when combined, 50 thickness measurements)
- per MC 5 units (when combined, 250 thickness measurements)

From a programmatic standpoint, the limiting factor in the magnitude of a study of fielded hardware likely rests with *the availability of MC units from the stockpile*, because once the units were obtained, there were plenty of solder joints to examine, and ample area within each solder joints to make the thickness measurements. Therefore, it would be desired to minimize the number of units requested from the field for dismantlement. The data acquired from the MC2839 was used to document the effect of unit sample size on the statistical description of the intermetallic compound layer measurements. The statistical metrics were: (1) the mean thickness, (2) standard deviation, and (3) the 95% confidence interval (on the mean).

As noted earlier, a total of five MC2839 units were dismantled. When all 250 intermetallic compound layer thickness measurements from those five units were combined, the statistical data were: mean, 0.86 μm; standard deviation, 0.35 μm; and a 95% confidence interval, 0.043 μm. If one of the units is dropped out so that the statistics are built upon only four units, then the mean thickness, etc. can be computed for all five possible combinations of four units, assuming that selection of four units for examination would be on a random basis. A similar analysis would then be performed for combinations of three, then two, and finally one unit. The results of such a matrix evaluation appear in Table 7 for each of the sets of combinations. Below each set, in bold face, are the mean values of the sample means, standard deviations, and 95% confidence intervals (CI) for the group; these summary data were included merely to show the trends in the statistical metrics as the number of sampled units decreased in descending order in Table 7.

Table 7. Intermetallic Compound Layer Thickness Combination Levels 5, 4, 3, 2, and 1 Units

Unit Comb.*	Mean Thickness (μm)	Standard Deviation (μm)	Confidence Interval (95%) (μm)
1-5	0.860	0.347	0.043
5 units	**0.860**	**0.347**	**0.043**
1-4	0.075	0.355	0.049
2-5	0.881	0.360	0.050
3-1	0.795	0.318	0.044
4-2	0.823	0.335	0.046
5-3	0.925	0.348	0.048
4 units	**0.864**	**0.343**	**0.048**
1-3	0.966	0.352	0.056
2-4	0.908	0.373	0.060
3-5	0.802	0.333	0.053
4-1	0.725	0.271	0.043
5-2	0.898	0.343	0.055
1,3,5	0.861	0.329	0.053
2,3,5	0.975	0.357	0.057
2,4,5	0.839	0.353	0.057
1,2,4	0.831	0.345	0.055
3 units	**0.867**	**0.340**	**0.054**
1-2	0.947	0.350	0.069
2-3	1.062	0.350	0.069
3-4	0.803	0.346	0.068
4-5	0.700	0.270	0.053
1,3	0.891	0.336	0.066
1,4	0.687	0.245	0.048
1,5	0.788	0.289	0.057
2,4	0.859	0.374	0.073
2,5	0.959	0.359	0.070
3,5	0.903	0.347	0.068
2 units	**0.860**	**0.327**	**0.064**
1	0.775	0.272	0.075
2	1.118	0.338	0.094
3	1.006	0.356	0.099
4	0.600	0.177	0.049
5	0.800	0.308	0.085
1 unit	**0.860**	**0.290**	**0.080**

* #1, 526676; #2, 219214; #3, 316030; #4, 469565; and #5, 661860.

It will be noted from the data in Table 7 that, moving from the bottom of the table to the top, that the average standard deviation (bold face) increased as the number of units in the hypothetical sampling group became greater. At first, the change was large when increasing from 1 to 2 units and from 2 to 3 units. The degree of change became less when increasing from 3 to 4 units and from 4 to 5 units. This trend suggests that the 1, 2, and 3 unit sampling regimes produced insufficient data that resulted in scatter terms that were sensitive to the number of measurements. The difference in standard deviation from 3 to 5 units shows a reduced sensitivity to number of samples taken in the analysis. This analysis suggests that a minimum sampling of 4 or 5 units would result in a data scatter (standard deviation) having a minimum sensitivity to the number of measurements.

The confidence interval (Table 7) exhibits a trend of decreasing value with an increasing number of samples in the test (again, proceeding from the bottom to the top of the table). The confidence interval does not necessarily have the same trend as the standard deviation, because of changes to the number of samples included in each group (in this case, an increase in the number of samples). The rate change in the confidence interval decreases and the value appears to reach a minimum at the 4 to 5 unit sample size. This behavior compliments that of the standard deviation parameter. In summary, either the standard deviation or the confidence interval analyses indicate that, if the sensitivity of the these parameters to the number of samples is the determining factor in the extent of sampling, then such a sensitivity tended to "bottom-out" at 4 units (or, 200 intermetallic compound layer thickness measurements).

As an alternative approach, a *desired* confidence interval can also serve as a quantitative criterion that determines the number of samples that are required for an analysis. For the intermetallic compound layer thicknesses of the MC2839 component, a sampling of 5 units (for a total of 250 solder joint measurements) resulted in a 95% confidence interval that was approximately 5% of the mean thickness value. If four units were to be examined at random, then the 95% confidence intervals ranged from 5.2% to 5.7% of the mean; three units, 5.8% to 6.7%; two units, 6.4% to 8.5%; and one unit, 8.2% to 10.6%. Therefore, if one wished to maintain a 95% confidence interval to be less than or equal to 5%, then 5 units would be required. At the other extreme, if 95% confidence intervals in the range of 8-11% were satisfactory, then only a single unit (that is, a combined 50 intermetallic compound layer thickness measurements) would be required for evaluation.

Clearly, the above analysis was made by having the data available, *a priori*. Unless the intermetallic compound layer thickness distribution is known, then sufficient units must be dismantled to establish those statistics. Simply examining one unit without such prior knowledge can give misleading results. This point can be illustrated with the MC2839 data. Initially, one (1) unit is dismantled and the intermetallic compound layer thicknesses are made from ten measurements on each of five joints for a total of 50 data points. The formula for the 95% confidence interval (95% CI) is:

$$95\%\ CI = 1.96[\ s / \sqrt{(n-1)}] \qquad (1)$$

where s is the sample standard deviation and n is the number of thickness data points. Knowing the value of s from the single unit and a desired 95% CI, the value of n, the number of test data, can be predicted from the rearranged form of equation (1):

$$n = 1 + [(1.96\ s) / 95\%\ CI]^2 \quad (2)$$

If unit #316030 were initially evaluated, then the 50 measurements showed a standard deviation of 0.356. If the desired confidence interval were set at 0.05 μm (for a mean of 1.01 μm), then the total number of joints required for examination would be 196. Because 50 had already been evaluated, an additional 146 would require measurement. At 50 joints per unit, an additional 3 units would need to be dismantled. Unit #316030 represents the worst case. On the other hand, if unit #469565 were selected, then only 48 such measurements would be required; that is, only that unit would be needed to arrive at the desired uncertainty.

Therefore, using the MC2839 data as a benchmark, it can be expected that in order to realize a 95% confidence interval of 0.05 μm for intermetallic compound layer thickness measurements, a minimum of 200 such measurements taken from amongst MC's from 4 different weapons would be required.

2.1.2.3 Quantitative Assessment - Pb-rich Phase Particle Size Distribution

A quantitative analysis of the size distribution of Pb-rich phase particles was performed from 500x magnification optical micrographs of the Region II (fillet "quadrant") location. The particles were counted as entirely Pb, even those having some Sn dissolved into them. The results of an evaluation of joint C from unit #526676 will be used to detail the evaluation. Shown in Figure 17 are 500x and 1000x photomicrographs of the fillet area II in joint C. The 500x photograph provided the input for the quantitative image analysis. The view at 1000x magnification was included simply to illustrate the presence of Sn within the Pb-rich phase. Either micrograph in Figure 17 demonstrates that the Pb-rich particles exist in a wide range of sizes and shapes. Thus, quantitative image analysis became an important tool for determining the size and counting statistics of these particles.

Shown in Figure 18 is a series of bar charts depicting the frequency of Pb-rich particles (y-axis) as a function of size categories (x-axis) for the solder joint C of #526676, using the micrograph in Figure 17a. The size parameter is the footprint *area* of the particle (in units of mm^2). Because the particles are of such widely varying shapes, the size categories were described in terms of areas rather than defined as a lineal dimension based upon some nominal geometry (e.g., diameters for assumed circular shape). Shown in Figure 18a is the frequency plot for all of the particles detected in Figure 17a. A total of 1469 particles were identified in the picture, of which, approximately 97% are in the size range of zero to 5×10^{-5} mm^2 (50 μm^2). The area range was further narrowed; the graph in Figure 18b shows that 90% of the particles have areas less than 2×10^{-5} mm^2 (20 μm^2). The process of redefining the area range to narrower values was continued, with the results illustrated by Figures 18c and 18d. An examination of Figure 18c indicated that approximately one-half of the particles have a size exceeding 2×10^{-6} mm^2 and one-half have an area less than this amount. Therefore, another sub-division was performed (Figure 18d) to determine the size frequency of the particles of a size less than 2×10^{-6} mm^2. The data in Figure 18d show that in this

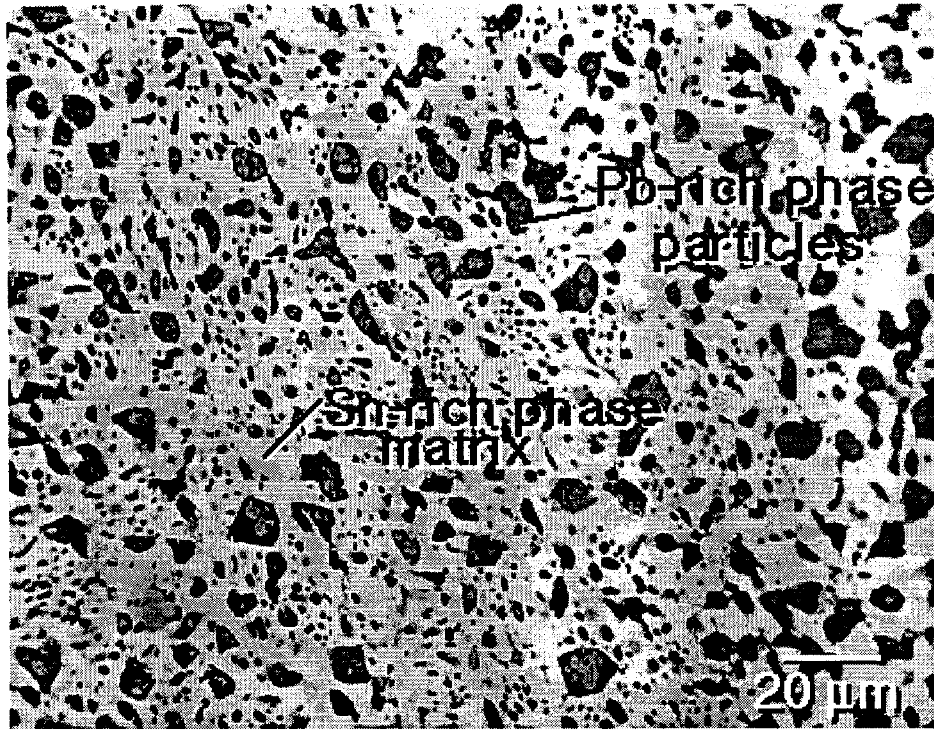

(a)

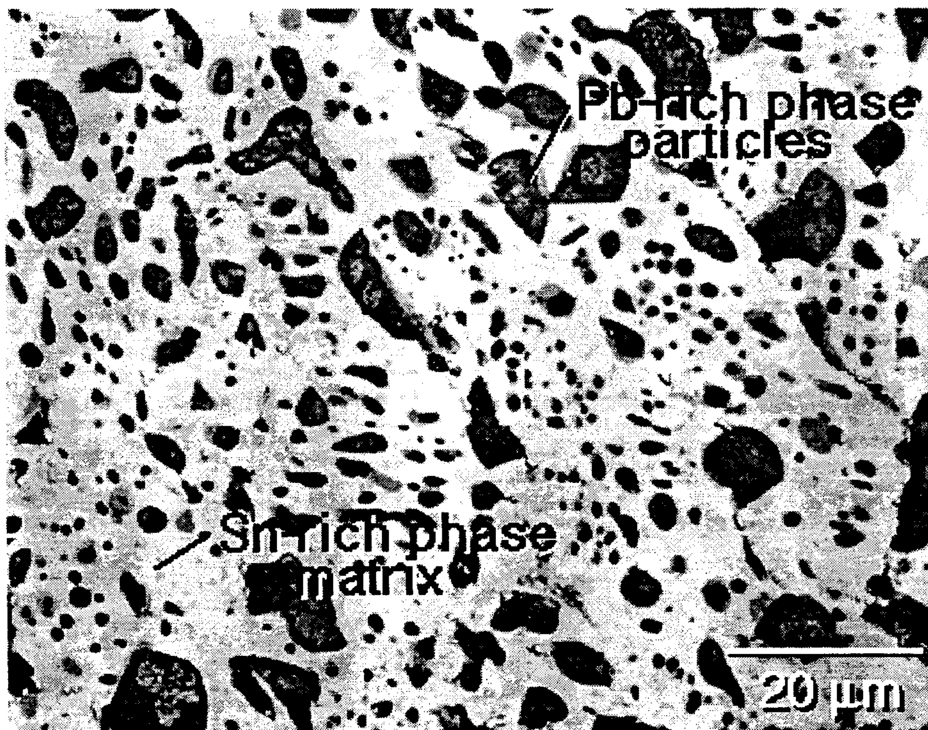

(b)

Figure 17. Optical micrographs of the fillet region II in joint C from unit 526676 at (a) 500x and (b)1000x. The 500x photo was used for the quantitative image analysis. The Sn contained in the Pb-rich phase particles is exemplified by the 1000x photomicrograph in (b).

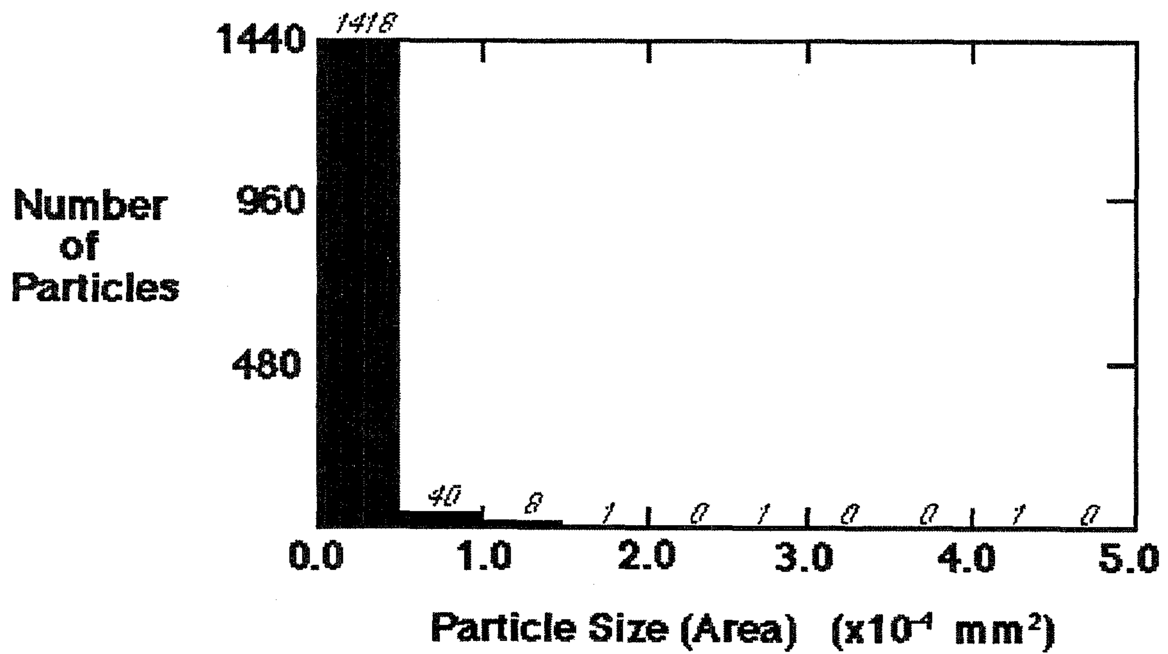

(a)

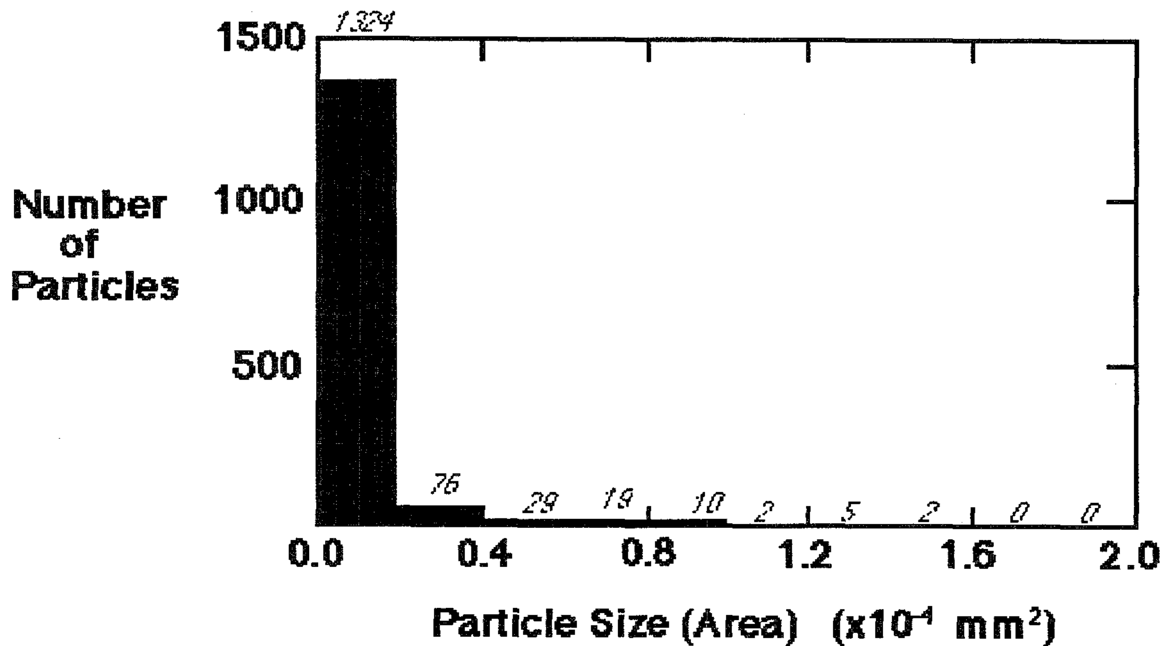

(b)

Figure 18. Pb-rich phase particle size distributions from the micrograph in Figure 17a from an MC2839 solder joint. The ranges indicating the degrees of refinement are: (a) 0 - 5 $\times$ 10^{-4} mm^2; (b) 0 - 2 $\times$ 10^{-4} mm^2; and (c) 0 - 2 $\times$ 10^{-5} mm^2, and (d) 0 - 2 $\times$ 10^{-6} mm^2.

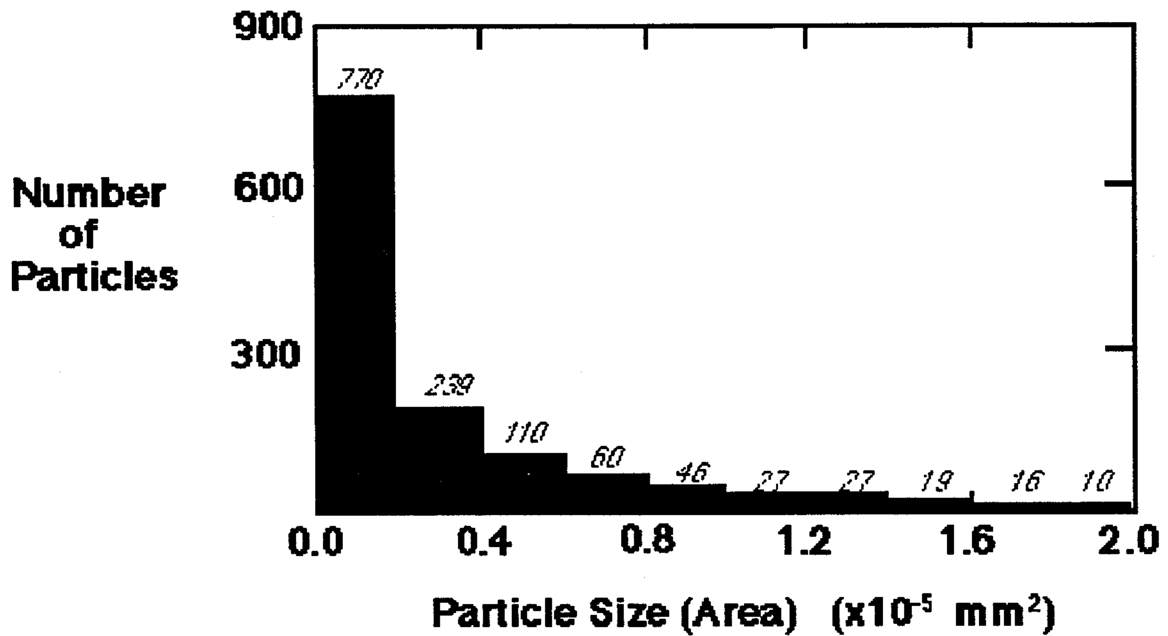

(c)

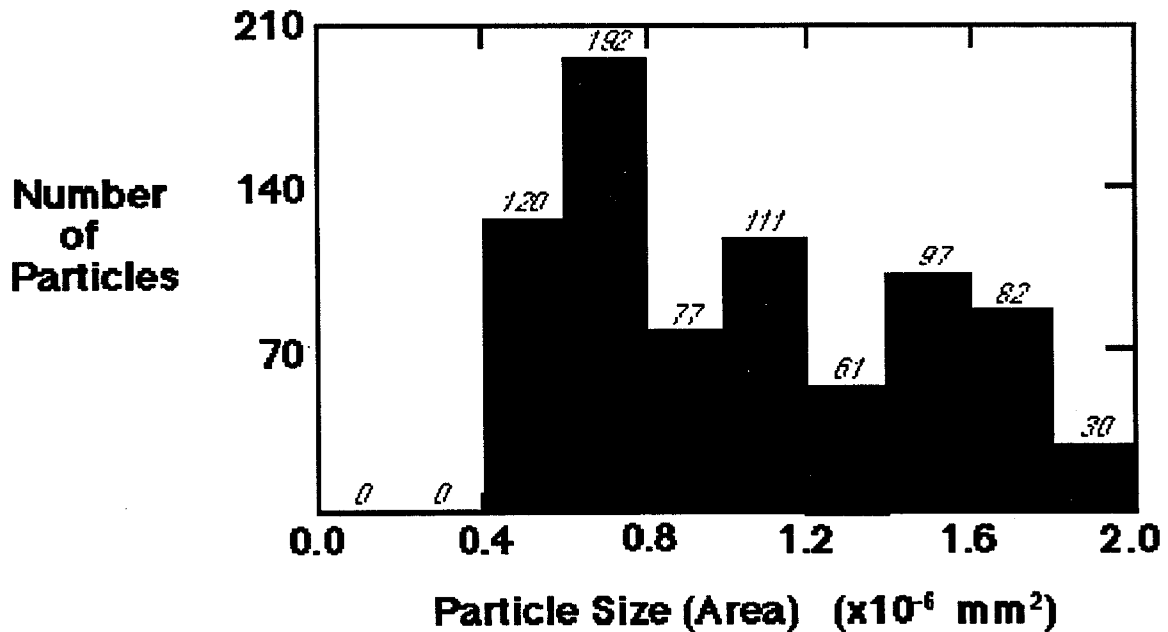

(d)

Figure 18. (Continued). Pb-rich phase particle size distributions from the micrograph in Figure 17a from an MC2839 solder joint. The ranges indicating the degrees of refinement are: (a) $0 - 5 \times 10^{-4}$ mm²; (b) $0 - 2 \times 10^{-4}$ mm²; and (c) $0 - 2 \times 10^{-5}$ mm², and (d) $0 - 2 \times 10^{-6}$ mm².

minimum sub-division set of 770 particles, 25% have a size of 6×10^{-7} to 8×10^{-7} mm^2 (6 to 8 μm^2). Over the entire distribution of sizes, the mean value was 8.12×10^{-6} mm^2. The standard deviation was 2.14×10^{-5} mm^2.

The frequency graphs presented in Figure 18 visually describe the particle size distribution. Clearly, the particle size distributions were skewed positive from a normal-type distribution. For the following analysis, it was assumed that the particle size distribution would be treated normally distribute. *The mean and the standard deviation served as the metrics used to describe each of the distributions.*

Shown in Table 8 are the particle size statistics for each of the solder joints in the dismantled units. These data include: (1) the mean of the particle size (area) distribution, (2) the standard deviation of each distribution, (3) the maximum particle size, (4) total number of particles that were included in the analysis, and (5) the calculated area percent of Pb-rich particles detected in the analyzed micrographs.

The mean of all of the "mean particle sizes" was 9.85×10^{-6} mm^2 (with a standard deviation of 3.9×10^{-6} mm^2). If it were assumed that the particles were of circular area, and therefore, had a spherical geometry in three-dimensions, then the overall mean particle *diameter* would be 3.54 μm.

As done with the intermetallic compound layer thickness measurements, the mean particle size (area) distribution was evaluated for variations between solder joints of the same unit. This analysis used the student's t-test to test the hypothesis of equivalent means. The F-test was used to establish the equivalence of the variances between the data pairs, in order to select the proper t-test format. However, unlike the case of the intermetallic compound layer data, a re-evaluation of the particle size data using each of the individual values was not possible. First of all, the analysis routine did not allow the particle size data to be available in such detail. Secondly, and more importantly so, it would have been hardly practical to input between several hundred and several thousand data points into the (packaged) software algorithms that performed the F-test and t-test evaluations.

Therefore, the following procedures were used. The "calculated" F-test parameter, F, was computed from the ratio of the sample variances (s^2_i, i=1,2) of the two data sets (with the larger value always serving as the numerator so that F>1):

$$F = s^2_1 / s^2_2 \tag{3}$$

Table 8. Pb-rich Particle Size Statistics from the MC2839 Units

Unit	Solder Joint	Mean Part. Area (mm^2)	Std. Dev. Area (mm^2)	Max Part. Area (mm^2)	No. of Part.	Pb-Rich Phase (%)
526676	C	8.12×10^{-6}	2.14×10^{-5}	4.42×10^{-4}	1469	28.6
	D	8.36×10^{-6}	1.96×10^{-5}	2.08×10^{-4}	1581	31.7
	E	9.59×10^{-6}	2.14×10^{-5}	2.53×10^{-4}	1152	24.6
	F	8.84×10^{-6}	2.06×10^{-5}	2.49×10^{-4}	1413	30.0
	G	5.76×10^{-6}	1.2×10^{-5}	2.48×10^{-4}	2023	27.5
469565	C	9.57×10^{-6}	2.37×10^{-5}	2.80×10^{-4}	1142	26.2
	D	6.35×10^{-6}	1.24×10^{-5}	1.38×10^{-4}	1598	24.4
	E	13.9×10^{-6}	3.03×10^{-5}	4.34×10^{-4}	860	28.7
	F	8.64×10^{-6}	1.65×10^{-5}	1.77×10^{-4}	1623	33.7
	G	12.1×10^{-6}	2.18×10^{-5}	2.98×10^{-4}	1118	32.5
661860	C	2.84×10^{-6}	0.67×10^{-5}	1.17 x 10-4	4046	27.6
	D	3.50×10^{-6}	0.81×10^{-5}	1.24 x 10-4	3937	33.1
	E	8.07×10^{-6}	1.65×10^{-5}	2.64 x 10-4	1594	30.9
	F	7.44×10^{-6}	1.99×10^{-5}	2.53 x 10-4	1925	34.4
	G	7.49×10^{-6}	1.72×10^{-5}	2.52 x 10-4	1933	34.8
316030	C	8.47×10^{-6}	2.00×10^{-5}	2.30 x 10-4	1470	29.9
	D	12.4×10^{-6}	3.18×10^{-5}	4.47 x 10-4	1214	36.3
	E	12.7×10^{-6}	2.62×10^{-5}	2.97 x 10-4	1205	36.7
	F	19.1×10^{-6}	3.98×10^{-5}	5.61 x 10-4	860	39.4
	G	18.0×10^{-6}	4.25×10^{-5}	83.6 x 10-4	895	38.6
219214	C	8.48×10^{-6}	2.24×10^{-5}	3.12 x 10-4	1380	28.1
	D	10.4×10^{-6}	2.68×10^{-5}	3.22 x 10-4	1040	26.0
	E	11.0×10^{-6}	2.45×10^{-5}	3.26 x 10-4	1137	30.0
	F	15.1×10^{-6}	3.40×10^{-5}	3.90 x 10-4	881	32.0
	G	9.95×10^{-6}	2.18×10^{-5}	3.02 x 10-4	1121	26.8

where s is the sample standard deviation of the data set. The "table" F-test parameter was determined from the table of F-distribution values for ν_1 and ν_2 degrees-of-freedom. The degree-of-freedom values equaled the respective number of data point entries, minus one[13]. Due to the large number of data points comprising each set, the "table" F-test parameter was equal to one for all cases. Because all "calculated" F-test parameters were greater than one, the sample variances tested "unequal" in all cases. Therefore, it was inferred that the distribution variances, σ^2_i, were, likewise, unequal. This trend was observed because of the large number of data points evaluated in each set. Even the slightest difference between the variances of the two data sets was sufficiently significant to establish the two variances as statistically "unequal" (by the F-test). As a consequence of this condition on the variances, the t-test used to test the hypothesis of equivalent means was that developed for the condition of *unknown distribution variances,* and assumed *unequal distribution variances*, as determined from the F-test procedure described above.

The t-test was performed under the two-tail criterion with a confidence interval of 95% (i.e., $\alpha = 0.05$). The t-test evaluation began by establishing a "composite" degree-of-freedom, f, by means of the following expression:

$$f = \left\{ [s^2_1/n_1 + s^2_2/n_2] \ / \ [(s^2_1/n_1)^2/(n_1-1) + (s^2_2/n_2)^2/(n_2-1)] \right\} \qquad (4)$$

where s^2_i is the sample variance and n_i is the sample size. The composite f-value (not to be confused with the F-distribution parameter for variances) was then used to determine the parameter $t_{f,\,1-\alpha/2}$, from the appropriate t-distribution tables, given f and α. The parameter $t_{f,\,1-\alpha/2}$,, was introduced into the following expression:

$$\left\{ [x_1 - x_2] - t_{f,\,1-\alpha/2} \sqrt{[(s^2_1/n_1 + s^2_2/n_2]} \right\} < (\mu_1 - \mu_2) < \left\{ [x_1 - x_2] + t_{f,\,1-\alpha/2} \sqrt{[(s^2_1/n_1 + s^2_2/n_2]} \right\} \qquad (5)$$

where x_i is the sample average; $(\mu_1 - \mu_2)$ is the difference in the population means; and the other symbols as previously described. The two limiting values were computed; if zero is included within those two boundaries, then the hypothesis of equal means tests positive; that is, the means of the hypothetical populations, μ_1 and μ_2, are statistically equal. The null hypothesis stands (i.e., unequal means) should zero be outside of the range established by the limiting values.

The above analysis was applied to the mean Pb-rich particle sizes for the solder joints within each of the units. The number of pairwise combinations evaluated by the t-test that tested positive for equality of the mean particle size were recorded for each units in Table 9.

Table 9. Equality of MC2839 Solder Joint Mean Pb-Rich Particle Sizes versus Total Number of Pairwise Comparisons per Unit

Unit	Equal/Total
526676	6/10
469565	2/10
661860	3/10
316030	2/10
219214	4/10

It is apparent from the data in Table 9 that the frequency of mean particle size equality varied considerably amongst the different units. Only 20% of the pairwise comparisons showed equal means for the 469565 and 316030 units. Sixty percent of those possible pairwise combinations in the 526676 exhibited equality. When all of the data in Table 9 is combined to represent the entire weapon, the number of pairs showing equal means is 34%. Again, the purpose of this analysis was to establish the variability of the Pb-rich phase particle distribution in the solder joints in the MC2839. There should be no inference made from the data, as yet, with respect to the impact of this variability on the properties of the solder joints, present or future.

A correlation was sought between mean particle size and the range of sizes as represented by the standard deviation of the size distributions. Previous studies on solder joint aging demonstrated that the Pb-rich phase can be expected to coarsen with time[14]. This trend should reflect itself in the particle size distribution, by an increase in the mean particle size that is accompanied by a reduction in the spread of particle sizes, as the smaller particles are lost to larger ones. Shown in Figure 19a is a plot of standard deviation versus mean particle size of the data compiled from all of the MC2839 units. It is observed that a strong correlation exists (R^2=0.93). However, this trend also contains behavior in which the standard deviation magnitude is dependent upon the size of the mean. Therefore, the data spread was represented by the standard deviation after having been normalized to the mean; this parameter represented the percent error (of the mean). The percent error as a function of the mean particle size is shown in Figure 19b. A very poor correlation is observed (R^2=0.03). Therefore, because the particle size and percent error did not correlate well, let alone with a positive slope, it is to be expected that the different particle sizes did not represent instances of different thermal histories for the solder joints. Rather, the distribution of particle sizes reflected the statistical variation inherent in the solidification and cooling processes of the solder joints during manufacture.

Quantitative data describing the extent of coarsening as a function of aging time and temperature has been described in the literature[15]. However, such *generic* data are not readily applicable to a particular case study such as reported here, because the starting microstructure must be known so that it may serve as a reference point. The as-fabricated microstructure is sensitive to the process used to assemble the joint, in particular, the cooling rate of the solder[16]. The faster the cooling rate, the finer the starting Pb-rich phase distribution. In the case of hand soldering, the cooling rate is determined by the soldering iron tip temperature, the heat sink capacity of the device lead, and the circuit board laminate. In the immediate investigation, comparable measurements of as-fabricated solder joints that were made 30 to 40 years ago does not exist.

Both the Pb-rich phase particle size distribution as well as the intermetallic compound layer thickness provide indicators of the thermal history of the solder joints. The intermetallic compound layer thickness and mean Pb-rich particle size are expected to increase with the severity of thermal aging (increased time and/or temperature). The existence of such a correlation between the intermetallic compound thickness and the associated Pb-rich particle distribute would suggest that the differences in these parameters amongst the various units was caused by a thermal history (aging) effect. In the first part of the analysis, the intermetallic compound layer thicknesses at each of locations I and III were compared individually with the corresponding Pb-rich phase particle size (from area II). That is, a thickness (I)-mean particle size (II) correlation was calculated for each of the joints labeled "C" from all five of the units. The comparison was repeated for thickness (III)-mean particle size (II). Then, joints "D," "E," etc. from all of the units were similarly analyzed. In all cases, no significant correlation was observed; in fact, the R^2 values were generally very poor. Lastly, the pairwise data comprised of all the mean intermetallic compound layer thicknesses (areas I and III) and the mean Pb-rich particle size from each unit were examined by linear regression analysis. An R^2 value of 0.06 was computed, indicating once again that no significant correlation was present. In conclusion, the intermetallic compound layer thickness data

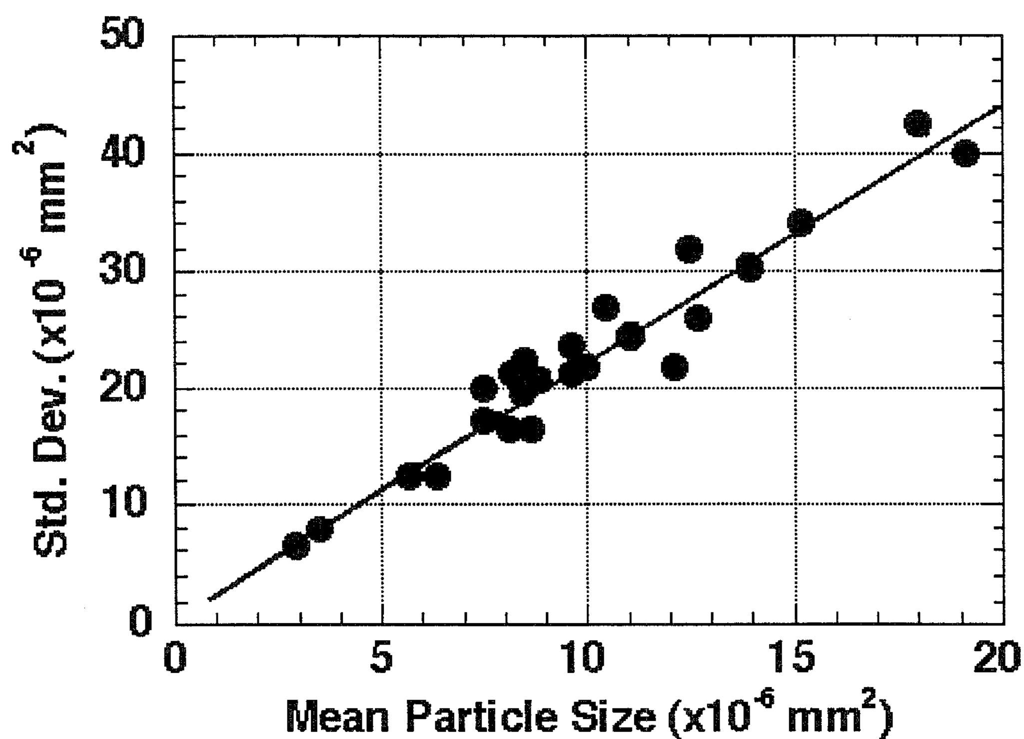

(a)

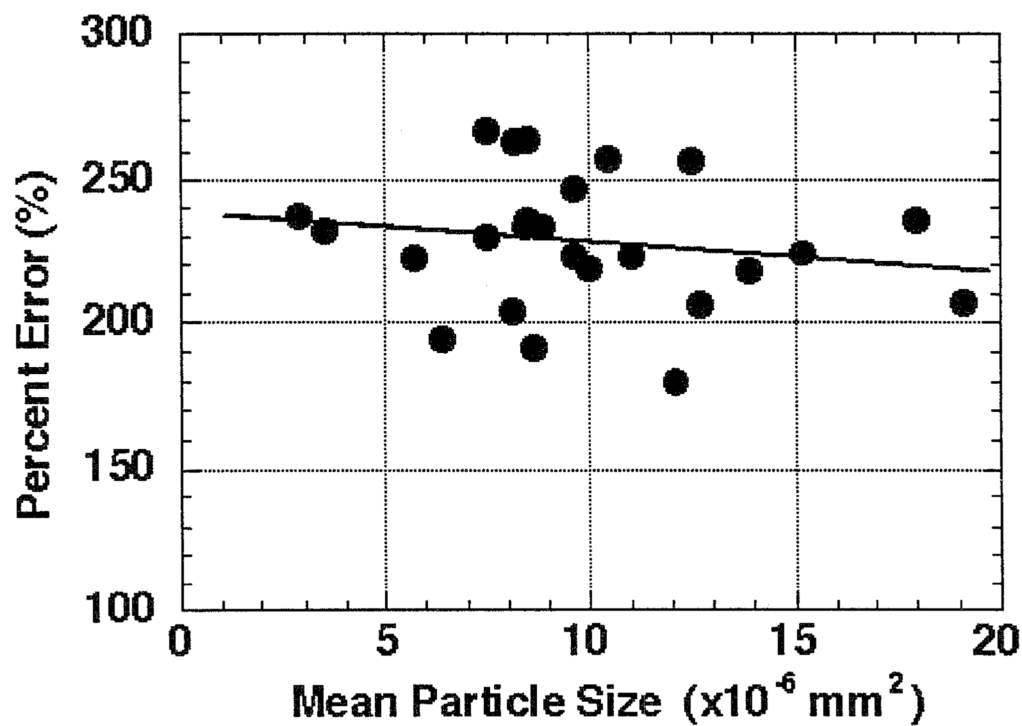

(b)

Figure 19. (a) Standard deviation and (b) percent error as a function of mean Pb-rich phase particle size for the data compiled from the MC2839 units.

and the Pb-rich phase particle sizes of the solder joints on the MC2839 units did not appear to be well correlated. This result confirms the conclusion drawn from the lack of correlation between the mean Pb-rich particle size and the normalized data spread; that is, the differences in Pb-rich particle sizes between solder joints from different units did not reflect different thermal histories, but rather, represented the customary variation in solidification microstructure arising from the cooling process.

The quantitative analysis of Pb-rich phase particle distributions (as exemplified by Figure 17a) also allowed a measurement of the area fraction of the microstructure that was the Pb-rich phase and, of course, the remainder that was the Sn-rich phase. When the area fraction data were computed for each of the solder joints and combined together to represent the entire MC2839, an overall mean area fraction was calculated to be 30.9±4.2%. The 95% confidence interval was [29.2%, 32.6%]. The area fraction of Pb-rich particles (see Table 8) provides a direct measure of the concentration of Pb in the solder. In order to use the area percentage values to verify the solder composition, it was assumed that the solder solidification did not create a texture to the Pb-rich phase in the solder. Therefore, the cross sections were considered to be random cuts through the solder so that *the area fraction represented the volume fraction*. Given the densities of Sn and Pb, the weight fraction of Pb was computed from the overall, mean area percentage of Pb to be the number above (30.9±4.2%). A solder composition was then calculated and that composition was 59Sn-41Pb. Given a 95% confidence interval, the Pb composition could vary from 39 to 43 wt.%. The quantitative image analysis did not distinguish the approximately 2 wt.% Sn dissolved in the Pb-rich phase. Therefore, the area fractions of Pb-rich particles are consistent with a commercial solder composition of 60Sn-40Pb.

The area percent of Pb-rich phase data also provided a verification of the appropriateness of the photomicrograph magnification (500x) used to perform the particle analyses. The variation in the mean Pb phase area percent value (±4.2%) provided an acceptance criterion on the magnification of the micrographs used in the analysis. Lower magnification images increased the sampling area, thereby making the Pb content determination more accurate. However, resolution limits on the imaging technique would have caused a loss of the smaller particles; that is, loss grows in severity as the magnification was further reduced. On the other hand, increasing the magnification in order to capture the smallest particles limited the sampling area, thereby increasing the likelihood of disparate Pb contents due to localized (small scale) variations.

A confirmation that the 500x magnification was suitably high was made by comparing the area percentage of Pb-rich particles against the mean particle size for all of the examined joints. The absence of a correlation would suggest that the sampling area is adequately large to smooth out localized concentration fluctuations caused by the different Pb-rich phase particle sizes. A plot of area fraction versus the mean particle size of all of solder joints in the units is shown in Figure 20. A linear regression analysis was performed on the data; the computed R^2 value of 0.27, indicating that no significant correlation was found between the two parameters. Therefore, the Pb-rich phase distribution appeared to be sufficiently uniform at 500x so as to minimize magnification effects on the Pb-rich phase particle statistics.

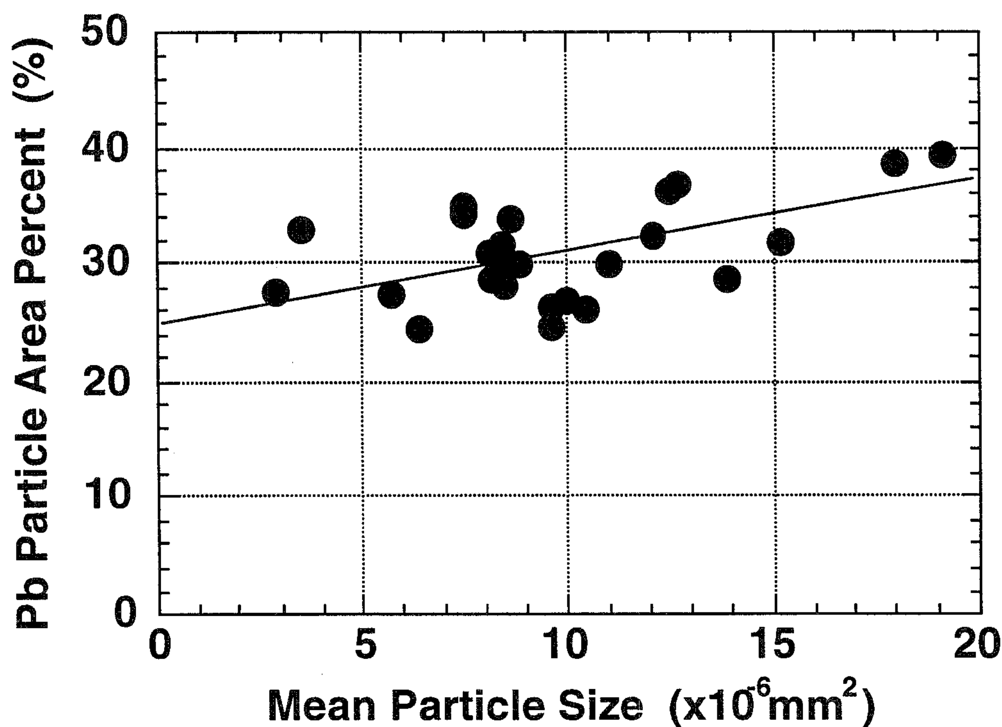

Figure 20. Area percent of Pb-rich phase versus the mean Pb-rich phase particle size for all of the solder joints.

2.2 MC1814 Junction Box

2.2.1 Procedures for the Extrication of Targeted Parts

Photographs of the MC1814 junction box unit is shown in Figure 21. The assembly is comprised of a thermosetting plastic housing. A total of 12 cable connectors was mounted to one side of the housing for signal transmission to the inside. Internally, the box is a collection of solder-assembled circuit boards. A foam potting material was placed into the unit to mechanically secure circuit boards in place. The positive print of an x-ray image of the junction box appears in Figure 22a. The circuit boards targeted for analysis were identified from the x-ray image. Their location has been indicated in Figure 22a as well as in Figure 22b, which shows a schematic diagram of the unit.

As was the case with the MC2839, chemical depotting techniques were initially used in an attempt to retrieve of the circuit boards. The first unit exposed to the depotting treatment described in Appendix A was serial number #26705. The housing was not affected by the chemicals. However, the potting foam and the circuit boards were harshly attacked in the process. The circuit boards had swelled and the weave layers delaminated as a consequence of this depotting procedure.

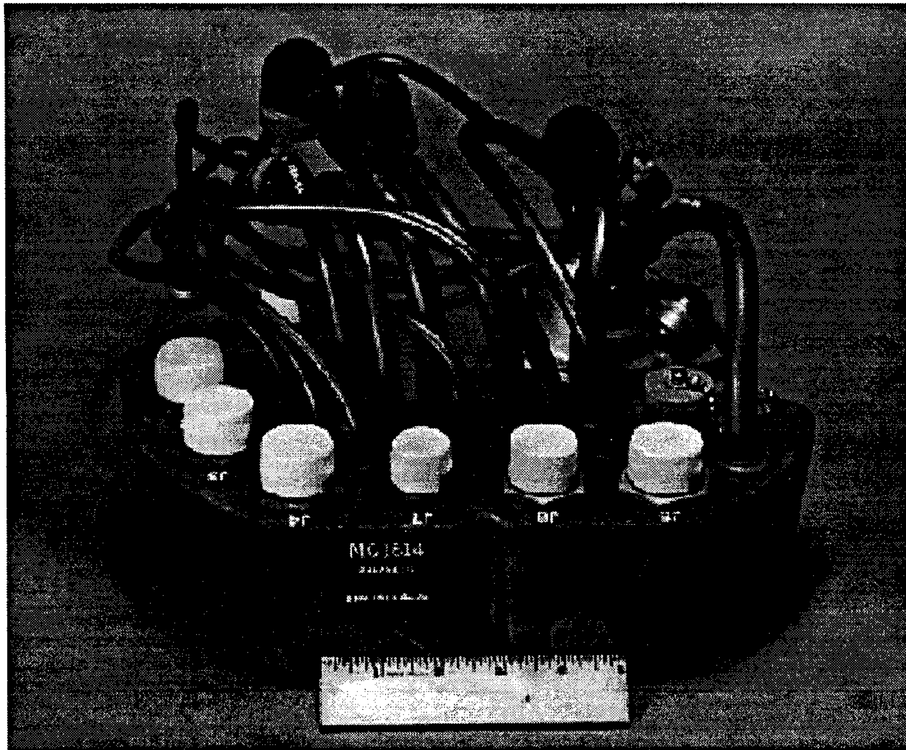

(a)

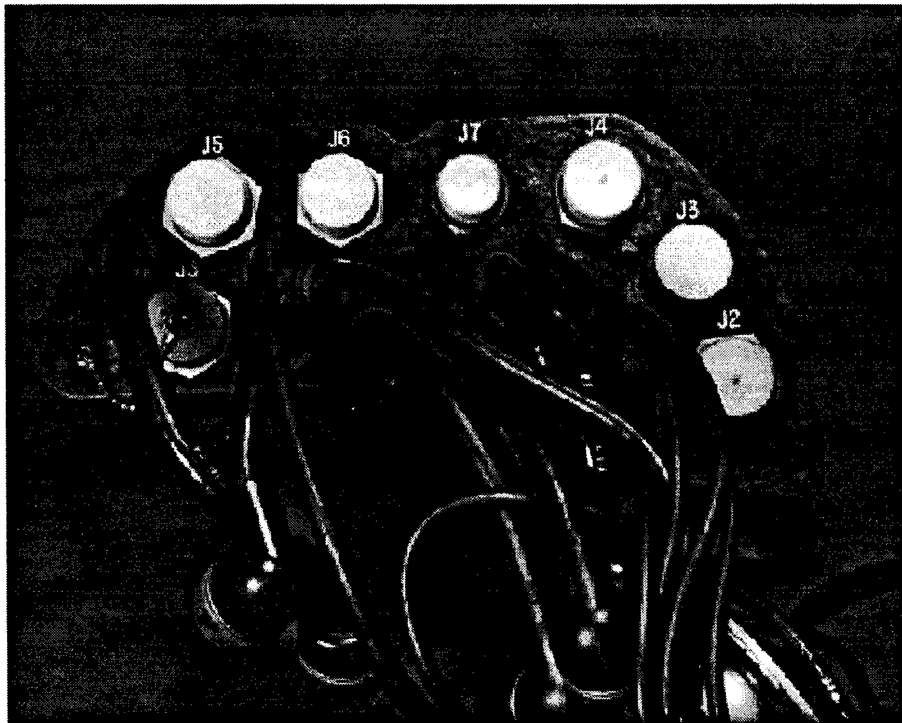

(b)

Figure 21. Photographs of the MC1814 junction box: (a) general view, (b) top view, and (c) bottom view.

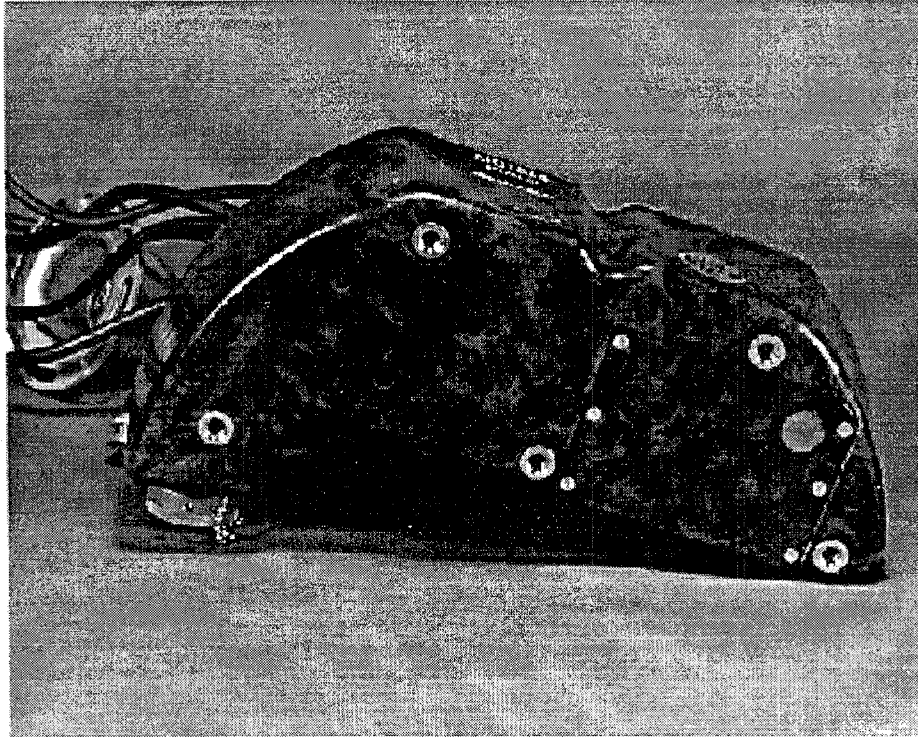

(c)

Figure 21. (Continued). Photographs of the MC1814 junction box: (a) general view, (b) top view, and (c) bottom view.

The extent of damage to the circuit boards resulting from the chemical depotting procedure was unacceptable. Therefore, the abrasive water jet process, in combination with a more limited chemical dissolution step or none at all, were used to extract the circuit boards from the units. Using x-ray images similar to that in Figure 21, a unit was initially placed in the abrasive water jet machine (Figure 23). Sections were made through the housing to cut out the "segments" which contained the circuit boards (Figure 24a). The circuit boards used in the analysis were labeled in Figure 24b. Figure 24c is simply a view of the segment from the opposing side.

First, it was necessary to remove the potting material from the circuit boards in order to identify the solder joints to be sectioned. Therefore, a segment from the unit #65517, for example, was exposed to a limited chemical depotting treatment with heated N-methyl-pyrolidinone (NMP). This procedure caused some damage to the laminate, but did allow identification of the solder joint positions. The analysis was extended to included another five of the eight remaining MC1814 units; the final three units were archived. In subsequent dissection of the other five units that were used in this study, the circuit board segments were retrieved by an abrasive water jet cutting the MC1814. Further sectioning of the units was then performed using either an abrasive saw or a cutting saw.

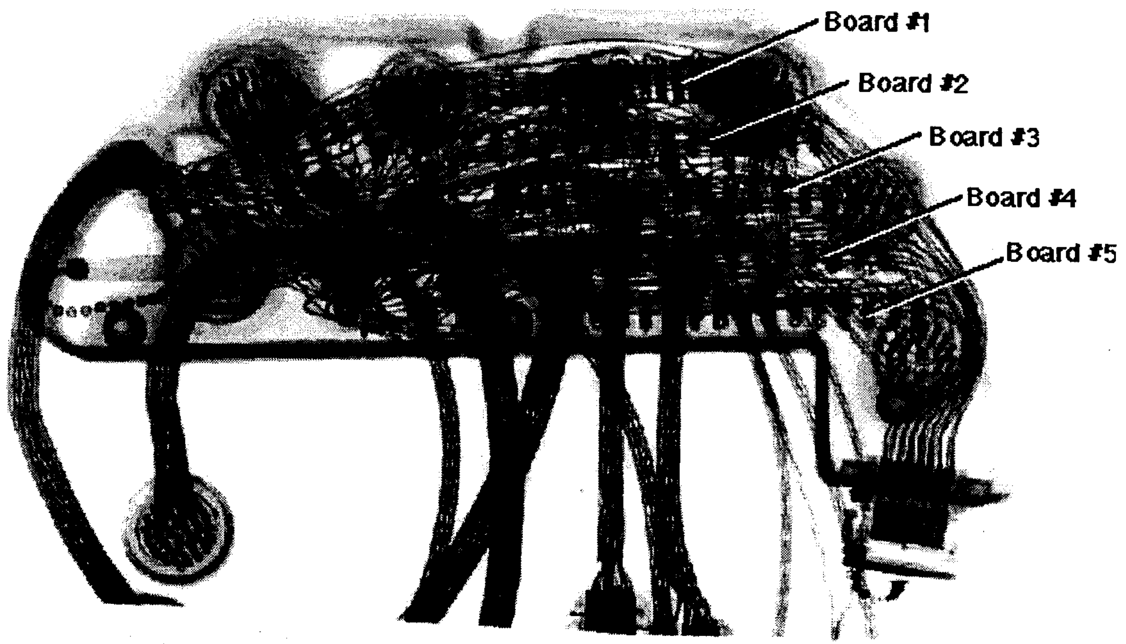

Figure 22a. Positive print of an x-ray of the MC1814 junction box.

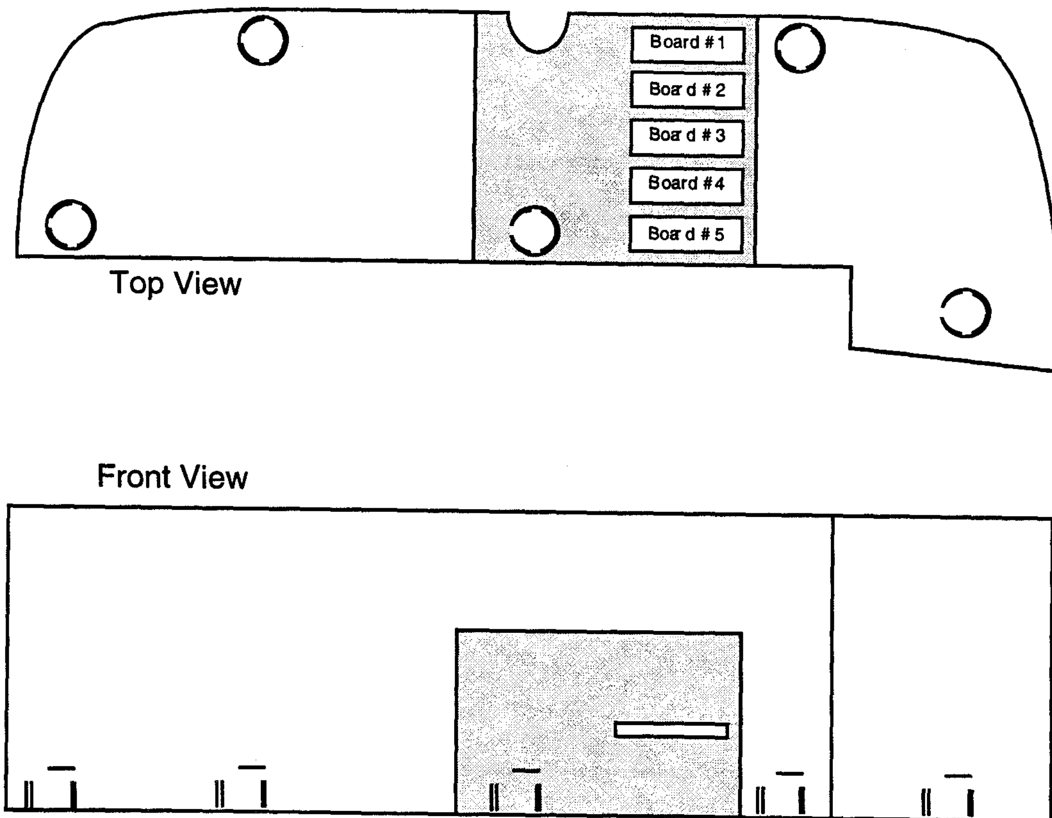

Figure 22b. The circuit boards targeted for analysis have been identified by a schematic diagram of the junction box showing their location.

Figure 23. An MC1814 unit in place in the abrasive water jet cutting machine.

Each of the circuit boards was cut up into five segments. Three of the five segments, labeled #3, #4, and #5, were selected for the study; the other two segments were discarded. The segment, #4, was relabeled as "M" and the segment #3 was relabeled "S" (Figure 25). The third board (#5) remained unlabelled and was kept for archival purposes. The solder joints analyzed from each of the segments M and S are identified in Figure 25. At this point, the analysis scenario of the first unit #65517 differed slightly from that used on the other five units. In the case of the #65517 unit, four solder joints (M1A, M1B, M2A, and M2B) were evaluated from the "M" segment and one solder joint (S1) was evaluated from the "S" segment. In the case of the other five units, only two solder joints from the "M" segment were evaluated (M1 and M2) and one solder joint was assessed from the "S" segment (S1).

For the unit #65517, an analysis protocol similar to that used for the MC2839 solder joints, and diagrammed in Figure 11, was used to evaluate the solder joint microstructure. That is, the intermetallic compound layer thickness was measured from a single 1000x optical micrograph taken at the land (copper)/solder interface (III) and one from the hole barrel (copper)/solder interface (I). A total of 13 thickness readings was taken at each location. The Pb-rich phase distribution was determined from a 500 x optical micrograph taken at location (II) as previously described.

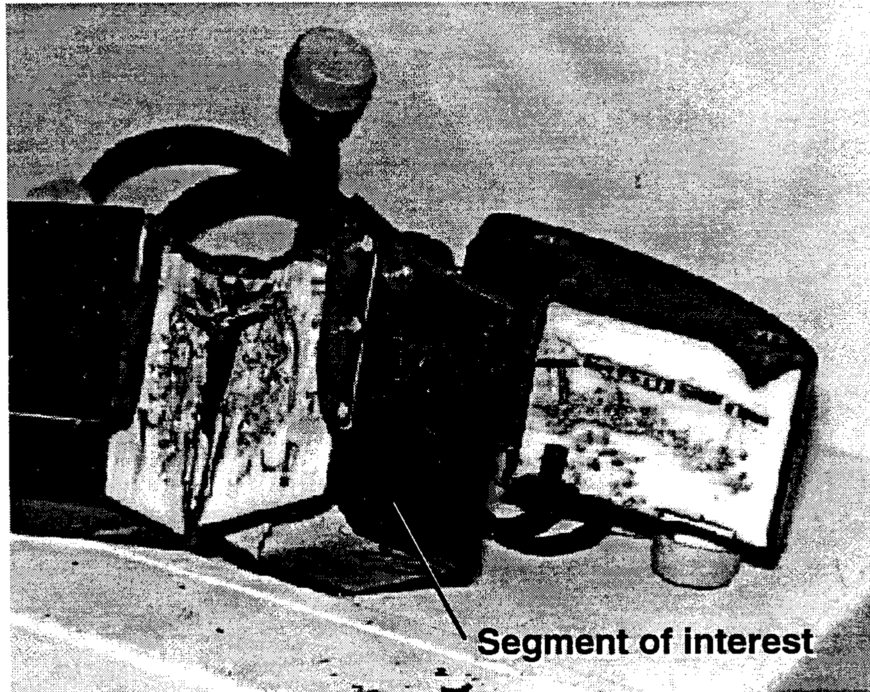

(a)

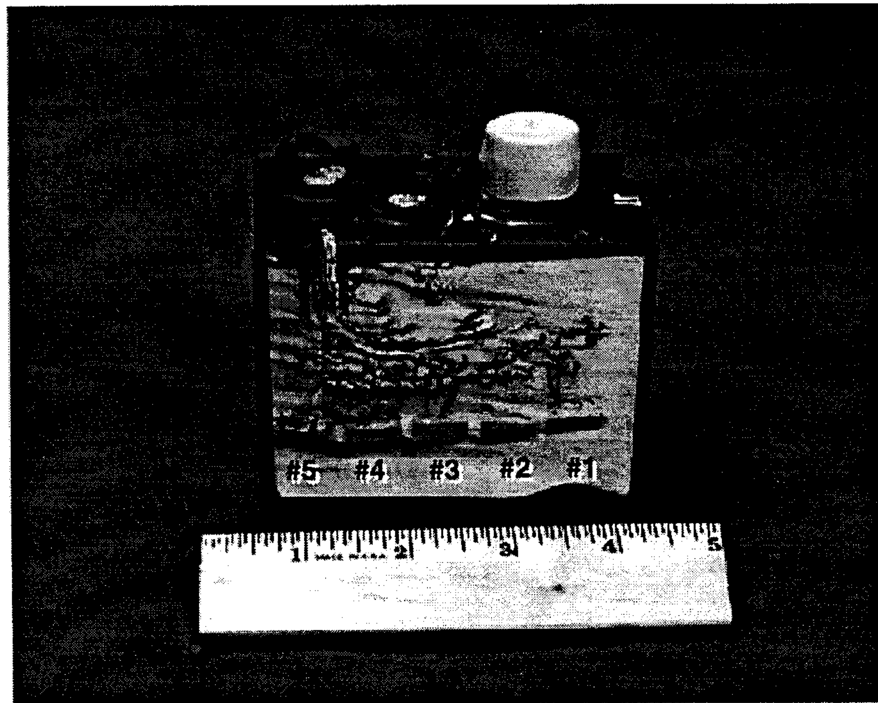

(b)

Figure 24. Segment of the MC1814 unit after water jet cutting which contains the targeted circuit boards: (a) First cut from the unit to separate the segment of interest. Segment of interest in (b) the front view and (c) rear view. In the front view (b), the numbers refer to the circuit boards in positions noted in Figure 22b.

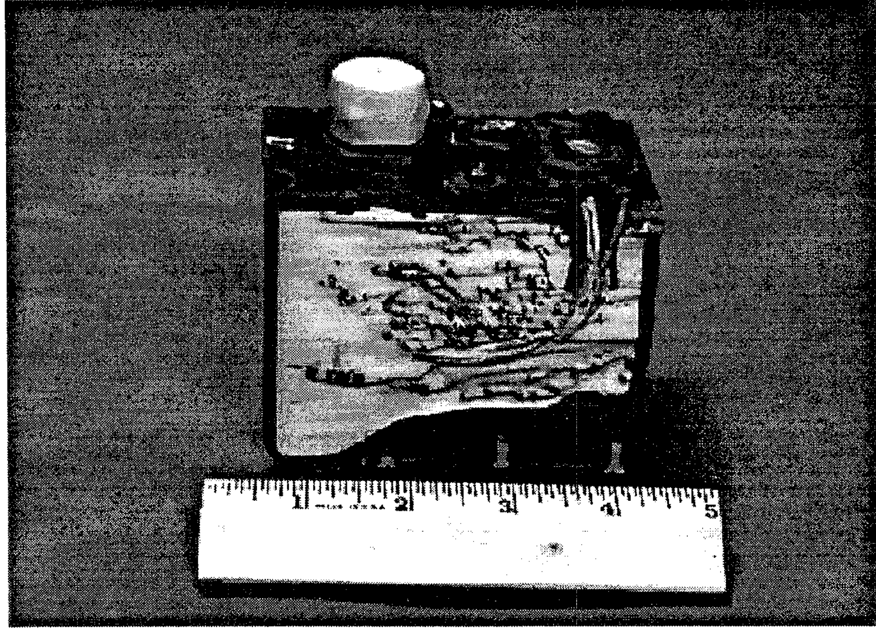

(c)

Figure 24. (Continued). Segment of the MC1814 unit after water jet cutting which contains the targeted circuit boards: (a) First cut from the unit to separate the segment of interest. Segment of interest in (b) the front view and (c) rear view. In the front view (b), the numbers refer to the circuit boards in positions noted in Figure 22b.

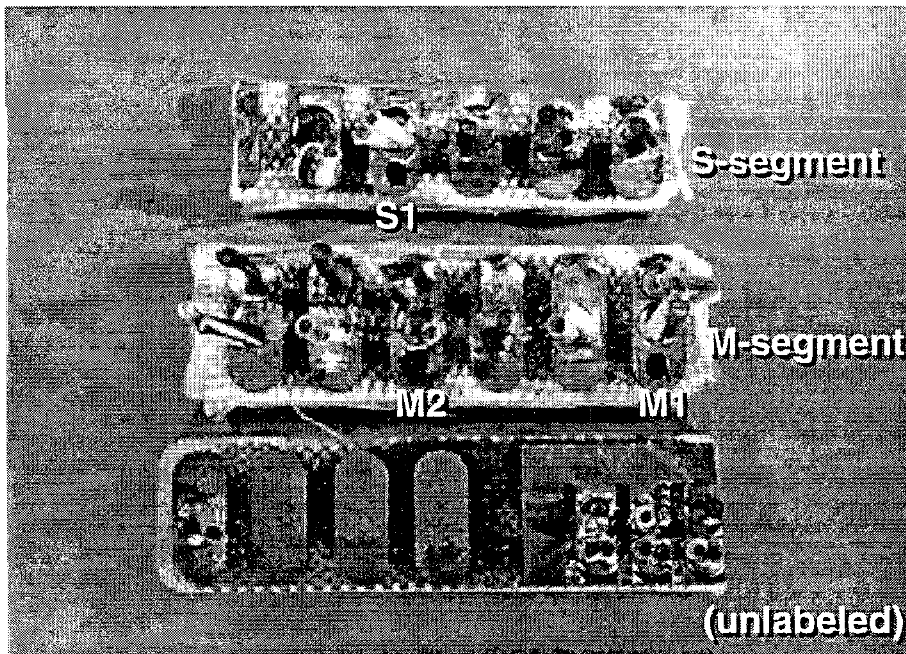

Figure 25. Photograph of the circuit board segments labeled "S", "M", and an unlabelled part, taken from circuit boards #5, #4, and #3 of the MC1814 unit, respectively. The solder joints used for analysis are identified in the photograph.

The analyses of the five remaining units differed from that of the #65517 unit in order to obtain some additional information. First of all, the intermetallic compound layer thickness was measured at two (III) positions, one on the top of the joint and labeled (III-A) and the second on the land at the bottom side of the board and labeled (III-B). The objective of this additional data was to determine the variation of the intermetallic compound layer thickness as a function of location within the joint real estate. A total of 10 thickness reading were taken at each location (as opposed to 13 data for the #65517 and MC2839 evaluations). Likewise, the Pb-rich phase particle distribution was extended to three locations: one location being in the topside fillet (A), the second was located in the bottom side fillet (B), and the third location was within the hole (H). A similar goal was the basis for the additional particle size measurements.

2.2.2 Results and Discussion

2.2.2.1 Qualitative Assessment

The circuit board laminate was composed of a fiber weave and thermosetting plastic filler. The laminate thickness was nominally 3.18 mm (0.125 in.). The conductor features (lands and strips) were 75 μm (0.003 in.) thick Cu foil bonded to the laminate. The hole diameters were 2.54 mm (0.100 in.). The wires were stranded Cu with a 0.787 mm (0.031 in.) nominal diameter. The construction of the holes was non-typical by current day practices. The unusual feature was that the holes were not plated-through for signal transmission between the two surfaces. Rather, a Cu sleeve (or "eyelet") was inserted into the hole. A schematic diagram of the hole construction is shown in Figure 26. The wall thickness of the cylinder measured approximately 0.178 mm (0.007 in.). The ends of the sleeve were flared into a flange on either side in order to secure it mechanically into place. Electrical continuity was provided by soldering the sleeve to the conductor (land) at the same time that the wire lead was soldered into the hole.

The use of the sleeve to effect signal transmission between the two surfaces of the circuit board was a likely consequence of circuit board technology that was available at the time of unit manufacture (early 1960's). The technology of the plated-through hole, in which Cu conductor is electroplated on the hole walls, was either not readily accessible at that time or was not sufficiently well developed to be used on such a thick laminate. Ancillary factors such as cost and schedule, while clearly quite distant from the technological scenarios, may certainly have driven the choice of the sleeve technique.

Irrespective of the reason(s) for the use of the sleeve, this approach can raise reliability concerns for the assembly in service. The primary issue is the presence of an empty cavity between the outer wall of the sleeve and the circuit board. Fluxes used in the solder process as well as volatiles emitted by the circuit board laminate during the elevated temperature excursion of the solder operation (including water vapor and organic contaminants) can lead to corrosion of the Cu and/or solder. Moreover, the rapid vaporization of these materials during the solder process can potentially damage the laminate. Although the potential for these scenarios to occur must be noted, it must also be stated that upon examination of numerous solder joint cross sections in this unit, there was no evidence of them having taken place.

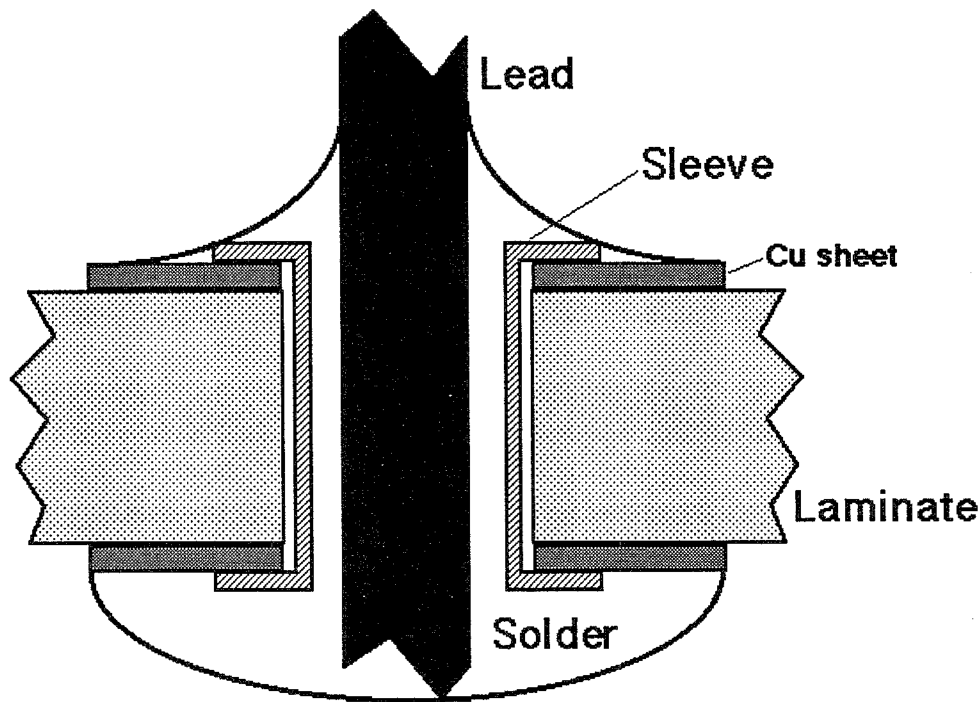

Figure 26. Schematic diagram of the hole construction for the circuit boards in the MC1814 junction box.

An evaluation of the solder joints was made prior to their cross sectioning. Low magnification optical microscopy (<50x) revealed no defects in the solder joints. Next, a portion of one board from the #65571 unit was examined by scanning electron microscopy. Shown in Figure 27a is a view of the top side of one of the solder joints. An outline of the hole diameter was apparent. Higher magnification views of areas "G" (Figure 27b) and "D" (Figure 27c) revealed that a circumferential crack had formed in the joint. Further observations about the crack showed that it extended around the entire circumference of the joint. Moreover, the majority of the crack opening contained the potting material; the view "G" (Figure 27b) was an isolated exception in which the foam appeared absent from the crack. It cannot be concluded that the presence of potting material in the cracks indicates that the cracks were present prior to the potting step. Residual potting material may have entered the cracks as a consequence of the chemical release process. Next, the bottom side of the joint was examined via scanning electron microscopy. A low magnification view appears as Figure 28a with higher magnifications in Figures 28b and 28c. A circumferential crack was also noted about the joint. Clearly, the crack opening was reduced with respect to that observed on the top side. In some areas such as that represented by Figure 28b, the "crack" was more accurately a line of extensive plastic deformation without the formation of a discontinuity that is a crack. Potting foam was not observed in these cracks.

In order to get a better view of the crack morphology, samples from the #65517 unit were cross sectioned. Shown in Figure 29 (a, b, and c) are optical micrographs of three of the four quadrants of a solder joint as it is viewed in cross section. In the

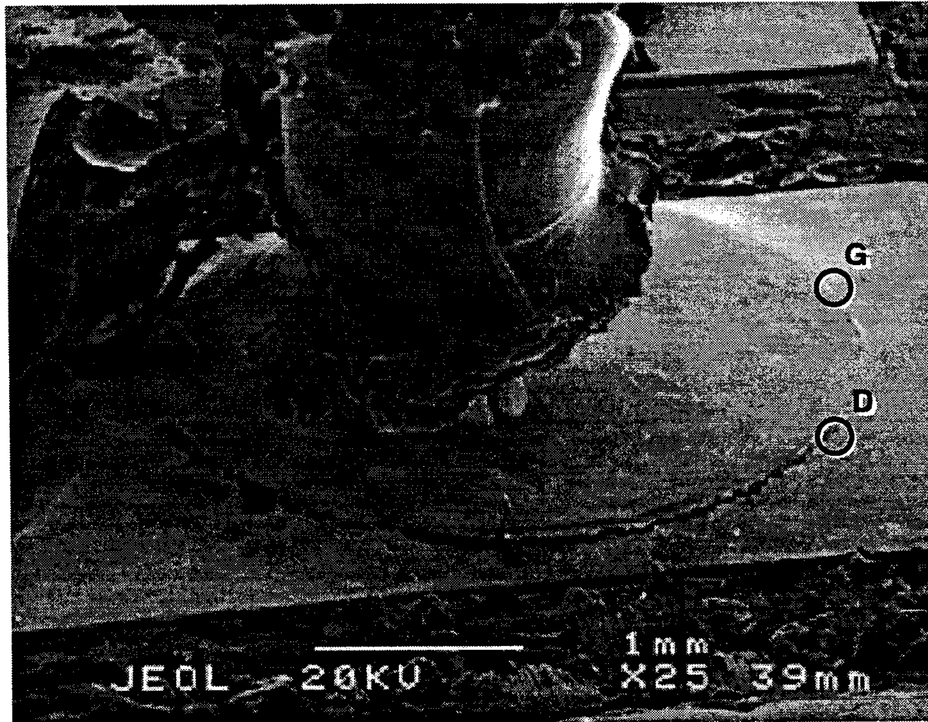

(a)

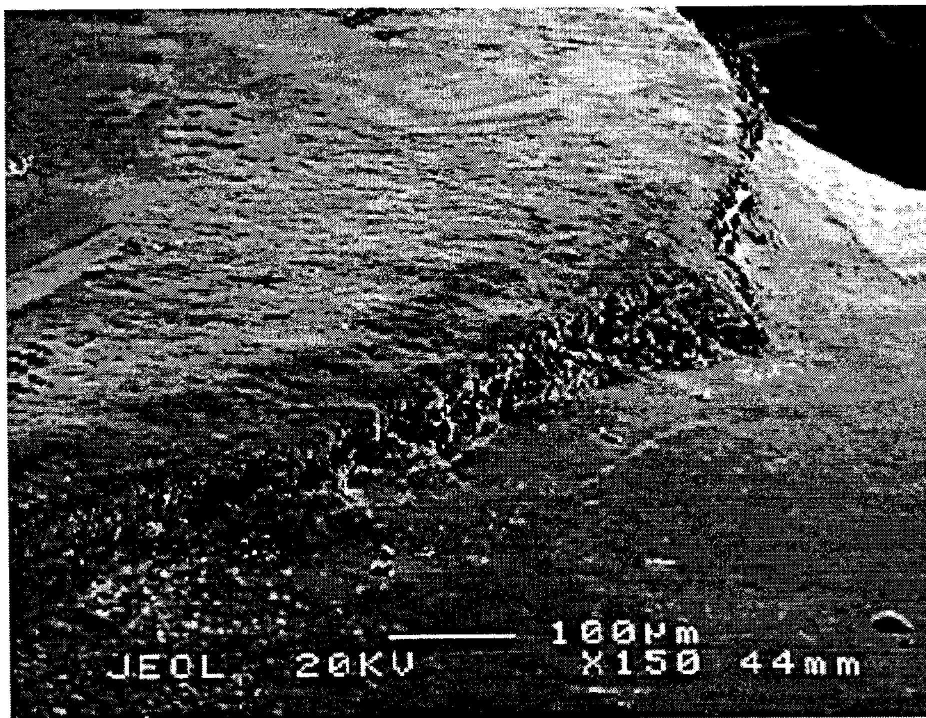

(b)

Figure 27. (a) Scanning electron micrograph of the top side of a solder joint from the unit serial number 65517 of the MC1814 assembly. Locations for higher magnification images have been noted; those regions are shown in (b) as "G" and (c) as "D".

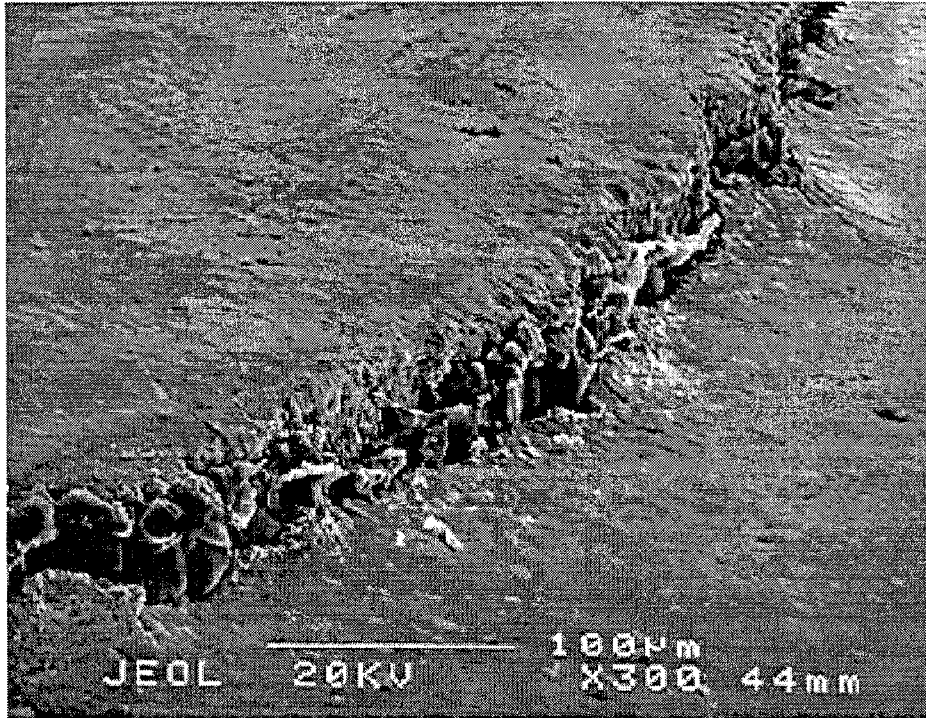

(c)

Figure 27. (Continued). (a) Scanning electron micrograph of the top side of a solder joint from the unit serial number 65517 of the MC1814 assembly. Locations for higher magnification images have been noted; those regions are shown in (b) as "G" and (c) as "D".

micrographs of Figure 29, there is no apparent flow of solder under the flange of the sleeve; this fact appeared to be the case in more instances than not. This series of micrographs was selected because they represent the varying degrees of crack progression that was observed between the eyelet and the pad. In the case of Figure 29a, no cracking was observed. Some limited crack propagation was recorded in Figure 29b, while the joint in Figure 29c had completely cracked through the section. Observation of these joints as well as others revealed that, in general, the extent of cracking was determined by the amount of solder in the joint. That is, the greater was the amount of solder, the lesser was the extent of cracking.

An investigation was performed to determine the source of the cracking. The cracks did not appear to be caused by lead clipping after the joints had been made. This scenario was discounted because additional evidence of overloading such as tearing of the solder at the top of the solder/lead fillet was not observed. The more likely scenario is that of fatigue damage to the solder due to thermal expansion mismatch between the Cu sleeve (plus solder plus lead) and the circuit board. Although not as extensively studied as thermal fatigue of solder joints in surface mount circuit boards, fatigue damage is not uncommon in through hole solder joints, particularly given the very large thermal expansion coefficient of the circuit board laminate in the z-direction (that is,

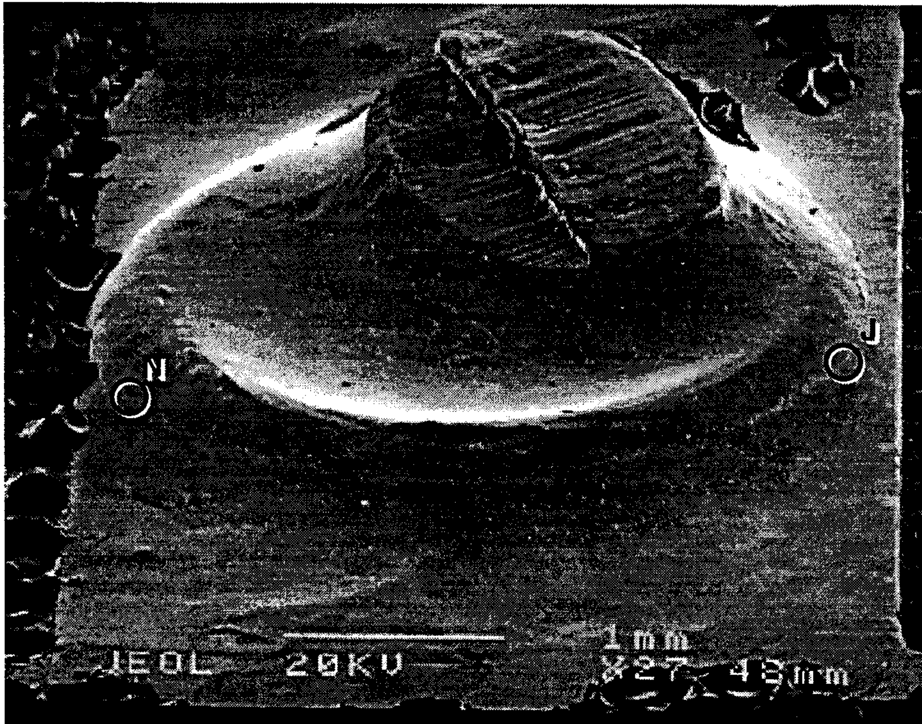

(a)

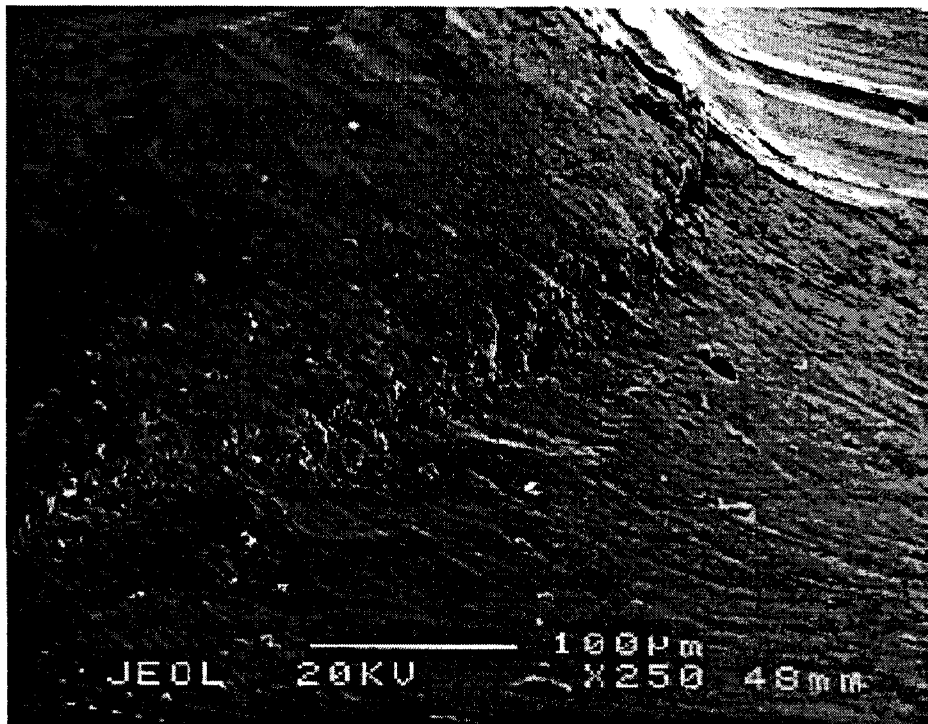

(b)

Figure 28. (a) Scanning electron micrograph of the bottom side of a solder joint from the unit serial number 65517 of the MC1814 assembly. Locations for higher magnification images have been noted; those regions are shown in (b) as "J" and (c) as "N".

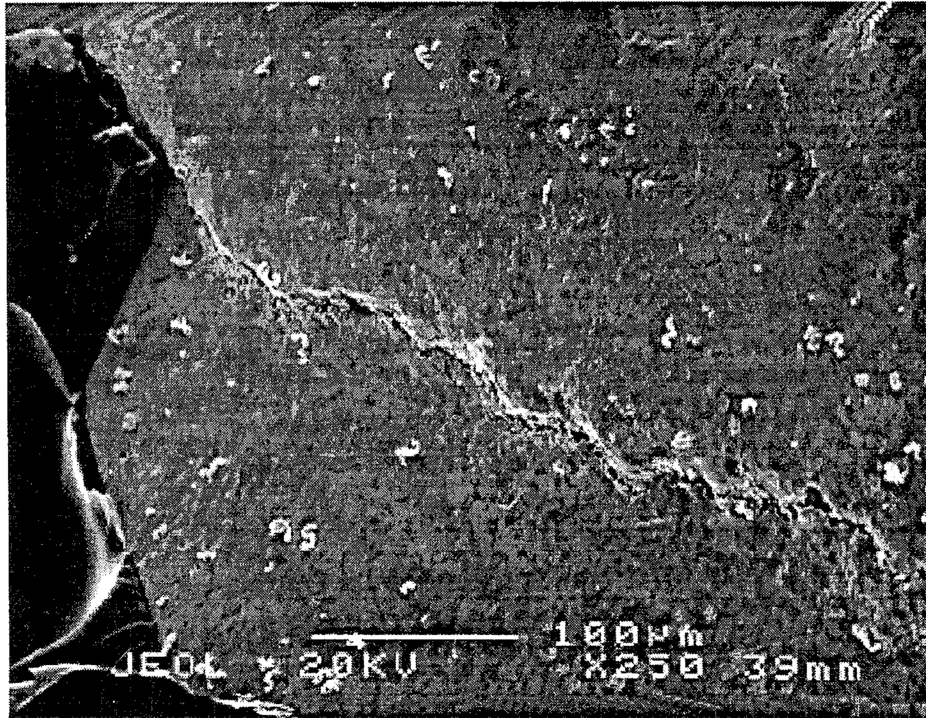

(c)

Figure 28. (Continued). (a) Scanning electron micrograph of the bottom side of a solder joint from the unit serial number 65517 of the MC1814 assembly. Locations for higher magnification images have been noted; those regions are shown in (b) as "J" and (c) as "N".

perpendicular to the board surface) as compared to the in-plane (x or y) directions. This difference arises from the fact that the weave of the laminate provides constraint in the in-plane directions, but not so in the out-of-plane direction.

The z-direction thermal expansion coefficient can be as much as an order of magnitude greater than the corresponding x and y directions[17]. Values of 100 to 200 ppm/°C are not uncommon. By contrast, the thermal expansion coefficients of Cu and 63Sn-37Pb are 17 ppm/°C[11] and 21 ppm/°C[11], respectively. The difference in expansion coefficients, coupled with the relatively large thickness of the board (3.18 mm), results in a potentially large relative displacement between the sleeve and the circuit board laminate. As a result, a substantial residual stress can build-up in the solder joint. For example, let it be assumed that during the solder assembly, the joint "area" (sleeve and immediate laminate volume) reaches a temperature commensurate with the soldering process. Upon cooling of the joint, the Cu sleeve will contract a distance, Δl , determined by the following equation:

$$\Delta l = \alpha \, \Delta T \, l$$

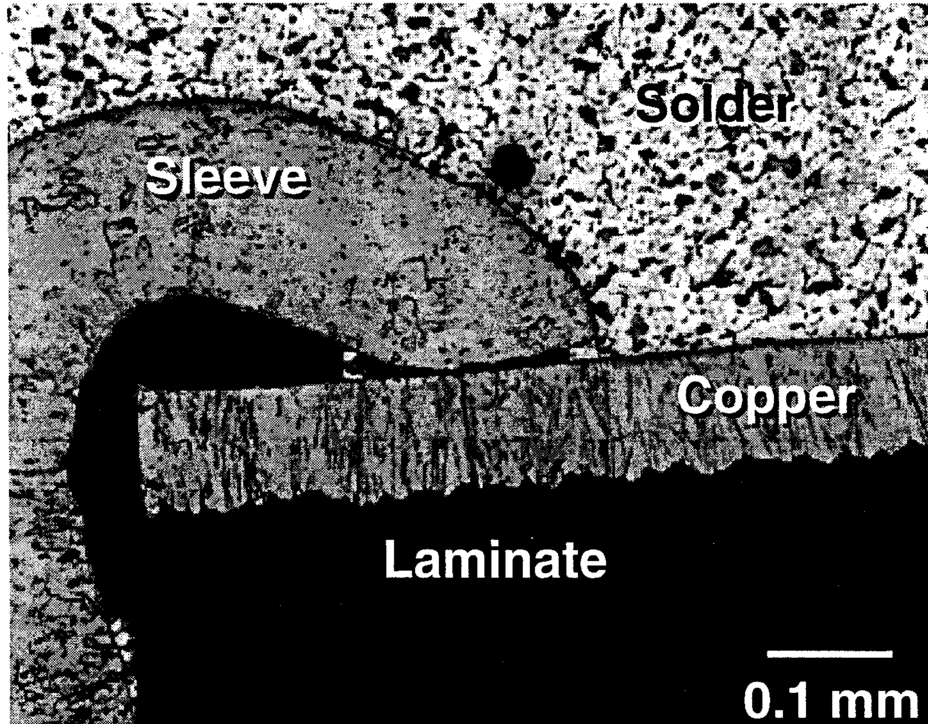

Figure 29a. Optical micrograph from one quadrant of a unit #65517 solder joint at the point where the sleeve ends on the surface at the conductor.

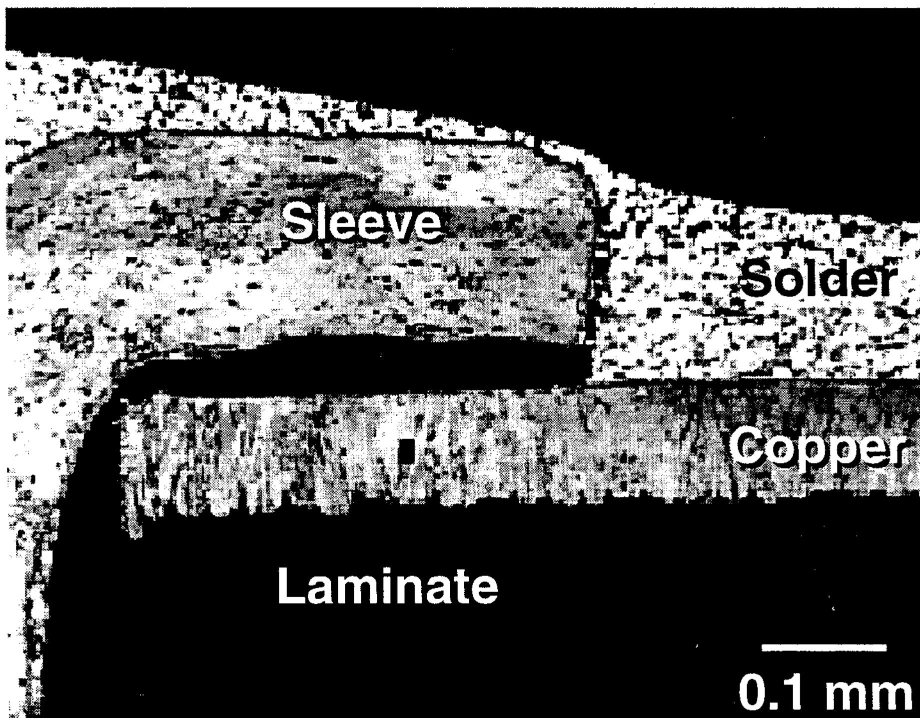

Figure 29b. A second quadrant showing partial cracking of the sleeve-to-conductor surface solder joint.

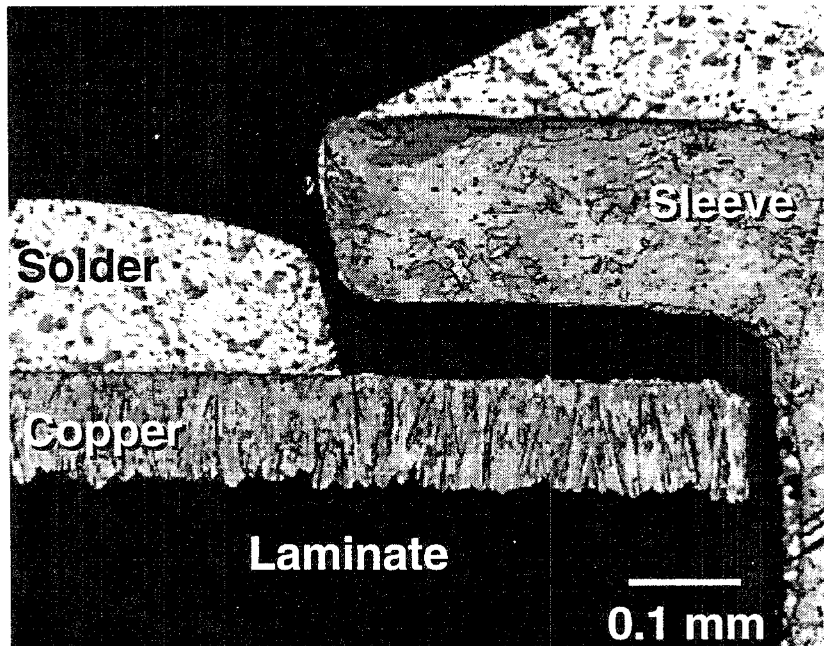

Figure 29c. A third quadrant in which complete cracking of the connection has occurred.

where α is the thermal expansion coefficient; ΔT is the temperature excursion; and l is the circuit board thickness. However, until the solder joint has solidified, the eyelet, solder, and printed circuit board are free to contract, unconstrained. A restraint on the mutual contractions, and hence the built-up of residual stresses, will begin as soon as the temperature has dropped past 183°C, the solidification temperature of the solder. Therefore, ΔT will equal (183°C - 20°C), or 163°C. The Cu eyelet will contract a distance of 0.0087 mm (3.5×10^{-4} in.). The printed circuit board would contract (given α = 200 ppm/°C) of 0.10 mm (4.1×10^{-3} in.), which is greater by an order of magnitude than that of the Cu eyelet.

The difference in displacement can then be used to determine the shear stress in the solder. That difference, Δx, was 0.94 mm (3.7×10^{-3} in.). It will be assumed that all of the strain took place at one surface. In order to determine a shear strain the at the solder experienced, a characteristic distance, x, over which deformation took place was determined to be approximately 0.127 mm (0.005 in.) from the geometry at the eyelet/pad interface. The shear strain was calculated from the expression:

$$\gamma = \Delta x / x$$

where γ is the shear strain; Δx is the displacement; and x is the "characteristic distance" equal to 0.127 mm. The computed shear strain of 0.75 is very large. This level of strain would clearly result in a shear stress level that exceeds the yield stress of the solder. Therefore, this calculation indicates that, while cyclic thermal fatigue from the service environment may have provided some limited contribution to crack propagation, the cooling cycle from the initial joint formation provided a single, overload stress that was most likely responsible for the fracture at the eyelet/pad solder joint.

The consequences of crack formation at these locations in the joint can be potentially serious. A complete loss of electrical continuity would require that the solder joint be fully cracked around the circumference of the hole on one of the two sides of the circuit board, causing the sleeve to lose contact with the Cu pad. The scanning electron micrographs in Figures 27 and 28 clearly showed that cracking could readily take place around the entire circumference of the joint. Loss of contact between the eyelet and the pad was observed in a number of solder joint cross sections (optical micrographs) in which cracking had taken place. Similar thermal expansion mismatch cracking experienced with PIN diodes showed complete electrical failure[18,19]. Therefore, the loss of electrical continuity in the joints was considered as a potential reliability problem with the MC1814 solder joints.

In addition to the solder cracking associated with the Cu sleeve, the remaining attributes of the joints were examined. Overall, the workmanship was very good. Adequate solder was present on both the top and bottom locations of the joint. As noted earlier, there was no indication of corrosion having taken place anywhere in the joints; also, flux residues were not observed. Some small voids were observed in the joint. Those voids were either associated with stranded wire leads or were found attached to the barrel walls. When stranded wire is used rather that solid leads, a greater amount of flux becomes included in the pre-soldered joint due to capillary retention of the flux liquid between the individual strands of the lead. Volatilization of this excess flux increases the likelihood that voids will form within the joint, specifically in the gap and between the strands. The extent of void formation would not jeopardize the mechanical or electrical performances of the joints, and was not entirely unexpected.

2.2.2.2 Quantitative Assessment - Intermetallic Compound Layer Thickness

The solder joints from six units were evaluated. Shown in Figure 30 is an optical micrograph of the intermetallic layer of the M1B solder joint at the solder/copper land interface. The microstructure is very similar to those noted on the MC2839 unit; there were no unusual features to the morphology. The composition of the layer appears to be entirely Cu_6Sn_5. Shown below in Table 10 are the mean intermetallic compound layer thicknesses, standard deviations, and 95% confidence intervals for the intermetallic compound layer thicknesses of from position (I) (barrel wall) and the two positions (III), A and B (copper land).

The magnitudes of the intermetallic compound layer thicknesses were comparable to those values observed in present-day, as-fabricated hardware, suggesting that the units did not experience any "significant" thermal excursions. The thicknesses would clearly not jeopardize the electrical or mechanical integrity of the solder joints.

The mean layer thickness when all of the data were combined (thereby, representing the MC1814 component as a whole) was 1.010 μm; the standard deviation was 0.053 μm; and the 95% confidence interval, 0.007 μm. These same parameters for the previously discussed MC2839 component were: mean, 0.86; standard deviation, 0.35; and the 95% confidence interval, 0.04. The latter standard deviation and confidence interval data demonstrated a greater degree of variability for solder joints in the MC2839 parts as compared to the MC1814 parts.

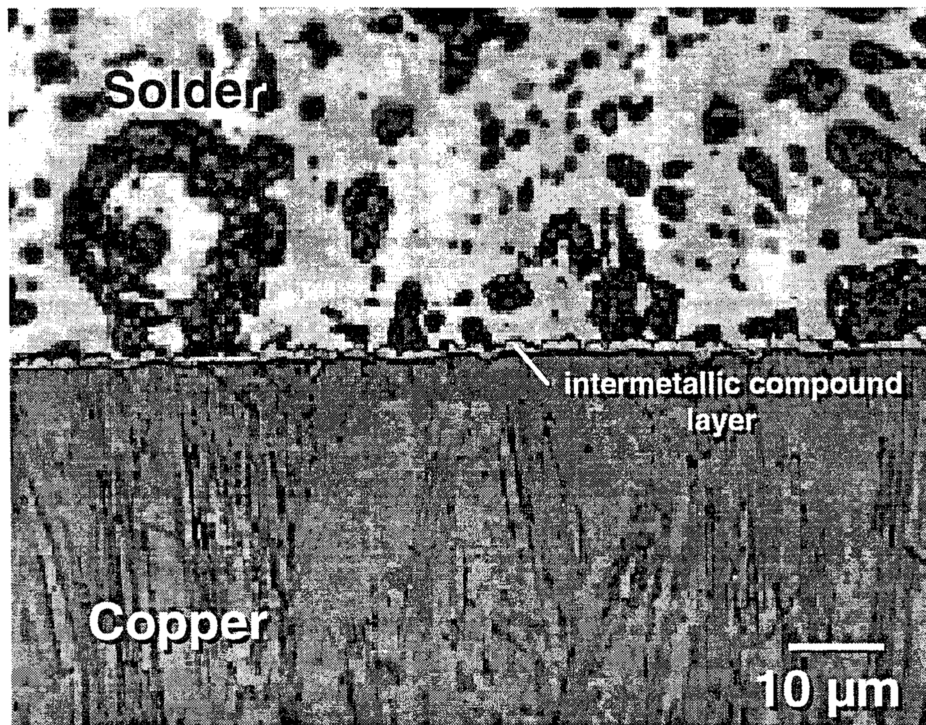

Figure 30. Optical micrograph of the intermetallic compound layer in the M1B solder joint (unit #65517) at the solder/copper land interface (location III).

The analysis of the individual units began by examining whether any significant intermetallic compound layer thickness differences existed between the various positions in each respective joint. The first evaluation was performed by a pairwise comparison of the two land positions on the solder joints, III(A) and III(B) (excluding the #65517 unit). As was previously described, the hypothesis of same or different thickness means was assessed by the Student's t-test (95% confidence interval), the particular test being determined by the similarity of the variances of the two data sets as determined by the F-test parameter. Based upon this analysis, it was observed that in four of five units, the mean layer thicknesses of the A and B positions were not statistically different. The exception was unit #82035, in which the intermetallic compound layer thicknesses at the III(A) and III(B) positions were 0.888 μm and 1.149 μm, respectively, from amongst the joints. In the cases of all five units, the variances were equal (F-test) so that thickness variations showed no significant difference between the two positions. Shown in Table 11 below is a summary of the layer thicknesses for the III(A) and III(B) positions, the respective data being combined from all of the solder joints in a given unit.

Table 10. Intermetallic Compound Layer Thickness MC1814 Junction Box Circuit Board

Unit #	Solder Joint/Location	Mean Thickness (μm)	Standard Deviation (μm)	Confidence Interval (95%) (μm)
22022	M1/I	0.585	0.225	0.122
	M1A/III	0.972	0.459	0.250
	M1B/III	1.082	0.337	0.183
	M2/I	0.909	0.415	0.226
	M2A/III	0.684	0.164	0.089
	M2B/III	0.768	0.201	0109
	S1/I	1.218	0.608	0.330
	S1A/III	0.945	0.380	0.207
	S1B/III	1.097	0.400	0.217
81735	M1/I	1.138	0.416	0.226
	M1A/III	0.905	0.270	0.147
	M1B/III	1.165	0.538	0.293
	M2/I	2.032	0.615	0.334
	M2A/III	1.040	0.658	0.358
	M2B/III	2.223	1.045	0.568
	S1/I	1.371	0.694	0.377
	S1A/III	1.946	0.790	0.429
	S1B/III	1.645	0.851	0.462
65517	M1A/I	0.909	0.480	0.297
	M1A/III	0.823	0.248	0.154
	M1B/I	0.697	0.274	0.170
	M1B/III	1.013	0.434	0.269
	M2A/I	1.310	0.713	0.442
	M2A/III	1.453	0.386	0.239
	M2B/I	1.346	0.870	0.539
	M2B/III	1.014	0.430	0.267
	S1/I	1.241	0.531	0.329
	S1/III	1.205	0.417	0.259
51470	M1/I	1.043	0.279	0.152
	M1A/III	1.358	0.851	0.462
	M1B/III	1.108	0.641	0.349
	M2/I	0.716	0.204	0.111
	M2A/III	0.865	0.424	0.230
	M2B/III	1.015	0.608	0.331
	S1/I	0.889	0.366	0.199
	S1A/III	1.000	0.459	0.250
	S1B/III	0.808	0.355	0.193

Table 10. Intermetallic Compound Layer Thickness MC1814 Junction Box Circuit Board (Continued)

Unit #	Solder Joint/Location	Mean Thickness (μm)	Standard Deviation (μm)	Confidence Interval (95%) (μm)
50462	M1/I	0.745	0.238	0.129
	M1A/III	0.658	0.275	0.150
	M1B/III	1.000	0.332	0.181
	M2/I	0.809	0.504	0.274
	M2A/III	0.812	0.299	0.162
	M2B/III	0.806	0.296	0.146
	S1/I	0.589	0.281	0.153
	S1A/III	0.919	0.308	0.167
	S1B/III	0.741	0.244	0.133
82035	M1/I	1.235	0.294	0.160
	M1A/III	0.950	0.420	0.228
	M1B/III	1.142	0.352	0.191
	M2/I	0.807	0.363	0.197
	M2A/III	0.591	0.148	0.081
	M2B/III	1.237	0.377	0.205
	S1/I	1.520	0.361	0.197
	S1A/III	1.124	0.320	0.174
	S1B/III	1.069	0.545	0.296

Table 11. Intermetallic Compound Layer Thickness for MC1814 Junction Box Circuit Boards - Unit Summaries for III Locations (A or B)

Unit #	Solder Joint/Location	Mean Thickness (μm)	Standard Deviation (μm)	Confidence Interval (95%) (μm)
22022	A	0.868	0.372	0.117
	B	0.982	0.350	0.110
50462	A	0.796	0.306	0.096
	B	0.849	0.298	0.094
51470	A	1.074	0.629	0.198
	B	0.977	0.550	0.173
81735	A	1.297	0.759	0.238
	B	1.678	0.926	0.291
82035	A	0.888	0.382	0.120
	B	1.149	0.428	0.134

The similarity of intermetallic compound layer thicknesses (location IIIA only) amongst solder joints in the same unit was analyzed by testing the hypothesis of equivalent means using the Student's t-test. Equivalence of variance in each pair was initially tested (F-test) to determine the appropriate t-test for use on the data pair. Shown in Table 12 is the frequency of equivalent means per total number of pair-wise combinations. There were six possible combinations for all, but unit #65517 in which there were ten such pairs.

Table 12. Intermetallic Compound Layer Thickness MC1814 Junction Box Circuit Boards Frequency of Equivalence, All Joints per Unit, Location IIIA

Unit #	Equal Means-Frequency
22022	3/6
50462	6/6
51470	6/6
65517	6/10
81735	3/6
82035	4/6

The data in Table 12 documented the extent of similarity of mean thicknesses between solder joints in a given unit varied considerably, depending upon the particular unit that was analyzed. This variability clearly underscores the statistical approach towards the quantitative analysis of the solder joint properties; however, from the applications point-of-view, given the relatively thin layers that were observed, the spread in intermetallic compound thickness values would not have impacted the reliability of those solder joints, if they were to have continued in service. Combined, 28 or 40 total comparisons (70%) showed equivalent layer thicknesses.

In order to determine the extent to which the layer thicknesses differed between units, a comparison was performed amongst all possible unit pairings. Only position III(A) was included in the analysis, because both A and B locations appeared to be similar in all but one unit. The hypothesis of equivalent means was tested, using the Student's t-test, based upon a 95% confidence interval. The equivalence of variance was computed for each sample pair by the F-test so that the correct t-test (for equivalent versus non-equivalent means) would be used. The data for unit #65517 were also included.

The t-test analyses showed that, of all possible pair-wise combinations (15) from amongst the five units, eight of the fifteen had the same means and seven had dissimilar means. A further analysis was made to determine which unit(s) differed from amongst the others. In the case of pairs with dissimilar means, the units #81735 and #65517 had mean thicknesses that were always greater than those of their counterparts from the other units,

that is, a frequency of three (3) instances. The unit #50462 exhibited all three (3) instances of having a mean less than the counterpart unit. On the other hand, from the category of pairs having the similar means in all of three (3) instances, units #22022, #51470, and #82035 were so characterized. Therefore, a summary of the six units would be described as follows: Unit #50462 had the significantly lowest intermetallic compound layer mean thickness (0.796 μm); units #81735 and #65517 had the highest values (1.297 μm and 1.100 μm, respectively, and were statistically similar); and units #22022, #82035, and #51470 were of similar mean thicknesses (0.867 μm, 0.888 μm, and 1.074 μm, respectively), in the middle of the group.

Lastly, the behavior of the variances (representing the scatter in the thicknesses) was evaluated. For nine of the 15 pair analyses, the F-test concluded that the variances were equal. Also, there did not appear to be a trend between the occurrence of equivalent variances and equal mean thickness values.

2.2.2.3 Quantitative Assessment - Pb-rich Phase Particle Size Distribution

The Pb-rich phase particle distribution was determined at locations (II) in each of the top and bottom solder joint fillets (Figure 11) as well as at a third location within the hole for five of the six units (unit #65517 being the exception). Shown in Figure 31 is an optical micrograph of the microstructure of the M1B solder joint from unit #65517. Along with the Pb-rich phase particles, there were observed small particles of Cu_6Sn_5 intermetallic compound distributed in the matrix. The source of these particles was Cu dissolved by the molten solder during formation of the joint. The Cu and Sn precipitated as the intermetallic phase upon cooling of the joint. Given the isolated occurrence of these particles in the solder microstructure, they presented no complications to the functionality of the joint, nor indicated unusual erosion of circuit board Cu features as a consequence of the soldering operation. The size distribution of the Pb-rich phase particles (in an area size of mm^2) is illustrated by the example from the S1 joint, shown in Figure 32. For example, those data show that approximately 93% of the particles were less than 5×10^{-5} mm^2; or, assuming spherical shape for illustrative purposes only, the particle diameters, d, would be $0 \leq d \geq 8$ μm. The mean and standard deviation of the particle distributions in Figure 32 were 1.4×10^{-5} mm^2 (d = 4.2 μm) and 3.6×10^{-5} mm^2 (d = 6.7 μm), respectively. The distributions shown in Figure 32 were representative of the quantitative analyses of the all of the solder joints in the MC1814 units.

In the case of the five units for which the particle size distribution measurements were made at two fillet locations, one at the top of the joint and the other at the bottom of the joint, a pairwise comparison of the particle sizes was made using the F-test/t-test procedure. Of the 15 such comparisons, 13 such pairs (87%) indicated equality of the mean Pb-rich phase particle diameters. Further, similar comparisons were also made between the solder in the fillets and that contained within the hole. That evaluation would be comprised of two such comparisons per joint, or six per unit. The results are listed in Table 13.

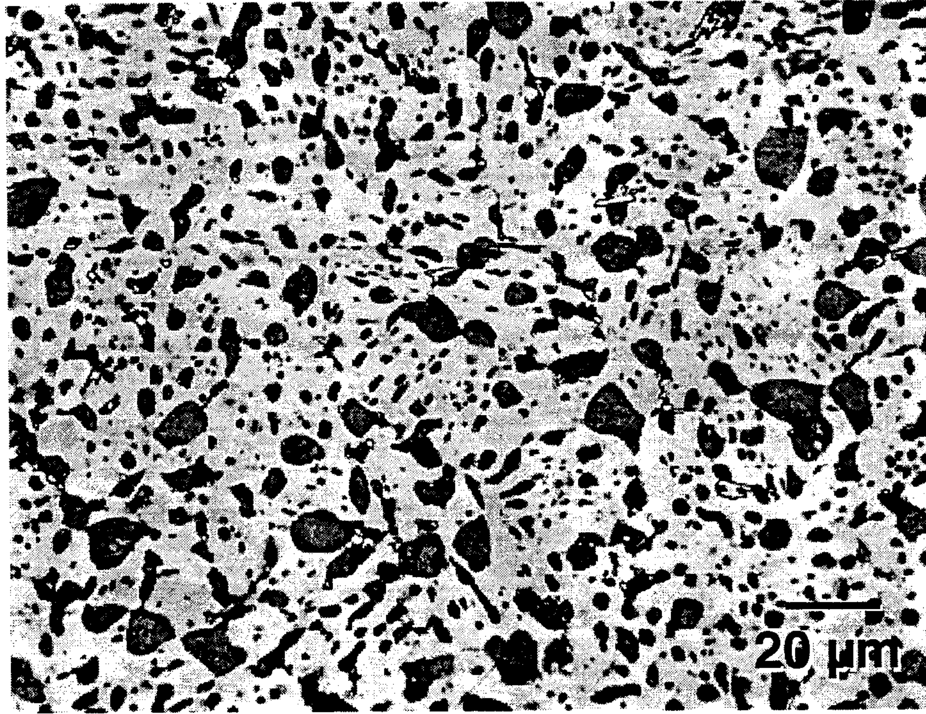

Figure 31. Optical micrograph of the solder microstructure in the M1B solder joint (unit #65517) in the fillet region (II).

There was variability between the different units; overall, a pairwise equality was observed in 67% of the cases. Therefore, the particle size data suggest that there is no significant difference in Pb-rich particle characteristics between the two fillet locations on the joint. However, the same conclusion does not appear be true when a comparison was made of the mean particle sizes between the fillets and the hole locations. In those cases, the pairwise equivalents dropped to 67% of the cases. When the ten cases of inequality were examined, it was observed that in seven of the ten cases, the particle size is larger in the hole (H) than at the fillets locations (A or B). This trend makes intuitive sense, because the hole interior would be expected to experience slower cooling rates than those found in the fillets at the circuit board surfaces, thereby resulting in a relatively larger mean particle size in the former case. However, the pairwise data indicate that this artifact was not very strong.

The graph in Figure 33, which shows the mean and ± one standard deviation of the Pb-rich particle sizes for the top side fillet location (A) from the joints that were examined from the MC1814 units, illustrates the relative variation of the mean values. The mean particle size from all of the MC1814 solder joints combined was computed to be $15.3 \pm 2.7 \times 10^{-6}$ mm^2 (4.4±1.8 µm).

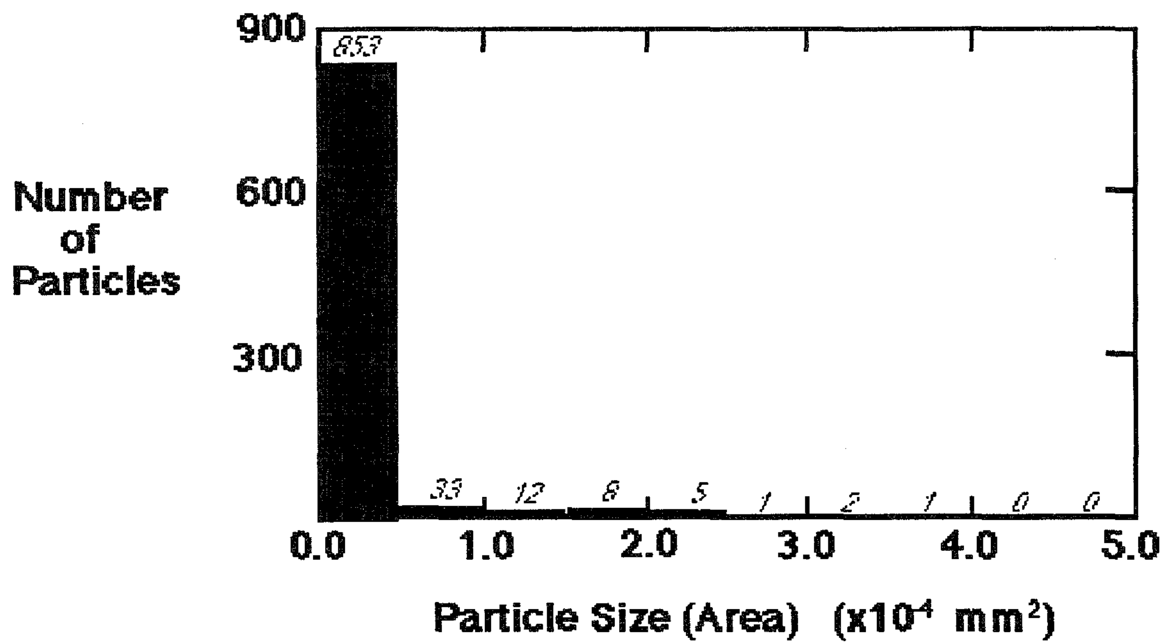

(a)

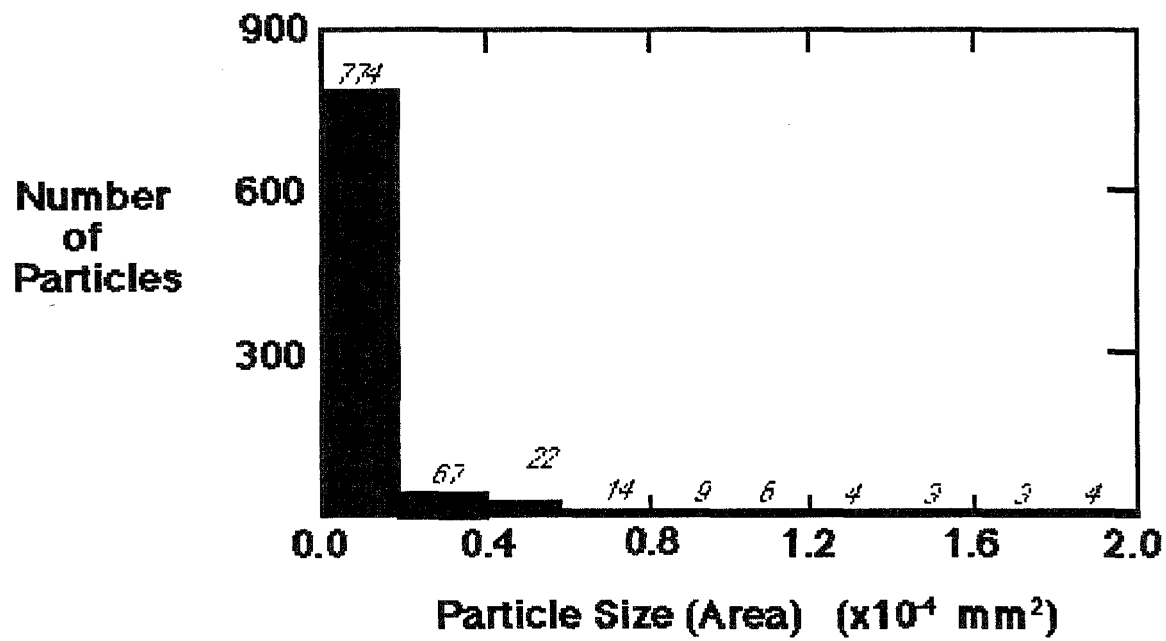

(b)

Figure 32. Pb-rich phase particle frequency distribution for the (II) regions of the S1 solder joint in the MC1814, #65517 unit. The ranges are: (a) 0 - 5 × 10^{-4} mm^2; (b) 0 - 2 × 10^{-4} mm^2; (c) 0 - 2 × 10^{-5} mm^2; and (d) 0 - 2 × 10^{-6} mm^2.

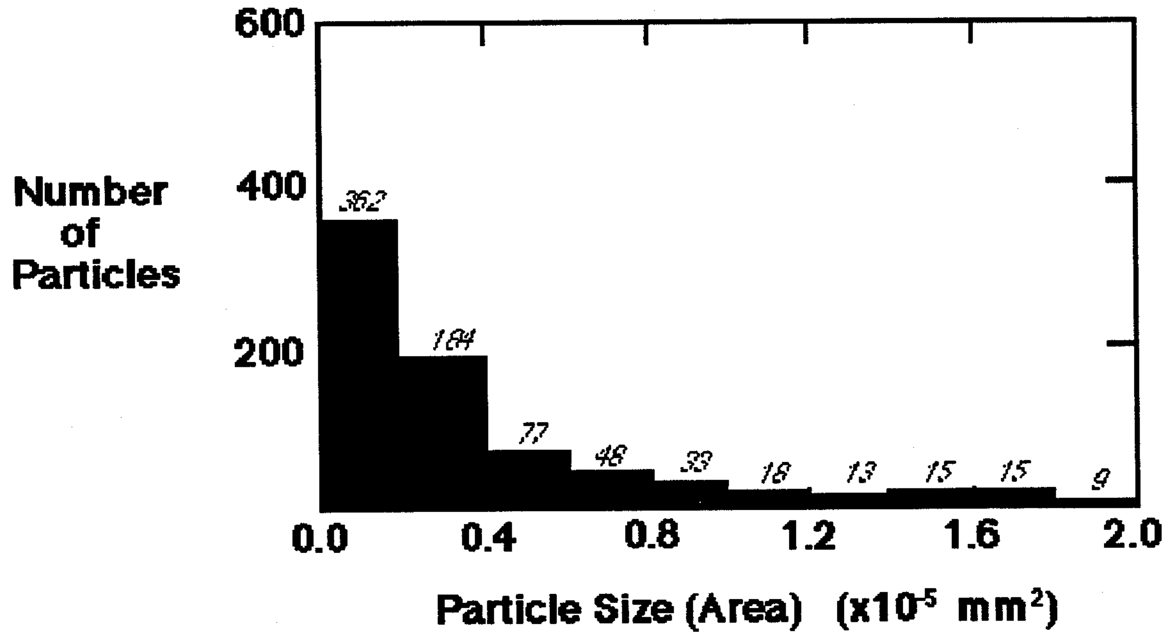

(c)

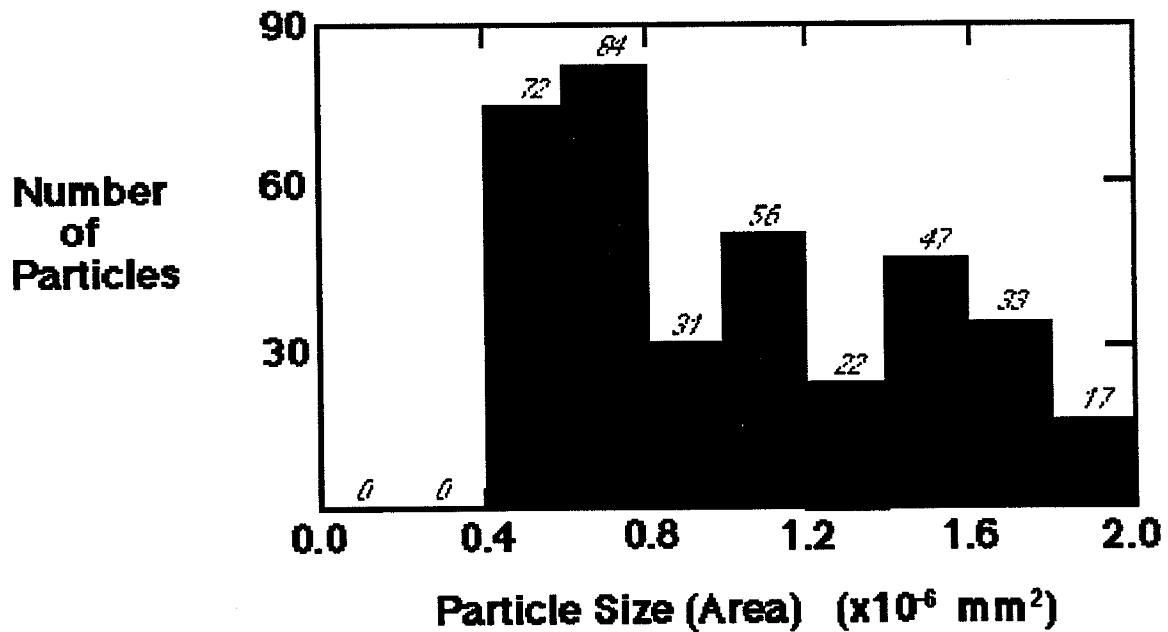

(d)

Figure 32. (Continued). Pb-rich phase particle frequency distribution for the (II) regions of the S1 solder joint in the MC1814, #65517 unit. The ranges are: (a) 0 - 5 × 10^{-4} mm^2; (b) 0 - 2 × 10^{-4} mm^2; (c) 0 - 2 × 10^{-5} mm^2; and (d) 0 - 2 × 10^{-6} mm^2.

Table 13. Pb-Rich Particle Phase Distribution MC1814 Junction Box Circuit Boards Frequency of Equivalence of the Mean Size of Paired Locations (A or B, versus H) of Unit Joints

Unit #	Equal Means-Frequency
22022	6/6
50462	6/6
51470	4/6
81735	3/6
82035	1/6

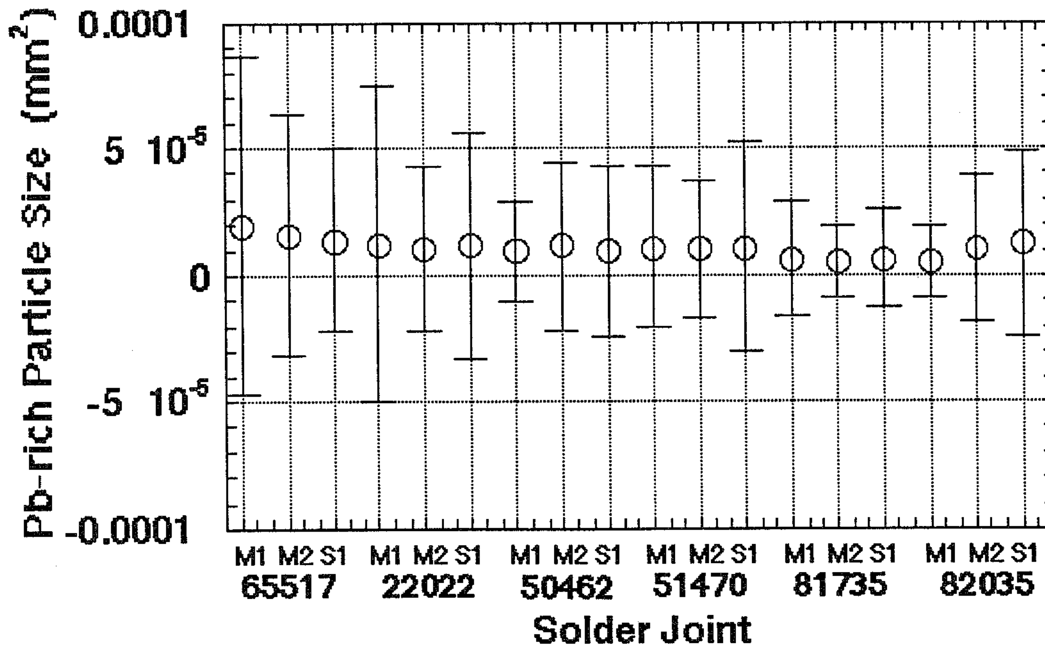

Figure 33. Pb-rich phase particle sizes (mean and ± one standard deviation) for each of the joints in the MC1814 units.

Finally, it is interesting to compare the MC1814 Pb-rich particle size parameters with those from the MC2839 parts. Recall that the mean particle size for the MC2839 solder joints was $9.8 \pm 3.9 \times 10^{-6}$ mm^2 as compared to $15.3 \pm 2.7 \times 10^{-6}$ mm^2 for the MC1814 unit. In the absence of rigorous statistical analyses such as those used thus far, simply comparing the mean values and variations represented by the scatter terms suggests that the two values may indicate a substantive difference between the MC2839 and MC1814 systems. Two potential sources for the different particle sizes are:

(1) different microstructural development of the joints due to variations in manufacturing practices or stockpile environments, or (2) variations in the composition of the solders used to make the joints.

Addressing point (2), the composition of the solder used for the MC1814 was computed from the volume percent (inferred from the area percent) of Pb-rich phase particles as measured from all of the joints. This computed solder composition for the MC1814 joints was 57Sn-43Pb, which was not significantly different from the composition, 59Sn-41Pb, computed for the MC2839 joints. Therefore, the larger Pb-rich phase particle size of the MC1814 solder joints appears to be a consequence of microstructural development in the solder (point (1) above). Assuming similar manufacturing practices (i.e., cooling rates of the solder during joint fabrication) and service temperatures in the field, the difference in Pb-rich particle size may rest upon the fact that the MC1814 components (B57) were older than the MC2839 parts (W70-1). In fact, the intermetallic compound layer data would also support this assessment, because the mean layer thicknesses from all of the joints of the MC1814 units were 1.010 μm (95% CI of 0.007 μm) as compared with a smaller value of 0.86 μm (95% CI of 0.04 μm) for the younger MC2839 joints. The future availability of a baseline having both parameters (i.e., intermetallic compound layer growth and Pb-rich particle coarsening) as a function of aging conditions will allow confirmation of this hypothesis.

The spread in the particle size was examined as a function of the mean particle size. As noted earlier, it would be expected that should thermally-induced coarsening take place to the Pb-rich phase, larger particles would grow at the expense of smaller ones until, ideally, upon completion there would be a relatively few particles left, all being of the same size. Shown in Figure 34a is the data spread represented by the standard deviation as a function of the mean particle size. The spread increased with mean particle sized as determined by a linear regression fit (R^2=0.74). However, in order to avoid any coupling between the standard deviation and the mean particle size, the standard deviation data was normalized as the percent error (standard deviation divided by the mean value) and this result is shown in Figure 34b. A linear regression analysis resulted in an R^2 value of 0.04. Therefore, there was no correlation between the different mean particle size values and the scatter to suggest that the variation was caused by different thermal environments. Rather, the different means of Pb-rich phase particle sizes from amongst the different joints reflected a random variation, possibly arising at the time of manufacture of the joint.

A comparison was made between the MC1814 Pb-rich phase particle data and that from the MC2839 units. That analysis showed that the trends of "standard deviations versus mean Pb-rich particle size" were similar (Figure 34b versus Figure 19b, respectively). The data in both Figures 19b and 34b express the same conclusion, that the differences in particle size distributions from solder joints in different units of the respective MC1814 and MC2839 systems did not support the cause as being that of differing thermal aging environments.

A confirmation that the 500x magnification of the photographs did not affect the Pb-rich phase particle measurements was obtained for the MC1814 solder joints by examining the Pb-rich phase particle distribution (total area %) as a function of mean

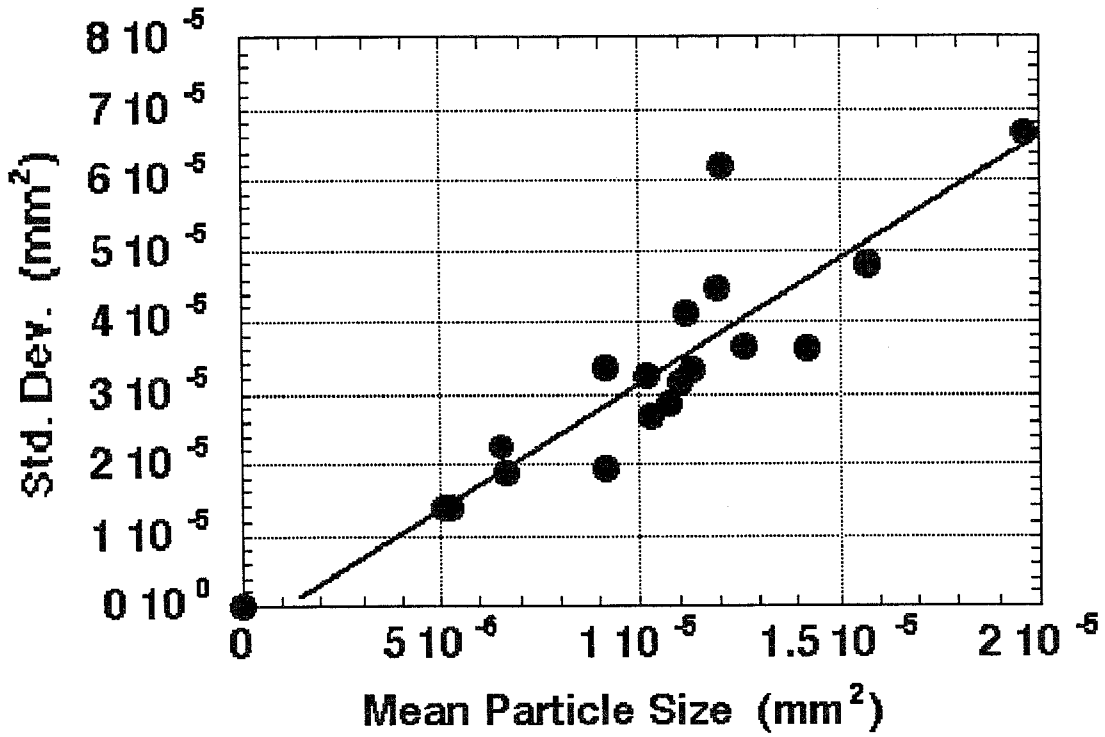

(a)

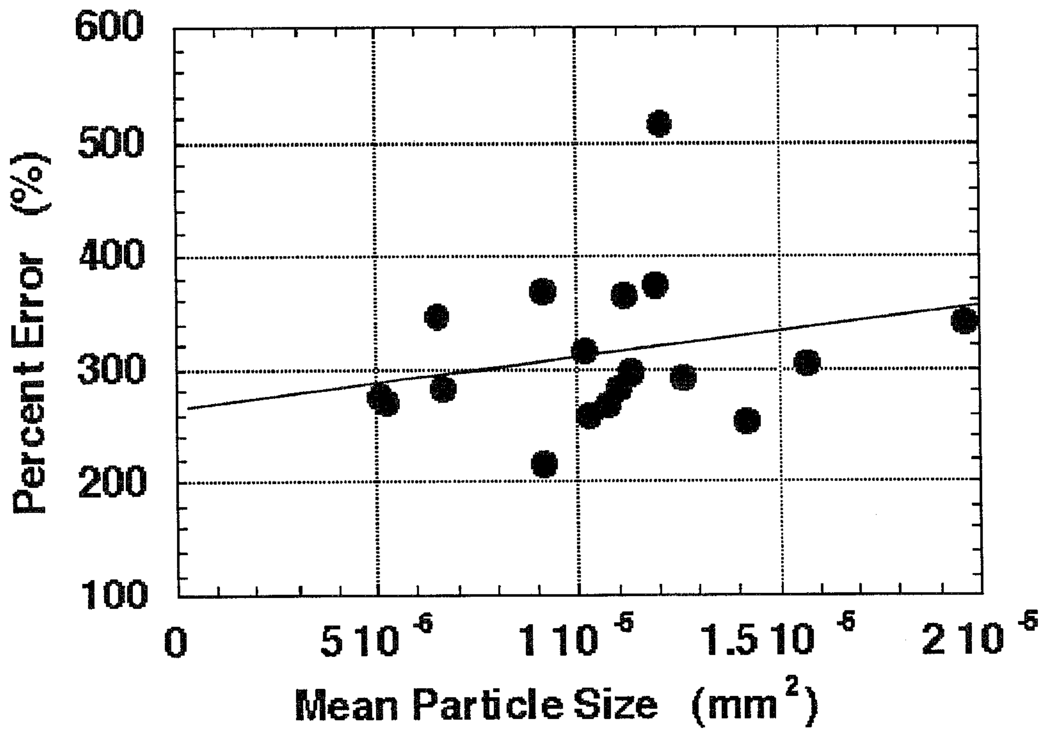

(b)

Figure 34. (a) Standard deviation and (b) percent error as a function of mean Pb-rich phase particle size for the data compiled from the MC1814 units.

particle size. This analysis was deemed pertinent because of the overall larger particle sizes observed in the MC1814 solder joints as compared with those measured for the MC2839 solder joints. An absence of any such influence would be noted by a lack of correlation between the two parameters. Shown in Figure 35 is a graph of the area percent of particles versus mean particle size from each of the solder joints. A linear regression analysis of the data showed that no correlation could be found between the two parameters and such was also the case with the MC2839 solder joints (Figure 20). Therefore, the 500x micrograph sampling area did not influence the composition measurements over the range of individual solder joint mean particle sizes.

As was also done with the MC2839 solder joints, the Pb-rich phase particle size distribution was examined with respect to the intermetallic compound layer thickness to determine whether any correlation existed between those two parameters. Again, such a correlation may be expected if variations in the two parameters resulted from exposure of the solder joints to elevated temperature conditions; the Pb-rich particle size would be expected to coarsen and the intermetallic compound layer to thicken, concurrently. The mean particle sizes were compared with the intermetallic compound layer thicknesses at both the (I) and (III) locations. Those plots appear as Figure 36a and Figure 36b, respectively. There was no correlation between the two parameters as determined by the linear regression analysis. This result confirmed that variations in the mean particle sizes and the intermetallic compound layer thicknesses were largely random and did not reflect the exposure by the units to thermal excursions.

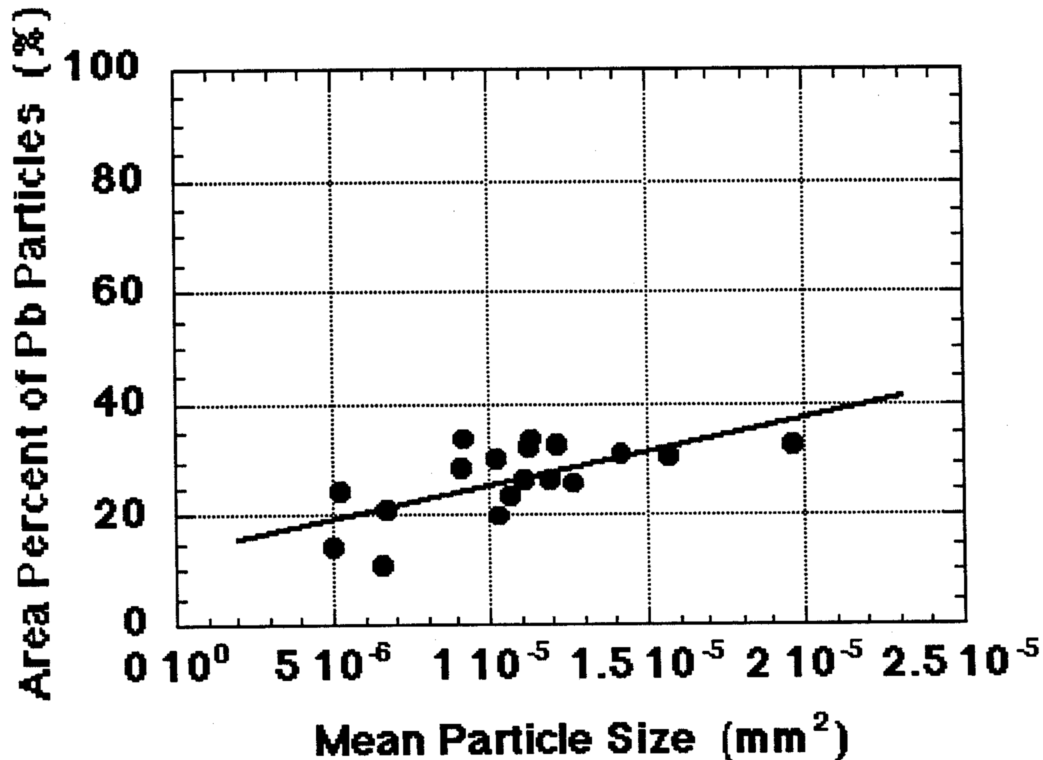

Figure 35. Area percent of Pb-rich phase versus the mean Pb-rich phase particle size for the top-side (A), solder fillet (G) location from all of the solder joints compiled for the MC1814 units.

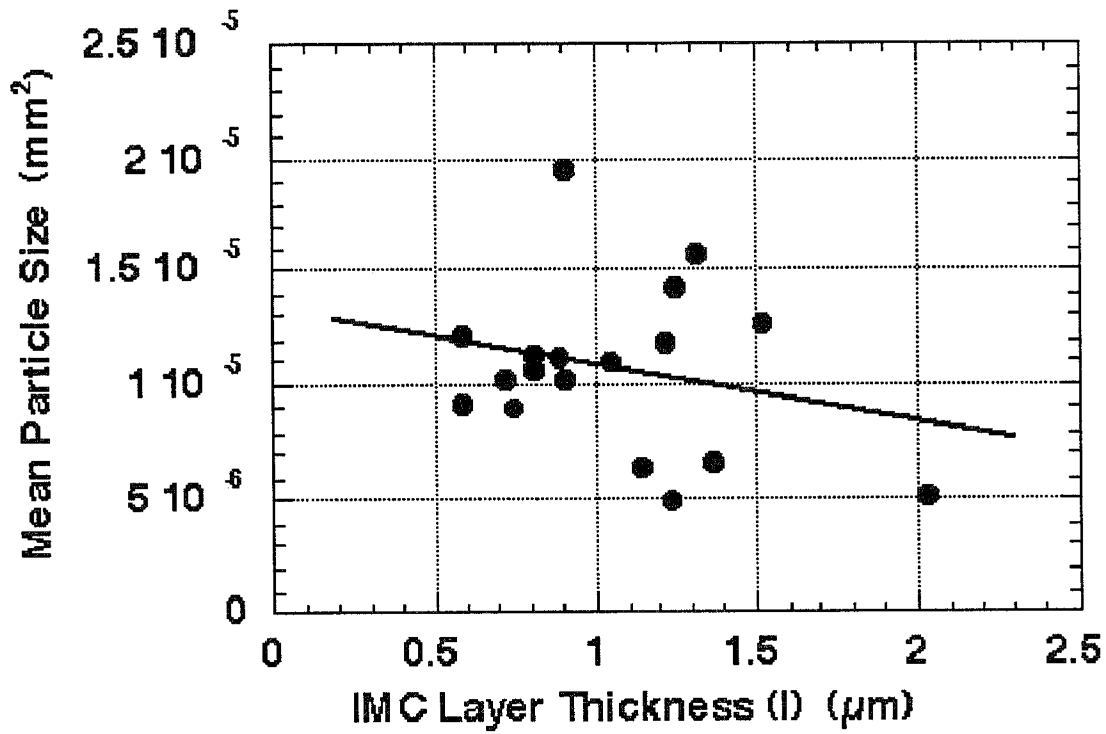

(a)

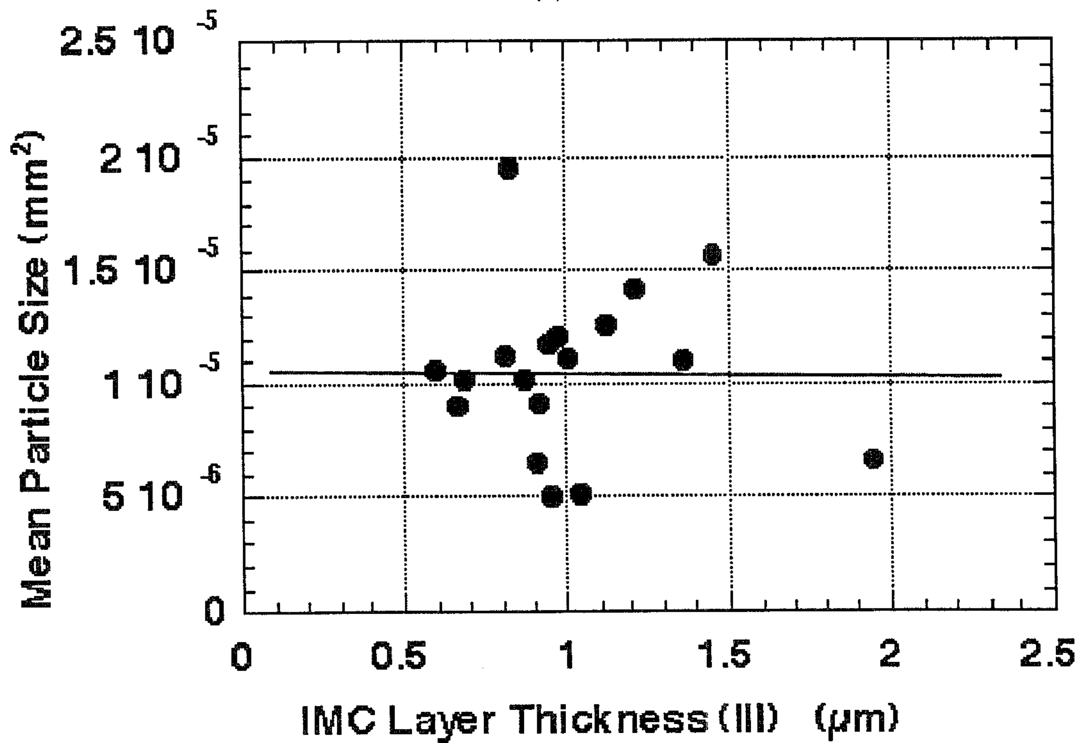

(b)

Figure 36. Mean Pb-rich phase particle size as a function of the solder/copper intermetallic compound layer thicknesses at (a) region (I) and (b) region (III).

3.0 Conclusions

1. MC1814 Interconnection Boxes from dismantled B57 bombs, and MC2839 Firing Sets from retired W70-1 warheads were obtained from the Pantex facility. Printed circuit boards were selected from these components for microstructural analysis of their solder joints. The analyses began with a qualitative assessment of the overall quality of the solder joints. Next, a quantitative analysis was performed. Two quantitative metrics were evaluated: (1) the thickness of the intermetallic compound layer that formed between the solder and circuit board Cu features, and (2) the Pb-rich phase particle distribution within the solder joint microstructure.

2. The MC2839 solder joints had very good workmanship qualities. Voids were largely absent from joints that contained a solid wire; voiding was more prevalent in those joints formed with stranded wire, but to a degree deemed typical for stranded wire joints. In neither case would the voiding have presented a significant impact on joint integrity. The intermetallic compound layer stoichiometry was determined to be that of Cu_6Sn_5. The mean intermetallic compound layer thickness for all solder joints was 0.885 µm. The values for joint locations (I) (barrel wall) and (III) (land) were 0.921 µm and 0.849 µm, respectively. The magnitude of these values did not indicate significant growth over the weapon lifetime. There was no indication of an excessive presence of Cu_6Sn_5 particles within the solder matrix, which would suggest excess heating of joint during the soldering process.

3. The size distribution of the Pb-rich phase particles for each of the joints were represented by the mean and the standard deviation. The mean particle size of the combined data was 9.85×10^{-6} mm^2. Assuming a spherical geometry, the mean particle diameter would be 3.54 µm. The joint-to-joint mean particle size variations were not due to thermal activated coarsening, but rather, were a result of random variations in the joint microstructure that probably existed at the time of manufacture.

4. The solder composition (wt.%) was computed from the Pb-rich phase particle distribution to be 59Sn-41Pb. This result indicated that the 500x images used in the particle size distribution analysis provided an adequate compromise between minimizing naturally occurring microstructural variations in particle distributions (requiring low magnification) versus the need to adequately resolve the particle by the imaging system (requiring higher magnifications).

5. No correlation was found between the mean intermetallic compound layer thickness and the mean Pb-rich phase particle size of the individual solder joints, further indicating that the joint microstructural variations were not the result of exposure to significant thermal environments.

6. The MC1814 solder joints were "through-hole" in nature; however, in place of electrodeposited Cu conducting layer used on the barrel walls, the copper sleeve ("eyelet") technology, which predated the plated through-holes of the MC2839 electronics, was used. The solder connection between the sleeve and the surface traces on the circuit boards exhibited cracking. The likelihood of loss of signal transmission between circuit board sizes as well as between the lead and either

surface was significant. Otherwise, the joints exhibited very good workmanship with no appreciable voiding and had excellent surface wetting.

7. The mean intermetallic compound layer thickness that was determined by evaluation of all of the solder joints was 1.102 μm, representing the Cu land location. The magnitude of these values did not indicate significant growth over the weapon lifetime. The intermetallic compound layer was entirely Cu_6Sn_5. There was some indication of Cu_6Sn_5 particles within the solder matrix, which would indicate excess heating of joint during the soldering process.

8. The mean particle size of the combined data was 15.3×10^{-6} mm^2. Assuming a spherical geometry, the mean particle diameter would be 4.41 μm. Trends in the joint-to-joint mean particle size variations did not indicate variations in mean particle sizes were due to thermal activated coarsening. Rather, they were a result of random fluctuations in the joint microstructure.

9. The solder composition (wt.%) was computed from the Pb-rich phase particle distribution to be 57Sn-43Pb. The data analyses indicated that the 500x images used in the particle size distribution analysis provided was adequate.

10. A comparison of the intermetallic compound layer data and Pb-rich particle size analyses of solder joints from the MC2839 and MC1814 units indicated that slightly larger values of both parameters in the MC1814 case likely reflected the longer field service lifetime of those units as compared with systems having the MC2839 assemblies. Otherwise, very similar trends in both metrics were documented for solder joints from the two MC systems.

11. ***Overall assessment.*** *The microstructural evaluation of the through-hole solder joints (intermetallic compound layer growth and Pb-rich phase particle coarsening) from the MC2839 and MC1814 components indicates that the environmental conditions to which these electronic units were exposed in the stockpile were benign with regards to solder joint aging. There was an absence of thermal fatigue damage in MC2839 circuit board, through-hole solder joints. The damage to the eyelet solder joints of the MC1814 more likely represented infant mortality failures resulting from a marginal design status of this type of solder joint design; there was no indication of traditional, thermal fatigue damage in these through-hole joints, as well. The few defects that were observed in MC2839 solder joints were largely those brought about <u>at the time of assembly (manufacture)</u> of the circuit board.*

4.0 References

[1] T. Massalski, J. Murray, L. Bennet, and H. Baker, eds., *Binary Alloy Phase Diagrams, Volume 2,* (ASM, Metals Park, OH; 1986), p. 1848.

[2] P. Vianco, Sandia National Laboratories, unpublished data.

[3] P. Vianco, P. Hlava, and A. Kilgo, "Intermetallic Compound Layer Formation Between Copper and Hot-Dipped 100In, 50In-50Sn, 100Sn, and 63Sn-37Pb Coatings," *Jour. of Elect. Materials,* 23, (1994), p. 583.

[4] B. Lampe, "Room Temperature Aging Properties of Some Solder Alloys," *Welding Jour.*, October 1976, p. 330-s.

[5] P. Vianco, A. Kilgo, and R. Grant, "Solid State Intermetallic Compound Layer Growth Between Copper and Hot Dipped Indium Coatings," *Jour. Mater. Sci.*, 30, (1995), p. 4871.

[6] P. Vianco, A. Kilgo, and R. Grant, "Intermetallic Compound Layer Growth by Solid State Reactions Between 58Bi-42Sn Solder and Copper," *Jour. Elect. Mater.*, 24, (1995), p. 1493.

[7] P. Vianco, K. Erickson, and P. Hopkins, "Solid State Intermetallic Compound Growth Between Copper and High Temperature, Tin-rich Solders, Part I - Experimental Analysis," *Jour. of Elect. Mater.*, 23, (1994), p. 721.

[8] M. Hashish, "A Modeling Study of Metal Cutting with Abrasive Waterjets," *Trans. ASME*, 106, (1984), p. 88.

[9] M. Hashish, "Cutting with Abrasive Waterjets," *Mechanical Eng.*, March (1994), p. 60.

[10] F. Yeaple, "Diamonds to Water Jets - Super Pressure Fluid Power," *Design News*, July 23 (1990), p. 59.

[11] *ASM Handbook - Volume 6 - Welding, Brazing, and Soldering*, (ASM Inter., Materials Park, OH; 1993), p. 992.

[12] D. Frear, W. Jones, and K. Kinsman, eds., *Solder Mechanics - A State of the Art Assessment*, (TMS, Warrendale, PA; 1991), p. 191.

[13] R. Bethea, B. Duran, and T. Boullion, *Statistical Methods for Engineers and Scientists* (Marcel-Dekkar, New York, NY; 1975), p. 197.

[14] H. Solomon, "Fatigue of 60/40 Solder," *IEEE Trans. CHMT*, 9, (1986), p. 423.

[15] R. Klein-Wassink, *Soldering in Electronics,* (Electrochem. Pub., Ltd., Ayr, Scotland, UK; 1989), p. 145.

[16] M. Nylen and S. Norgren, "Temperature Variations in Soldering and Their Influence on Microstructure and Strength of Solder Joints," *Soldering and Surface Mount Technology*, June (1990), p. 15.

[17] R. Prasad, *Surface Mount Technology - Principles and Practice,* (Van Nostrand-Rheinhold, New York, NY; 1989), p. 116-117.

[18] "Interim Report - Failure of PIN Diodes on Microwave T/R Switch Boards," (memo from P.T. Vianco to R.T. Sparks, dtd. March 3, 1992, Sandia National Laboratories, Albuquerque, NM).

[19] "Review of Engineering Change Proposal (ECP) 76-940-293 for Diode Installation on Microwave Circuit Boards," (memo from P.T. Vianco to R.T. Sparks, dtd. March 19, 1992, Sandia National Laboratories, Albuquerque, NM).

Appendix A
Chemical Dissolution Process for Depotting MC2839 Assemblies

This appendix describes the procedure used to remove the potting material (polyurethane elastomer, 9927087-00) from the MC2839 housing as a *whole unit.*

1. Chemical used: N-methyl-pyrolidinone (NMP).
2. Place firing set upside down in pan of NMP.
3. Place pan and unit in oven at 180°F (82°C) for four-hour increments to check for dissolution progress, the removal of by-products, and the replenishment of NMP.
4. Clean with acid brush and turn unit right-side up.
5. Pour NMP material into cavity, cover with aluminum foil, and monitor every one-half hour to one hour, adding material as needed and removing by-products.
6. After foam has been removed, rinse cavity with isopropyl alcohol.
7. Bake assembly for about 2 hours at 180°F (82°C).

Notes:

(a) Time in the oven, suspended upside down in the oven, took about 4 hours at 180°F (82°C).

(b) Time duration of potting removal, right-side up, in the oven at 180°F (82°C), took 20 hours.

Appendix B
Procedures for Analyzing Intermetallic Compound Layer Thicknesses

1. Photographic image taken at 1000x.
2. Scan image to 200%. File designate: **(Board#)-(Joint Letter)/(Pad Letter)**
3. Open *Adobe*™ *Photoshop* application.
4. Optimize image contrast and filter (1x or 2x) with software tools.
5. Resave file.
6. Open *Canvas* application.
7. Paste "Grid Overlay" file on top of photograph image. The "Grid Overlay" provides the ten (10) positions at which the intermetallic compound layer measurements are taken, along with a calibration box.
8. Resave file as **.1** extension in PICT format.
9. Open *Ultimage* application.
10. Calibrate the image with line tool and calibration box.
11. Perform line length analysis at each of the ten (10) locations, then save in *Exel*™ compatible format with extension **.1.lg**.
12. Open *Exel*™ application.
13. Perform statistical analysis of mean and standard deviation on the data.

Appendix C
Procedures for Analyzing Lead-Rich Phase Distribution

1. Photographic image taken at 1000x.
2. Scan image to 200%. File designate: **(Board#)-(Joint Letter)/(Pad Letter)**
3. Open *Adobe*™ *Photoshop* application.
4. Optimize image contrast and filter (1x or 2x) with software tools.
5. Using "Magic Wand", select Sn matrix and delete to a white background.
6. Resave file with **.1** extension.
7. Open *Ultimage*™ application.
8. Create line 28 pixels long.
9. "Geometry Calibrate:" 0.01 mm as calibration.
10. "Process Threshold:" (0-250).
11. Create new file with **.2** extension.
12. "Analysis Particle:" thresholds 1-255
13. "Analysis Distribute:" create histograms of particles vs. particle size, using the ranges:

    $0 - 5x10^{-04}$
    $0 - 2x10^{-04}$
    $0 - 2x10^{-05}$
    $0 - 2x10^{-06}$

14. Print histograms.

Distribution List

Name	Mailstop	Organization
R. Eagan	0513	1000
R. Bair	1070	1200
E. Royer	0527	1231
T. Fischer	0525	1235
G. Dulleck	0525	1235
C. Collins	0525	1235
J. Harris	0523	1251
A. Romig	1079	1300
D. Palmer	1082	1333
J. Searcy	0960	1400
W. Alzheimer	0953	1500
P. Wilson	0501	1565
H. Saxton	1435	1800
G. Pike	1434	1802
J. Jellison	1434	1803
R. Salzbrenner	0342	1805
D. Frear	1407	1811
R. Clough	1407	1811
R. Goehner	1405	1822
F. Greulich	1405	1822
A. Kilgo	1405	1822
A. Carter	1405	1822
W. Cieslak	0340	1832
P. Vianco (5)	1411	1833
J. Rejent	1411	1833
F. Hosking	1411	1833
J. Stephens	0367	1833
B. Damkroger	0367	1833
F. Yost	1405	1841
A. Hurd	1405	1841
D. Dimos	1411	1831
M. Cieslak	1411	1860
H. Schmitt	0457	2000
W. Reynolds	0427	2103
R. Martin	1394	2106
C. Knapp	9033	2262
R. Monson	9035	2265
R. Miller	9013	2266
W. Williams	0509	2300
D. Pierce	0311	2671
M. DeSpain	0311	2671
J. Wilder	0328	2674
R. Hagengruber	0463	5000
A. Medina	0972	5722
R. Stulen	9409	8250
L. West	9420	8200
A. West	9430	8420
T. Dyer	9904	8700
M. Perra	9402	8711
M. Baskas	9403	8712
A. Ratzel	0834	9112
P. Hopkins	0834	9112
K. Erickson	0834	9112

Distribution List (Continued)

H. Morgan	0439	9117
S. Burchett	0439	9117
M. Nielsen	0439	9117
W. Nickell	0631	12300
K. Diegert	0829	12323
M. Dvorack	0491	12333
D. Carlson	0405	12333
J. Sjulin	0830	12335
E. Saverino	0637	12336
O. Hernandez	1390	12354
R. Hahn	0634	12361
J. Middleton	0633	12363

1	MS9018	Central Technical Files, 8940-2
5	0899	Technical Library, 4414
2	0619	Review & Approval, 12690 For DOE/OSTI
1	1380	Technology Transfer, 4212